DESIGN, CONTROL, AND GUIDANCE OF A TACTICAL MISSILE WITH LATERAL THRUSTERS

A THESIS SUBMITTED TO
THE GRADUATE SCHOOL OF NATURAL AND APPLIED SCIENCES
OF
MIDDLE EAST TECHNICAL UNIVERSITY

BY

FAHRETTIN KAĞAN İPEK

IN PARTIAL FULFILLMENT OF THE REQUIREMENTS
FOR
THE DEGREE OF MASTER OF SCIENCE
IN
ELECTRICAL AND ELECTRONICS ENGINEERING

SEPTEMBER 2015

Approval of the thesis:

DESIGN, CONTROL, AND GUIDANCE OF A TACTICAL MISSILE WITH LATERAL THRUSTERS

submitted by **FAHRETTIN KAĞAN İPEK** in partial fulfillment of the requirements for the degree of **Master of Science in Electrical and Electronics Engineering Department, Middle East Technical University** by,

Prof. Dr. Gülbin Dural Ünver _____
Dean, Graduate School of **Natural and Applied Sciences**

Prof. Dr. Gönül Turhan Sayan _____
Head of Department, **Electrical and Electronics Engineering**

Prof. Dr. M. Kemal Leblebicioğlu _____
Supervisor, **Electrical and Electronics Eng. Dept., METU**

Examining Committee Members:

Prof. Dr. Sencer Koç
Electrical and Electronics Engineering, METU _____

Prof. Dr. Mehmet Kemal Leblebicioğlu
Electrical and Electronics Engineering, METU _____

Prof. Dr. Mehmet Önder Efe
Computer Engineering, Hacettepe University _____

Prof. Dr. Ozan Tekinalp
Aerospace Engineering, METU _____

Prof. Dr. Ömer Morgül
Electrical and Electronics Engineering, Bilkent University _____

Date: _____

I hereby declare that all information in this document has been obtained and presented in accordance with academic rules and ethical conduct. I also declare that, as required by these rules and conduct, I have fully cited and referenced all material and results that are not original to this work.

Name, Last Name: FAHRETTIN KAĞAN İPEK

Signature :

ABSTRACT

DESIGN, CONTROL, AND GUIDANCE OF A TACTICAL MISSILE WITH LATERAL THRUSTERS

İpek, Fahrettin Kağan

M.S., Department of Electrical and Electronics Engineering

Supervisor : Prof. Dr. M. Kemal Leblebicioğlu

September 2015, 100 pages

Maneuverability is a key concept for tactical missiles. In this thesis different aerodynamic configurations of a tactical missile is investigated. Effect of fixed wing position on stability and agility is discussed at different phases of the flight. A secondary actuator, lateral thruster system, is introduced. This system employs reaction forces obtained by ejecting high velocity gases at desired times. Unlike aerodynamic fins or thrust vector controlling of the main engine, thruster system control effect is constant at all phases of the flight. This makes it an interesting actuator for low speed conditions when main engine is not vector controlled and aerodynamic fin effectiveness is weak. One peculiarity of the system is that it can only work in on-off fashion; hence thruster modulator is introduced in the controller design to mitigate the nonlinear behavior of the thrusters. Missile initial turnover maneuvers are studied in vertical ground launch and in horizontal airborne launch. Terminal phase guidance is also examined. These scenarios are modeled in a 6 DoF simulation environment and lateral thruster effect is discussed.

Keywords: Tactical missile, lateral thrusters, guidance, control, maneuverability, agile maneuver

ÖZ

YANAL İTİCİLERE SAHİP BİR TAKTİKSEL FÜZENİN TASARIMI, KONTROLÜ VE GÜDÜMÜ

İpek, Fahrettin Kağan
Yüksek Lisans, Elektrik ve Elektronik Mühendisliği Bölümü
Tez Yöneticisi : Prof. Dr. M. Kemal Leblebicioğlu

Eylül 2015 , 100 sayfa

Manevra kabiliyeti taktik füzeler için önemli bir ölçüttür. Bu çalışmada farklı aerodinamik yapıya sahip taktik füzeler araştırılmıştır. Füze üzerinde bulunan sabit kanat yerinin kararlılık ve çeviklik üzerindeki etkisi farklı uçuş sahfalarında gösterilmiştir. İkinci bir eyleyici olarak füzeye yanal iticiler yerleştirilmiştir. Bu iticiler yüksek hızda gaz dışarı atarak gövde üzerinde reaksiyon kuvvetleri oluşturmaktadırlar. Aerodinamik kontrol yüzeylerinin ve ana motor itki vektör kontrolünün aksine bu sistemin kontrol etkisi bütün uçuş boyunca sabittir. Ana motoru vektör kontrollü olmayan bir füze için, düşük hız durumlarında bu tür eyleyiciler, aerodinamik kontrol yüzeylerinin aksine etkili olmaktadır. Bu tür sistemler aç-kapa şeklinde çalıştıklarından geleneksel doğrusal eyleyici yapısından farklıdırlar. Bu nedenle kontrol tasarımında itici modülatörü adı verilen bir algoritma ile iticilerin çalışması sağlanmıştır. Füze ilk dönüş manevraları yanal iticiler göz önüne alınarak 6 serbestlik dereceli benzetimde modellenmiştir. Yerden dik kalkış, havadan yatay atış senaryoları ve terminal güdüm yanal iticiler de göz önüne alınarak incelenmiştir.

Anahtar Kelimeler: Taktik füze, yanal iticiler, güdüm, kontrol, manevra, çevik manevra

to my family

ACKNOWLEDGMENTS

The author thanks to Prof. Dr. Kemal Leblebicioğlu for his guidance, advice, criticism, and insight throughout the thesis.

The author thanks to ROKETSAN for its support in the duration of the work.

TABLE OF CONTENTS

LIST OF TABLES

TABLES

LIST OF FIGURES

FIGURES

LIST OF ABBREVIATIONS

X, Y, Z	Axes of inertial reference frame
X_B, Y_B, Z_B	Axes of body reference frame
$\hat{C}^{(B/I)}$	Transformation matrix from inertial frame to body frame expressed in either frame
$\vec{V}$	Velocity vector of the missile
V_∞	Relative speed of the missile with respect to the air
$\bar{V}^{(I)}$	Velocity vector expressed in inertial frame
$\bar{X}^{(I)}$	Position vector expressed in inertial frame
ϕ, θ, ψ	Euler angles in roll, pitch and yaw planes
$\vec{\omega}_{B/I}$	Rotation vector of body frame with respect to inertial frame
$\tilde{\omega}$	Skew symmetric matrix form of angular velocity vector
u, v, w	Velocity components in body frame
p, q, r	Angular velocity components in body frame
$\vec{F}$	Forces acting on the missile
$\bar{F}^{(B)}$	Force vector expressed in body frame
F_x, F_y, F_z	Force components in body frame
$\bar{F}_A$	Aerodynamic force vector expressed in body frame
$\bar{F}_T$	Thrust force vector expressed in body frame
$\bar{F}_G$	Gravitational force vector expressed in body frame
F_{ME}	Main engine force
F_{thr}	Lateral thruster force
m	Mass of the missile
$\vec{M}$	Moments acting on the missile
M_x, M_y, M_z	Moment components in body frame
$\bar{M}_A$	Aerodynamic moment vector expressed in body frame
$\vec{H}$	Angular momentum of the missile about its center of mass
$\hat{I}$	Inertia matrix
I_{xx}, I_{yy}, I_{zz}	Principal inertia terms
I_{xy}, I_{xz}, I_{yz}	Cross inertia terms

$\vec{i}_i, \vec{j}_i, \vec{k}_i$	Unit vectors of intermediate frames
$\bar{X}_{cg}$	Center of gravity vector expressed in body frame
X_{cg}	Center of gravity position along X_B axis from nose of the missile
$\bar{X}_{cp}$	Center of pressure vector expressed in body frame
X_{cp}	Center of pressure position along X_B axis from nose of the missile
g	Gravitational acceleration
G	Universal gravitational constant
M_E	Mass of the Earth
R_E	Radius of the Earth
$\bar{g}^{(I)}$	Gravity vector expressed in inertial frame
C_X	Force coefficient in body frame X axis
C_Y	Force coefficient in body frame Y axis
C_Z	Force coefficient in body frame Z axis
C_L	Moment coefficient in body frame X axis
C_M	Moment coefficient in body frame Y axis
C_N	Moment coefficient in body frame Z axis
M	Mach number
α	Angle of attack
β	Angle of side slip
$\delta_e, \delta_r, \delta_a$	Aerodynamic control surface deflections of elevator, rudder, aileron.
δ_i	Aerodynamic control surface deflections of individual panels
G_{fin}	Transfer function of fin actuators
ω_n	Natural frequency of fin actuators
ζ	Damping ratio of fin actuators
δ_{max}	Maximum deflection of fins
$\dot{\delta}_{max}$	Maximum deflection rate of fins
G_{thr}	Transfer function of thruster actuators
τ	Time constant of thruster actuators
h	Altitude
Q	Dynamic pressure
S	Reference (cross sectional) area of the missile

d	Reference length (diameter) of the missile
γ	Specific heat ratio
T_0	Absolute temperature at mean sea level
T	Absolute temperature at given altitude
ρ_0	Air density at mean sea level
ρ	Air density at given altitude
a	Speed of sound at given altitude
L	Lapse rate
R	Characteristic gas constant
$\bar{x}$	State vector
$\bar{u}$	Input vector
$\bar{y}$	Output vector
A	System matrix
B	Input matrix
C	Output matrix
DoF	Degree of Freedom
PWPF	Pulse Width Pulse Frequency
AoA	Angle of Attack
PNG	Proportional Navigation Guidance
TVC	Thrust Vector Control
LQR	Linear Quadratic Regulator
MIMO	Multi Input Multi Output
LOS	Line of Sight

CHAPTER 1

INTRODUCTION

Missile systems can be grouped into two types in general: strategic and tactical. Strategic missiles are generally used against ground targets at long ranges. They usually follow a ballistic trajectory and for very high ranges, some portion of the flight takes place outside the atmosphere. Their range can extend to thousands of kilometers. Tactical missiles on the other hand, are generally used against moving targets at short ranges, in the order of tens of kilometers. They are much smaller and more agile than strategic systems. They are also categorized among themselves according to the mission requirements. Surface to air (anti air), surface to surface (anti tank), air to surface are the main types of tactical missiles. Many tactical missiles have the ability to be launched at ground from a canister or from an aircraft. There are also different approaches to the ground launch concept. Some systems have an active launcher that can track targets to launch the missile towards the target. Some systems use vertical launch concept. In this method, missile always leaves the launcher vertically and then executes a maneuver towards the target. Although this concept requires an additional turn to target motion, it reduces the complexity of the launcher and provides more storage room for missiles. Figure 1.1 shows the vertical launch of Sea Wolf missile.

Vertical launch missiles employ novel control techniques to cover the challenges of vertical launch. For example MICA missile uses thrust vector controlling as well as aerodynamic control [11]. In this thesis lateral thrusters are introduced as a secondary actuator in order to increase the agility of the missile and design, control and guidance of such a tactical missile is discussed.

In [16] there are aerodynamic characteristics of typical tactical missile configurations

Figure 1.1: Vertical Launch of Sea Wolf [1]

obtained by panel method. It is a good source to see how lift drag coefficients of a tactical missile change with Mach number and angle of attack. [18] discusses the validity of the Missile DATCOM results and gives several specific conditions in which Missile DATCOM performs well. [6] is a good source on tactical missile guidance. It contains existing systems' characteristics. Besides it has information on missile aerodynamics and control.

There are many sources on the missile linear analysis and controller design. [5] and [23] are comprehensive books on the subject. In addition [24] is a PhD thesis on the subject of guidance and control of a homing missile. [9] and [8] discusses the multi loop structures in missile control design.

[21] examines the effectiveness of three different control systems: aerodynamic fins, thrust vector control and lateral thrusters. It also discusses the interactions of the lateral thruster jets with the flow around the missile body.

[19] is a master's thesis on a similar subject. It considers a vertical launch tactical missile with thrust vector control and aerodynamic fins. [20] discusses a missile with lateral thrusters in stall conditions. It employs a sliding mode controller algorithm.

Outline of the thesis is as follows: in Chapter 2, missile equations of motion are derived; aerodynamic, atmosphere and gravity models are presented. In Chapter 3, missile aerodynamics are examined, static stability and agility of the missile are related through aerodynamic characteristics and a geometry is proposed. In Chapter 4, nonlinear dynamics of the missile is linearized around trim points and analyzed in linear domain. Controllers for both fins and thrusters are designed. Two types of controllers are considered for different phases of flight. In Chapter 5, several maneuvers are simulated with 6 DoF equations of motion and results are presented. Finally in Chapter 6, the study is summarized and possible future work is proposed.

CHAPTER 2

SIX DEGREE OF FREEDOM EQUATIONS OF MOTION

In order to simulate the missile motion and to design controller equations of motion are needed. In this chapter, reference coordinate frames and equations of translational and rotational motion are given.

2.1 Reference Coordinate Frames

In order to define motion of the missile, two reference coordinate frames are used. One is the inertial reference frame and the other is the body reference frame.

Considering the range, the flight ceiling and the flight time of the missile, non rotating and flat Earth model is used. Gravity is only changing with altitude and always in the Z direction of the inertial frame. X and Y of the inertial frame obeys the right hand rule with the sequence of X-Y-Z. Since flat Earth is assumed, direction of X axis of the inertial frame does not matter.

Body reference frame is fixed to the missile. The origin of the frame is coincident with the center of mass of the missile. X_B axis points towards to the nose, Y_B axis points towards to the right (when the missile is viewed from the rear in 0° roll position) and Z_B axis completes the right hand triad. See Figure 2.1.

It is convenient to write differential equations that define motion in the body frame, since aerodynamic and thrust forces/moments are easily defined in the body coordinate frame.

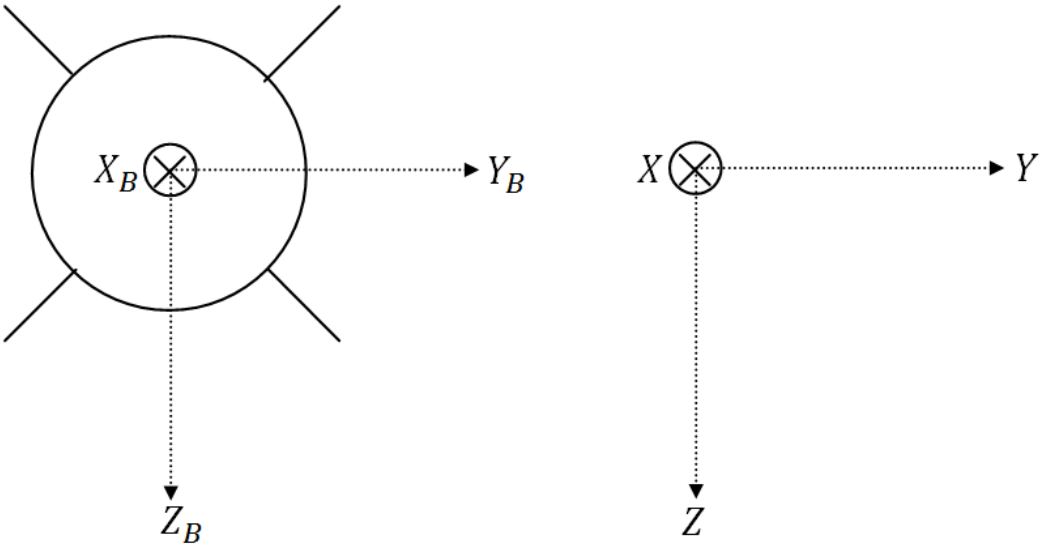

Figure 2.1: Body (left) and Inertial (right) Coordinate Frames. (Missile roll = 0°)

2.2 Translational Dynamics

Assume that the mass is constant, then the differential equation for translational motion is obtained from Newton's 2nd law of motion as:

$$\sum \vec{F} = m \frac{d}{dt}\bigg|_I \vec{V} \tag{2.1}$$

where $\bigg|_I$ denotes that vector is differentiated in the inertial frame. Since it is desired to write the equations in the body frame, Coriolis theorem is used to switch the differentiation frame, which can be stated as:

$$\frac{d}{dt}\bigg|_I \vec{A} = \frac{d}{dt}\bigg|_B \vec{A} + \vec{\omega}_{B/I} \times \vec{A} \tag{2.2}$$

which relates differentiation of a vector $\vec{A}$ in two frames rotating with respect to each other. Note that $\vec{\omega}_{B/I}$ denotes the rotation vector of B frame with respect to I frame. Then Newton's 2nd law can be expressed as:

$$\sum \vec{F} = m(\frac{d}{dt}\Big|_B \vec{V} + \vec{\omega}_{B/I} \times \vec{V}) \tag{2.3}$$

Express the vectors in Eq. (2.3) in body frame as:

$$\bar{F}^{(B)} = \begin{bmatrix} F_x \\ F_y \\ F_z \end{bmatrix}, \bar{V}^{(B)} = \begin{bmatrix} u \\ v \\ w \end{bmatrix}, \bar{\omega}^{(B)} = \begin{bmatrix} p \\ q \\ r \end{bmatrix} \tag{2.4}$$

where $\bar{A}^{(B)}$ is the column matrix obtained by resolving the vector $\vec{A}$ in B frame and write the equation in the matrix domain (as opposed to vector domain) and drop "body frame" superscript :

$$\bar{F} = m(\dot{\bar{V}} + \tilde{\omega}\bar{V}) \tag{2.5}$$

Note that $\tilde{\omega}\bar{V}$ operation is the equivalent matrix multiplication to the cross product where

$$\bar{\omega} = \begin{bmatrix} 0 & -r & -q \\ r & 0 & -p \\ -q & p & 0 \end{bmatrix} \tag{2.6}$$

is the skew symmetric matrix obtained from the column matrix $\bar{\omega}$. Substituting Eq. (2.4) in Eq. (2.5) and rearranging to get velocity derivatives:

$$\begin{aligned} \dot{u} &= \frac{F_x}{m} + vr - wq \\ \dot{v} &= \frac{F_y}{m} - ur + wp \\ \dot{w} &= \frac{F_z}{m} + uq - vp \end{aligned} \tag{2.7}$$

In Eq. (2.5) $\bar{F}$ is the net force acting on the missile and can be expressed as the sum of aerodynamic, thrust and gravitational forces, which is explained in detail in the following sections.

2.3 Translational Kinematics

In the previous chapter velocity derivatives are obtained in the body frame, by simply integrating the derivatives, velocity in the body frame is obtained. To calculate the velocity and the position in the inertial frame, first transform the velocity in the body frame to the inertial frame with "direction cosine matrix" and then integrate to obtain position. Direction cosine matrix and rotation angles are explained in the following sections.

$$\begin{aligned} \bar{V}^{(I)} &= \hat{C}^{(I/B)}\bar{V}^{(B)} \\ \bar{X}^{(I)} &= \int \bar{V}^{(I)}dt \end{aligned} \tag{2.8}$$

where $\hat{C}^{(I/B)}$ is the transformation matrix from the body frame to the inertial frame.

2.4 Rotational Dynamics

Define the inertia matrix in the body frame as:

$$\hat{I} = \begin{bmatrix} I_{xx} & I_{xy} & I_{xz} \\ I_{yx} & I_{yy} & I_{yz} \\ I_{zx} & I_{zy} & I_{zz} \end{bmatrix} \tag{2.9}$$

Define the angular momentum as:

$$\vec{H} = \check{I} \cdot \vec{w} \tag{2.10}$$

Moment equation, similar to Newton's force equation, is:

$$\sum \vec{M} = \frac{d}{dt}\bigg|_I \vec{H} \tag{2.11}$$

Again it is convenient to differentiate the expression in the body frame; hence Coriolis theorem can be applied:

$$\sum \vec{M} = \frac{d}{dt}\bigg|_B \vec{H} + \vec{\omega}_{B/I} \times \vec{H} \tag{2.12}$$

Substituting Eq. (2.10) in Eq. (2.12) and assuming moment of inertia is constant:

$$\sum \vec{M} = \check{I}\frac{d}{dt}\bigg|_B \vec{\omega} + \vec{\omega}_{B/I} \times \check{I} \cdot \vec{\omega} \tag{2.13}$$

where $\vec{\omega} = \vec{\omega}_{B/I}$ and will be written as $\vec{\omega}$ in the following equations and $\check{I}$ is the inertia dyadic. One can express Eq. (2.13) in matrix domain and resolve vectors in body frame:

$$\sum \bar{M} = \hat{I}\dot{\bar{\omega}} + \tilde{\omega}\hat{I}\bar{\omega} \tag{2.14}$$

Substituting Eq. (2.4) and Eq. (2.10) in Eq. (2.14) and rearranging to get angular velocity derivatives:

$$\begin{aligned}
\dot{p} &= \frac{\sum M_x + I_{xz}\dot{r} + I_{xz}pq + (I_{yy} - I_{zz})rq}{I_{xx}} \\
\dot{q} &= \frac{\sum M_y + (I_{zz} - I_{xx})pr + I_{xz}(r^2 - p^2)}{I_{yy}} \\
\dot{r} &= \frac{\sum M_z + I_{xz}\dot{p} + (I_{xx} - I_{yy})pq - I_{xz}qr}{I_{zz}}
\end{aligned} \tag{2.15}$$

Notice that there are $\dot{r}$ and $\dot{p}$ terms in $\dot{p}$ and $\dot{r}$ equations, respectively. For controller design it will be assumed that cross inertia terms are zero, hence these terms will be dropped and Eq. (2.15) can be used.

2.5 Rotational Kinematics

Define three rotation (Euler) angles (ϕ, θ, ψ) about inertial axes (X, Y, Z) respectively, such that when the inertial frame is rotated with a particular sequence (ZYX for this case), inertial frame coincides with the body frame.

Body angular rate ω was obtained previously in body frame. Since Euler angles also describe body rotation, time derivative of Euler angles should be equal to ω (Eq. (2.16)); however they should be first expressed in body frame.

$$\vec{\omega} = \dot{\vec{\phi}} + \dot{\vec{\theta}} + \dot{\vec{\psi}} \tag{2.16}$$

In Figure 2.2 (X, Y, Z) is the body frame and the frame with the subscript 1 (inertial frame) is being rotated by the above fashion (ZYX sequence) with the Euler angles (ϕ, θ, ψ). After each individual rotation frame subscript is changed (e.g., 2 and 3) and finally after the last rotation, rotated frame coincides with the body frame.

For the following equations, (i, j, k) are the unit vectors and the subscripts indicate which frame they belong to. Then,

$$\begin{aligned} \dot{\vec{\psi}} &= \dot{\psi}\vec{k_1} = \dot{\psi}\vec{k_2} \\ \dot{\vec{\theta}} &= \dot{\theta}\vec{j_2} = \dot{\theta}\vec{j_3} \\ \dot{\vec{\phi}} &= \dot{\phi}\vec{i_3} = \dot{\phi}\vec{i} \end{aligned} \tag{2.17}$$

Substituting Eq. (2.17) in Eq. (2.16):

$$\vec{\omega} = \dot{\psi}\vec{k_2} + \dot{\theta}\vec{j_3} + \dot{\phi}\vec{i} \tag{2.18}$$

Using Euler angles, transformation matrices can be written from one frame to another. For instance, let $\bar{A}^{(1)}$ be a vector expressed in frame 1, then transformation from frame 1 to frame 2 can be obtained as:

$$\bar{A}^{(2)} = \begin{bmatrix} c\psi & s\psi & 0 \\ -s\psi & c\psi & 0 \\ 0 & 0 & 1 \end{bmatrix} \bar{A}^{(1)} \tag{2.19}$$

where $s\psi$ and $c\psi$ are shorthand notations for $sin(\psi)$ and $cos(\psi)$ respectively.

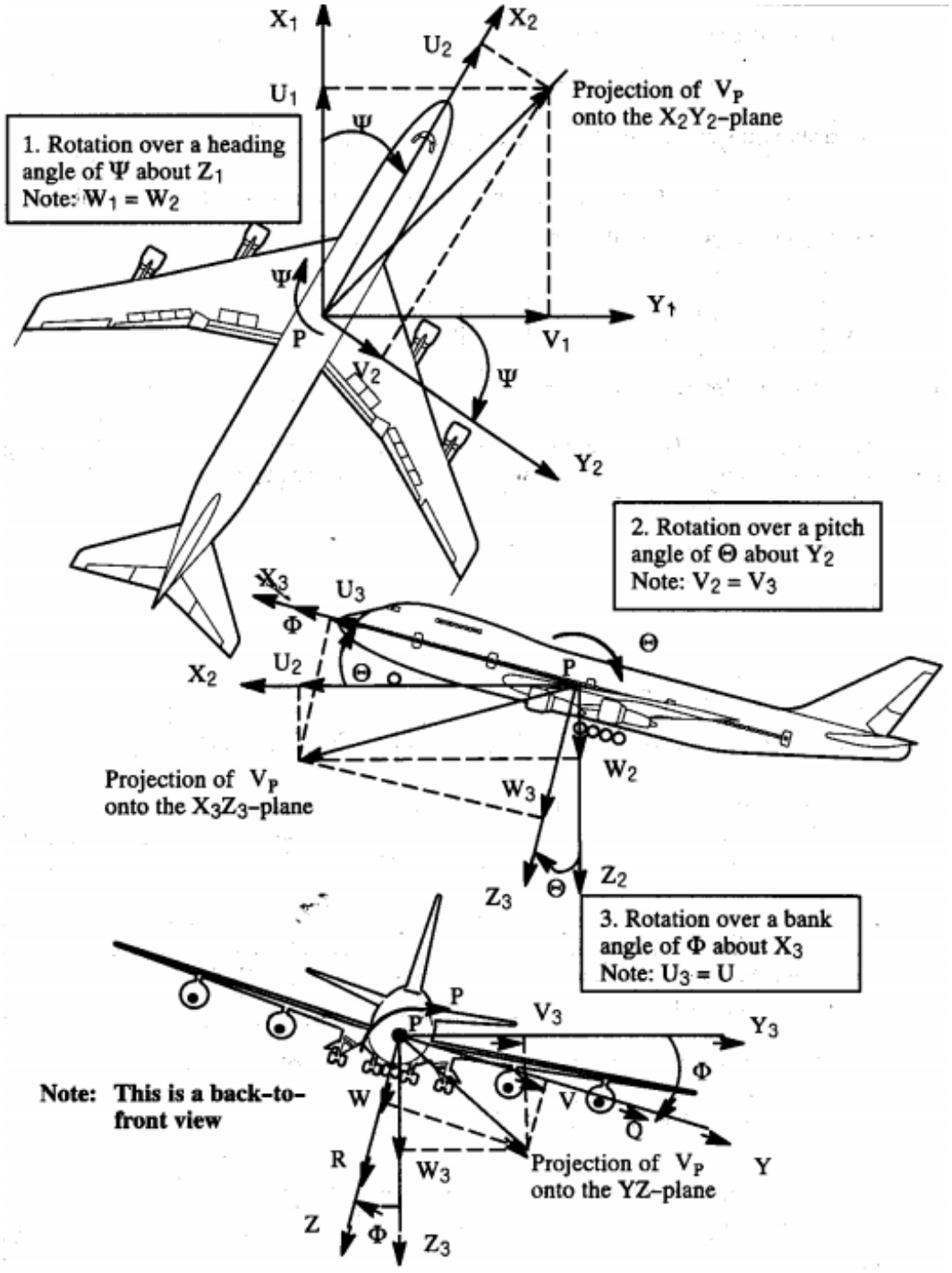

Figure 2.2: Euler Angles and Axis Rotations [17]

Similarly, transformation matrices from frame 2 to 3 and 3 to body frame can be obtained. Moreover by multiplying these three transformation matrices, the transformation matrix between inertial frame and body frame can be obtained.

Now, k_2 and j_3 from Eq. (2.18) can be expressed in body frame with the use of transformation matrices:

$$\begin{aligned} \vec{k_2} &= -\vec{i_3}s\theta + \vec{k_3}c\theta = -\vec{i}s\theta + (\vec{j}s\phi + \vec{k}c\phi)c\theta \\ \vec{j_3} &= \vec{j}c\phi - \vec{k}s\phi \end{aligned} \tag{2.20}$$

Substituting Eq. (2.20) in Eq. (2.18):

$$\vec{\omega} = (-\dot{\psi}s\theta + \dot{\phi})\vec{i} + (\dot{\psi}c\theta s\phi + \dot{\theta}c\phi)\vec{j} + (\dot{\psi}c\theta c\phi - \dot{\theta}s\phi)\vec{k} \tag{2.21}$$

Then components of $\bar{\omega}$ can be written as:

$$\begin{aligned} p &= -\dot{\psi}s\theta + \dot{\phi} \\ q &= \dot{\psi}c\theta s\phi + \dot{\theta}c\phi \\ r &= \dot{\psi}c\theta c\phi - \dot{\theta}s\phi \end{aligned} \tag{2.22}$$

After rearranging Eq. (2.22) to get Euler angle derivatives:

$$\begin{aligned} \dot{\phi} &= p + qs\phi t\theta + rc\phi t\theta \\ \dot{\theta} &= qc\phi - rs\phi \\ \dot{\psi} &= q\frac{s\phi}{c\theta} + r\frac{c\phi}{c\theta} \end{aligned} \tag{2.23}$$

where $t\theta$ denotes $tan(\theta)$.

By integrating Euler angle derivatives, Euler angles can be obtained and using Euler angles, transformation matrix ($\hat{C}^{(I/B)}$) in Eq. (2.8)) between the inertial and the body coordinate axes can be obtained. Note that for $\theta = 90^\circ$ there appears to be division by

zero in Eq. (2.23). However, this problem is not present in the solution of equations of motion, because of the discrete nature of the solver. Exact value of 90° does not appear in the solution; hence, division by zero does not occur.

2.6 Forces and Moments

In the previous chapters, force and moment equations are derived in the body coordinate frame and $\bar{F}$ and $\bar{M}$ are defined as the sum of all forces and moments acting on the missile expressed in body coordinate frame. In this chapter these forces and moments are explained. They are considered as aerodynamic, thrust and gravitational in general.

2.6.1 Aerodynamic Forces and Moments

In order to calculate the aerodynamic effects on the missile, aerodynamic coefficients of the missile should be obtained and a proper atmosphere model should be used.

2.6.1.1 Aerodynamic Coefficients

Aerodynamic forces and moments are calculated from the coefficients obtained in the body frame. In general aerodynamic forces can be written as:

$$\bar{F}_A = QS \begin{bmatrix} C_X \\ C_Y \\ C_Z \end{bmatrix} \tag{2.24}$$

where Q is the dynamic pressure and S is the reference area of the missile.

In general aerodynamic coefficients are non-linear function of many variables: Mach number (M), angle of attack (α), angle of side slip (β); aileron (δ_a), elevator (δ_e), rudder (δ_r) deflections and body rotational rates (p, q, r). However, the missile studied in this work is axisymmetrical and some of the cross dependence terms are ne-

glected (Appendix [A]). Dependence of aerodynamic force coefficients are given in Eq. (2.25).

$$\bar{F}_A = QS \begin{bmatrix} C_X(M,\alpha,\beta) \\ C_Y(M,\beta,\delta_r,\dot{\beta},r) \\ C_Z(M,\alpha,\delta_e,\dot{\alpha},q) \end{bmatrix} \tag{2.25}$$

In order to calculate aerodynamic coefficients Missile DATCOM is used. Missile DATCOM generates the coefficients for a given geometry at desired flight conditions. Missile DATCOM gives some dependence relations as linear for coefficients, e.g., C_Z dependence on rotation rate q is given through the coefficient C_{Z_q}, which is derivative of force coefficient with respect to rotation rate q. Overall, aerodynamic forces are written as:

$$\bar{F}_A = QS \begin{bmatrix} C_X(M,\alpha,\beta) \\ C_Y(M,\beta,\delta_r) + C_{Y_{\dot{\beta}}}(M)\dot{\beta}\frac{d}{2V_\infty} + C_{Y_q}(M)q\frac{d}{2V_\infty} \\ C_Z(M,\alpha,\delta_e) + C_{Z_{\dot{\alpha}}}(M)\dot{\alpha}\frac{d}{2V_\infty} + C_{Z_q}(M)q\frac{d}{2V_\infty} \end{bmatrix} \tag{2.26}$$

where d is the reference length, V_∞ is the relative airspeed of the missile and $\frac{d}{2V_\infty}$ term is the non-dimensionalization term for rate derivatives ($C_{Y_{\dot{\beta}}}$, C_{Z_q}, etc.).

Aerodynamic moments are similarly calculated. Equation below shows the moment function structure.

$$\bar{M}_A = QSd \begin{bmatrix} C_L(M,\alpha,\beta,\delta_a) + C_{L_p}(M)p\frac{d}{2V_\infty} \\ C_M(M,\alpha,\delta_e) + C_{M_{\dot{\alpha}}}(M)\dot{\alpha}\frac{d}{2V_\infty} + C_{M_q}(M)q\frac{d}{2V_\infty} \\ C_N(M,\beta,\delta_r) + C_{N_{\dot{\beta}}}(M)\dot{\beta}\frac{d}{2V_\infty} + C_{N_r}(M)r\frac{d}{2V_\infty} \end{bmatrix} \tag{2.27}$$

Moment and force coefficients are referenced to a point on the missile longitudinal (X_B) axis. Since the missile center of mass is changing during main engine burn, aerodynamic moment should be moved to the new center of mass. Therefore, center of mass is input as the tip of the missile to Missile DATCOM and then aerodynamic coefficients are moved to the instantaneous center of mass position. Then moment equation becomes:

$$\bar{M}_A = QSd \begin{bmatrix} C_L(M,\alpha,\beta,\delta_a) + C_{L_p}(M)p\frac{d}{2V_\infty} \\ C_M(M,\alpha,\delta_e) + C_{M_{\dot{\alpha}}}(M)\dot{\alpha}\frac{d}{2V_\infty} + C_{M_q}(M)q\frac{d}{2V_\infty} \\ C_N(M,\beta,\delta_r) + C_{N_{\dot{\beta}}}(M)\dot{\beta}\frac{d}{2V_\infty} + C_{N_r}(M)r\frac{d}{2V_\infty} \end{bmatrix} + \bar{X}_{cg} \times \bar{F}_A \quad (2.28)$$

where $\bar{X}_{cg}$ is the position of the center of mass of the missile.

Attack angles (α, β) of the missile are defined as follows:

$$\begin{aligned} \alpha &= arctan(\frac{w}{u}) \\ \beta &= arctan(\frac{v}{V}) \end{aligned} \quad (2.29)$$

Coefficients are calculated at some points in the flight envelope of the missile using Missile DATCOM and then tabulated to be interpolated in the simulation.

A model for atmosphere is needed to calculate dynamic pressure and Mach number. Atmosphere density is used to calculate dynamic pressure and speed of sound is used to calculate Mach number.

$$\begin{aligned} Q &= \frac{1}{2}\rho V_\infty^2 \\ M &= \frac{V}{a} \end{aligned} \quad (2.30)$$

where ρ is the density and a is the speed of sound. To calculate these values International Standart Atmosphere (ISA) model is used. See Appendix [B] for details.

Missile DATCOM is used to generate aerodynamic coefficients between $\alpha = -40^\circ$ and $\alpha = +40^\circ$. For values of angle of attack outside this interval, missile is slow in the cases studied in the thesis. Therefore, the missile is assumed to be in the stall condition for angle of attack values outside this interval. In the stall condition, aerodynamic moments are assumed to be zero and a constant drag coefficient of 2.5 is assumed. The resulting force is added in the missile body axis according to the angle of attack and angle of side slip [20].

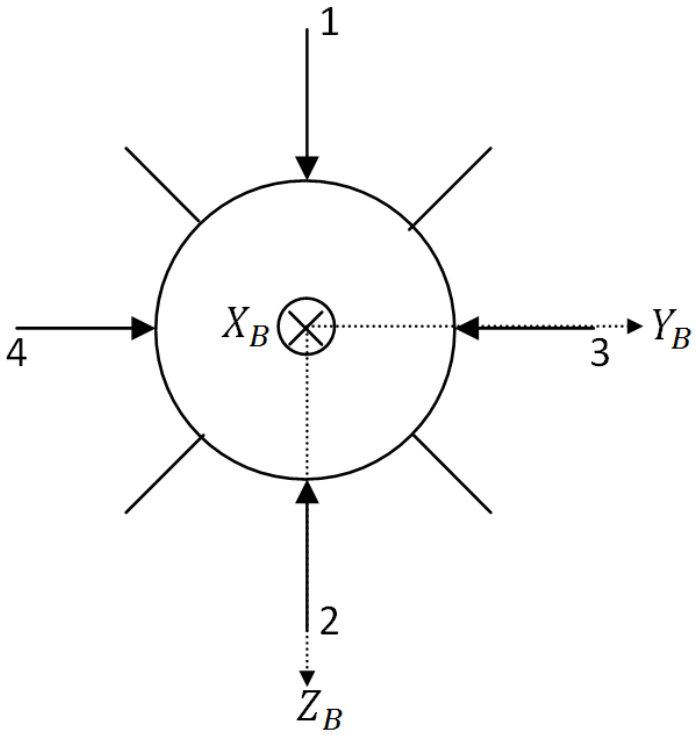

Figure 2.3: Thruster Locations, Force Directions and Numbering

2.6.2 Thrust Forces and Moments

There are two kinds of source of thrust in the missile. One is the traditional main rocket engine that propels the missile forward and other is the lateral thrusters placed at the aft of the missile. Main purpose of the lateral thrusters is to apply moment in pitch and yaw planes to the missile. Figure 2.3 shows the thrusters locations, force directions and numbering.

Main engine has a rectangle thrust profile, which is a constant 12.5 kN during 8 seconds. Its thrust is in the X_B direction only since it has a fixed nozzle.

Lateral thrusters produce 200 N at command, they are operated in on-off fashion. More information can be found in Appendix [C].

In the body coordinate frame, thrust forces can be written as:

$$\bar{F}_T = \begin{bmatrix} F_{ME} \\ 0 \\ 0 \end{bmatrix} + \begin{bmatrix} 0 \\ 0 \\ F_{thr} \end{bmatrix} u_1 + \begin{bmatrix} 0 \\ 0 \\ -F_{thr} \end{bmatrix} u_2 + \begin{bmatrix} 0 \\ -F_{thr} \\ 0 \end{bmatrix} u_3 + \begin{bmatrix} 0 \\ F_{thr} \\ 0 \end{bmatrix} u_4 \quad (2.31)$$

where F_{ME} and F_{thr} are the main engine and single lateral thruster thrust value respectively. u_i's are the commands for the lateral thrusters and take the values 0 or 1 only.

2.6.3 Gravitational Forces

As mentioned in Section 2.1, gravity direction is the Z axis of the inertial frame. Since all motion equations are derived in the body frame, gravity should also be written in the body frame. It can be done using the transformation matrix obtained in Section 2.5.

$$\bar{g}^{(I)} = \begin{bmatrix} 0 \\ 0 \\ g \end{bmatrix} \quad (2.32)$$

$g = g(h)$ is the simple gravity model of Newton:

$$g(h) = \frac{GM_E}{(h + R_E)^2} \quad (2.33)$$

where G is the universal gravitational constant, M_E is the mass of the Earth and R_E is the radius of the Earth. Next, the gravity is transformed from the inertial frame to the body frame:

$$
\begin{aligned}
\bar{F}_G &= m\hat{C}^{(B/I)}\bar{g}^{(I)} \\
\bar{F}_G &= m \begin{bmatrix} c\psi c\theta & s\psi c\theta & -s\theta \\ c\psi s\theta s\phi - s\psi c\phi & s\psi s\theta s\phi + c\psi c\phi & c\theta s\phi \\ c\psi s\theta c\phi + s\psi s\phi & s\psi s\theta c\phi - c\psi s\phi & c\theta c\phi \end{bmatrix} \begin{bmatrix} 0 \\ 0 \\ g \end{bmatrix} \\
\bar{F}_G &= mg \begin{bmatrix} -s\theta \\ c\theta s\phi \\ c\theta c\phi \end{bmatrix}
\end{aligned} \tag{2.34}
$$

Thus, aerodynamic, thrust and gravitational effects on the missile are modeled and expressed in the body coordinate frame for the solution of the equations of the motion.

CHAPTER 3

MISSILE DESIGN

In this chapter missile geometry and its effect on missile aerodynamic characteristics are explained. Tactical missiles have the general structure shown in Figure 3.1.

Guidance section usually houses a seeker to lock on to a target. Control section drives the aerodynamic fins to execute guidance commands. Fixed long wings placed around the motor section increases the lift generated by the missile and improves agility with the cost of increased drag.

Size of the control fins and the fixed wings greatly affect the missile aerodynamic behavior; hence it is important to investigate different fin and wing configurations. Missile DATCOM is used as the tool to generate aerodynamic properties. However, since center of mass is also very important in aerodynamics, first mass and center of gravity of the missile should be decided. Using estimation equations, taken from a thesis work (Appendix [D]), and analyzing similar systems, missile mass properties are determined as shown in Table **??**.

The missile considered in this work is 2m long, has a diameter of 0.15 m and 100

Table 3.1: Missile Characteristics

	Guidance/Control	Warhead	Main Engine	Overall
Mass [kg]	30	15	55/11	100/56
Length [m]	0.6	0.4	1	2
Diameter [m]	0.15	0.15	0.15	0.15
Center of Mass [m]	0.45	0.8	1.5	1.0/0.75

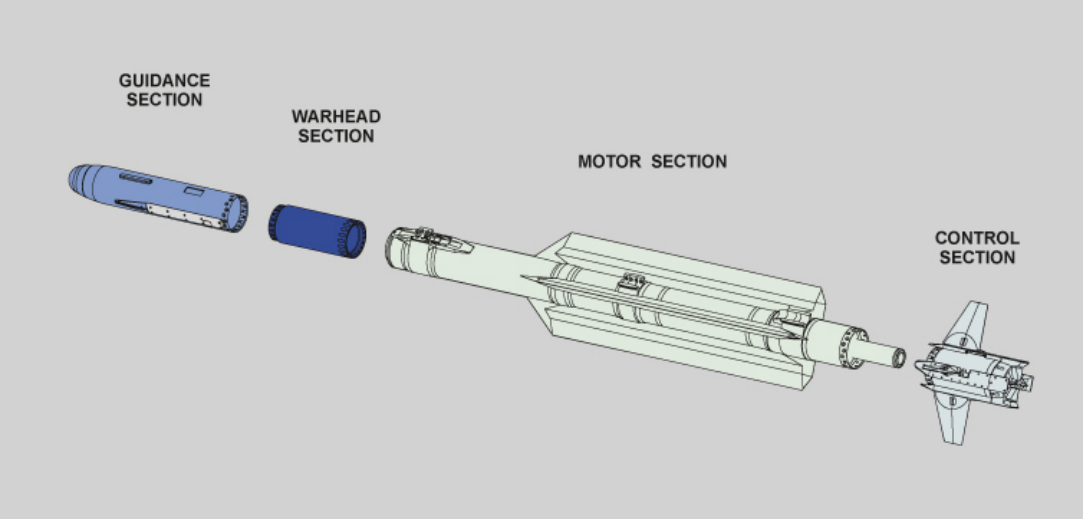

Figure 3.1: IRIS-T Tactical Missile

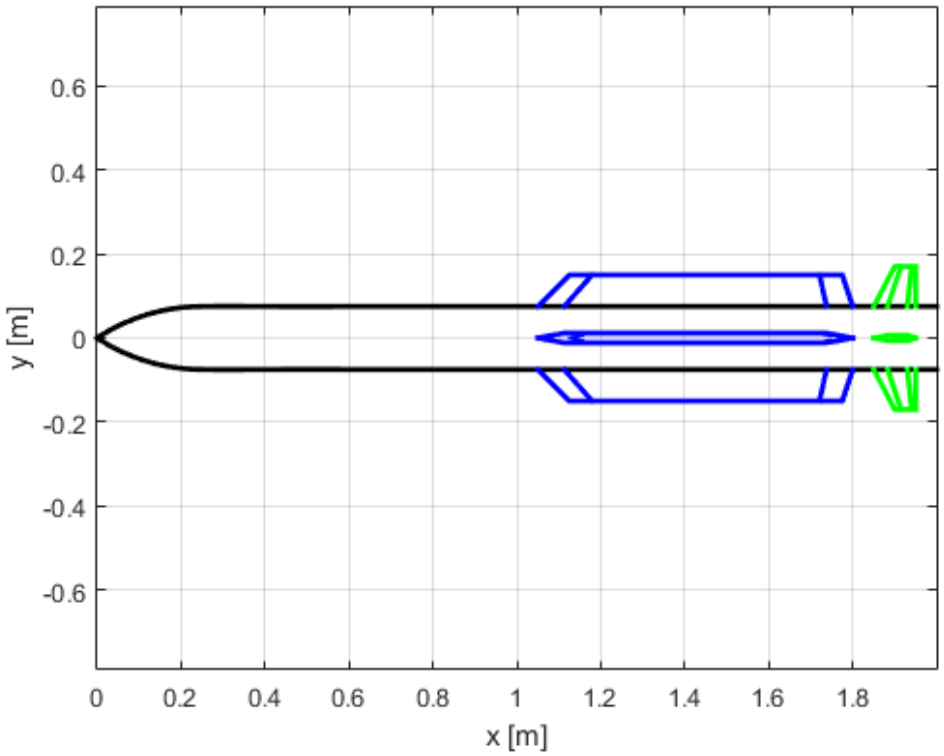

Figure 3.2: Typical Missile Geometry

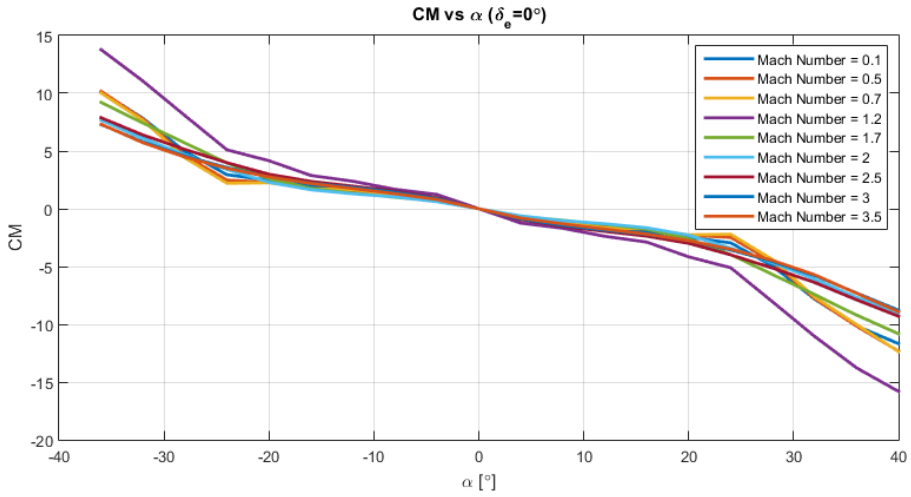

Figure 3.3: Pitching Moment Coefficient @ $X_{cg} = 1m$

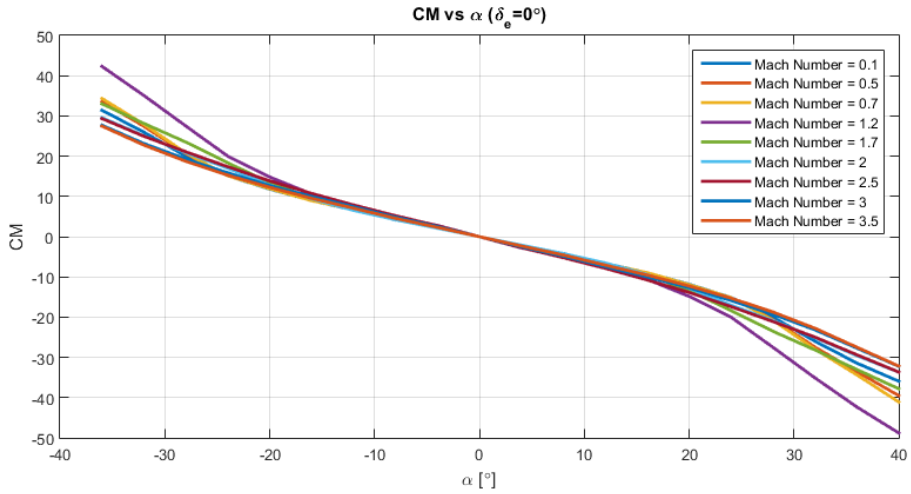

Figure 3.4: Pitching Moment Coefficient @ $X_{cg} = 0.75m$

kg of launch weight. 100/56 and 1.0/0.75 indicate the values at the start of the main engine and at the end of the main engine operation. Note that lateral thruster system mass is included in the guidance and control section.

First, the typical missile geometry shown in Figure 3.2 is considered. Primarily pitching moment coefficient is interesting, since it determines how agile the missile is. Figure 3.3 how the pitching moment coefficient changes versus angle of attack (α) at $X_{cg} = 1m$, which corresponds to main engine ignition time.

As it can be seen from the figure, C_{M_α}, pitching moment derivative with respect to angle of attack, is negative. Hence the missile is aerodynamically stable. Moreover,

as the main engine burns, the center of mass moves forward because of the propellant expelled from the aft of the missile. Therefore, the missile becomes more stable as it burns its engine. Figure 3.4 shows the same coefficient at $X_{cg} = 0.75$, at the burnout. As it is obvious from the figure, slope is increased in the negative direction.

In order to maneuver the missile, it should be trimmed at an angle of attack. The needed aerodynamic fin deflection is closely related to the missile stability margin. In simple terms, trim condition can be stated as $C_M = 0$. For the sake of simplicity, assume that:

$$C_M = C_{M_\alpha}\alpha + C_{M_{\delta_e}}\delta_e \tag{3.1}$$

Then, in order to satisfy trim condition:

$$\begin{aligned} 0 &= C_{M_\alpha}\alpha + C_{M_{\delta_e}}\delta_e \\ \delta_e &= -\frac{C_{M_\alpha}}{C_{M_{\delta_e}}}\alpha \end{aligned} \tag{3.2}$$

Hence, for a given α, higher C_{M_α} means higher δ_e, fin deflection. Keeping C_{M_α} low makes it possible to trim the missile with less fin deflections at higher angle of attack values. Same phenomenon can be observed by comparing center of gravity (X_{cg}) with the center of pressure (X_{cp}) of the missile. Figure 3.5 shows the missile center of pressure and center of gravity with respect to Mach number. As the missile accelerates (center of gravity moves forward) difference between center of pressure and center of gravity increases and the missile becomes more stable.

Considering this conclusion, the typical missile model is modified. Two configurations are discussed according to their stability and agility.

3.1 Alternative 1 - Agile Missile After Burnout

In this configuration, the aim is to get an agile missile after main engine burnout, i.e. X_{cg} and X_{cp} close to each other after burnout. Hence, it is more unstable than the

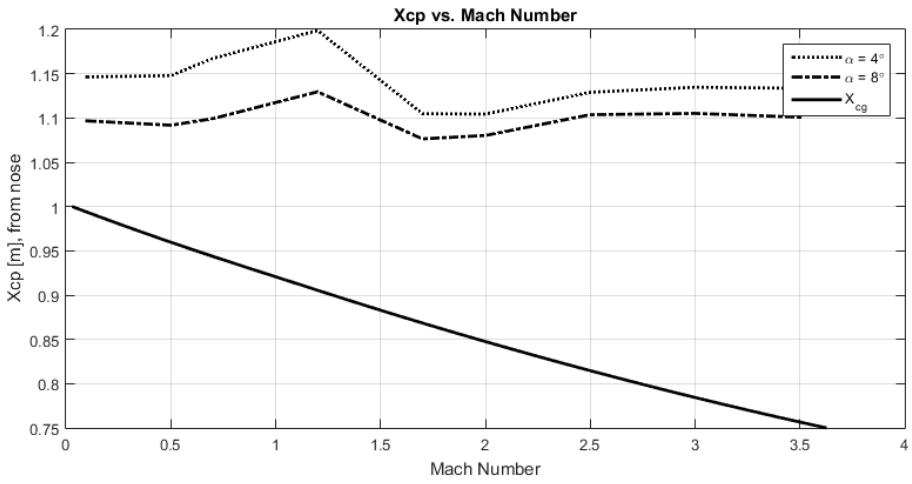

Figure 3.5: X_{cp} and X_{cg} vs Mach Number

typical missile. In order to move X_{cp} to X_{cg}, wings are moved towards the nose. New geometry is shown in Figure 3.6.

Figure 3.7 shows the pitching moment coefficient at ignition of the main engine. As expected, because of the movement of the wings towards to the nose, the missile became unstable when $X_{xg} = 1m$. However, at $X_{cg} = 0.75m$ the center of pressure is very close to the center of gravity (Figure 3.9) and C_{M_α} is close to zero (Figure 3.8). Hence, the missile is very easy to trim at high angles of attack after burnout.

A drawback of this configuration is the unstable behavior at the start of the main engine. If the missile is expected to perform sharp turns at the start, then it can easily become unstable and lose control.

Another interesting point to note for this configuration is the natural trim points at high angle of attacks (25°, red rectangles in Figure 3.8). At these points, even though fin deflections are zero and angle of attack is not, pitching moment is zero. Hence the missile can be trimmed at these points and execute maneuvers with zero control effort. Also note that around these points, missile is stable so it will try to conserve this state. This phenomena occurs because as the angle of attack increases center of pressure moves backwards, i.e., the missile becomes more stable. This behavior also illustrated in Figure 3.10.

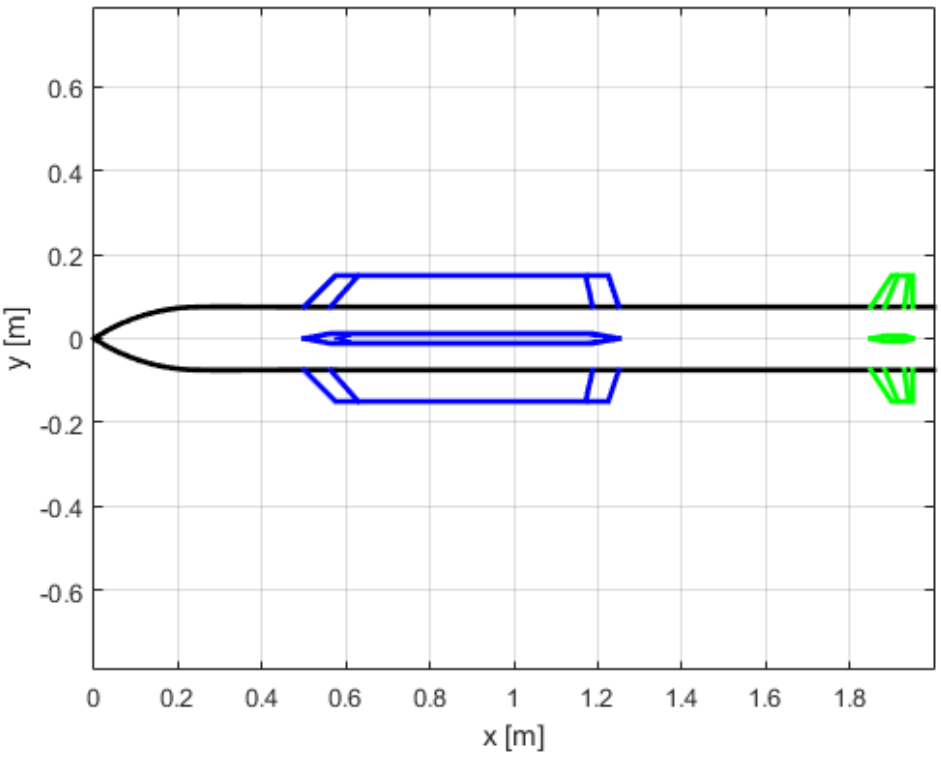

Figure 3.6: Alternative 1 Missile Geometry

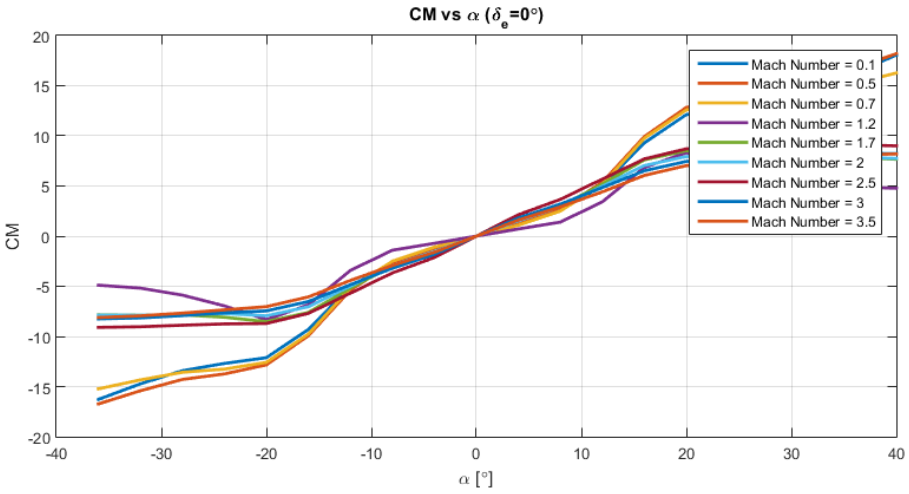

Figure 3.7: Alternative 1 Pitching Moment Coefficient @ $X_{cg} = 1m$

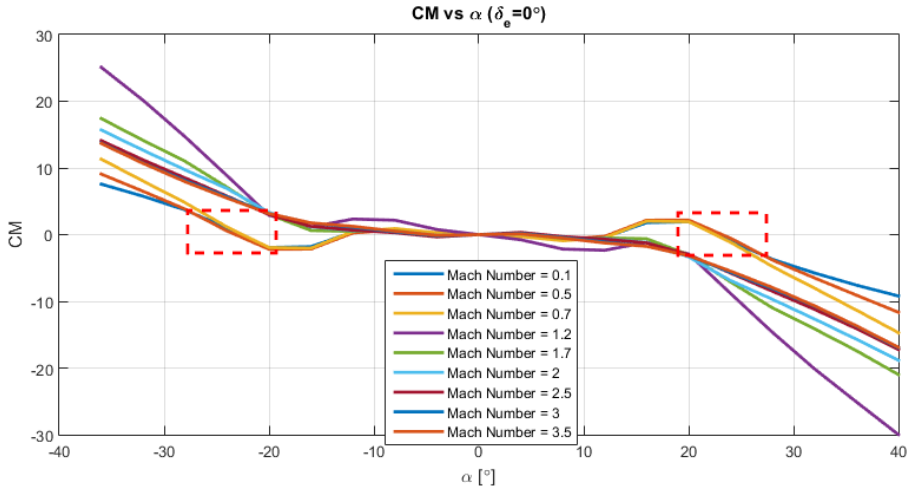

Figure 3.8: Alternative 1 Pitching Moment Coefficient @ $X_{cg} = 0.75m$

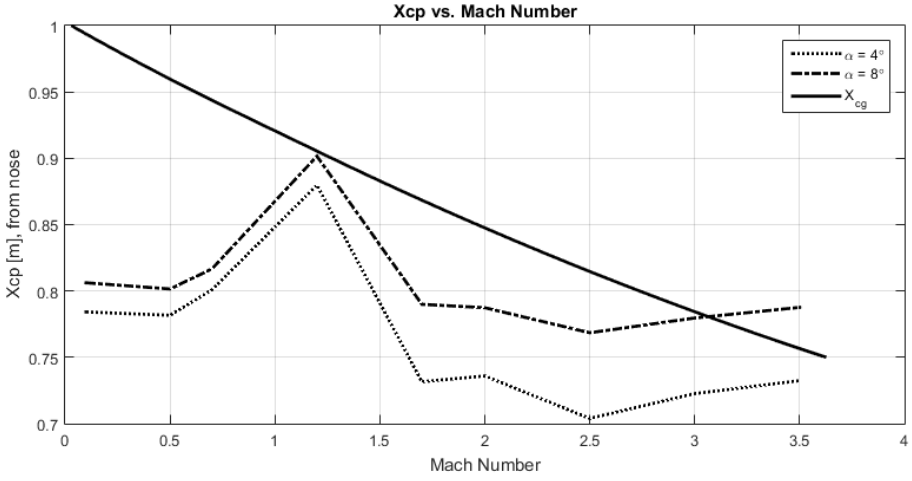

Figure 3.9: Alternative 1 X_{cp} and X_{cg} vs Mach Number

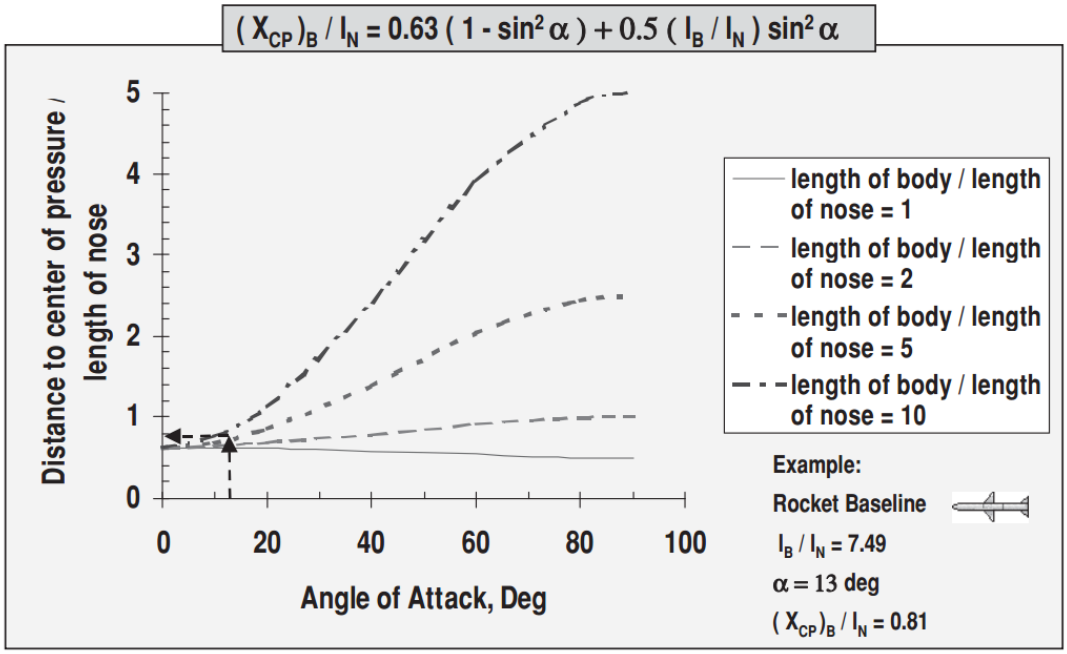

Figure 3.10: X_{cp} vs. Angle of Attack [6]

3.2 Alternative 2 - Agile Missile at Launch

In order to have an agile missile at the launch wings can be moved towards to the nose but not as much as in the case with "Alternative 1" missile. Hence it is between typical missile and alternative 1 missile in terms of stability. It is more stable than alternative 1 and less stable than typical missile configurations. Figure 3.11 shows the missile geometry.

Figures 3.12, 3.13, 3.14 show the properties discussed for this missile configuration. As it is seen from the figures, the missile center of pressure is close to the center of mass at the launch. This will be advantageous when utilizing lateral thrusters at launch, which is discussed in detail in the following chapters.

Alternative 2 missile configuration is a good compromise between typical missile and Alternative 1 missile. For the remaining of this study Alternative 2 missile geometry is used. Aerodynamic coefficients of this geometry can be found in Appendix [A].

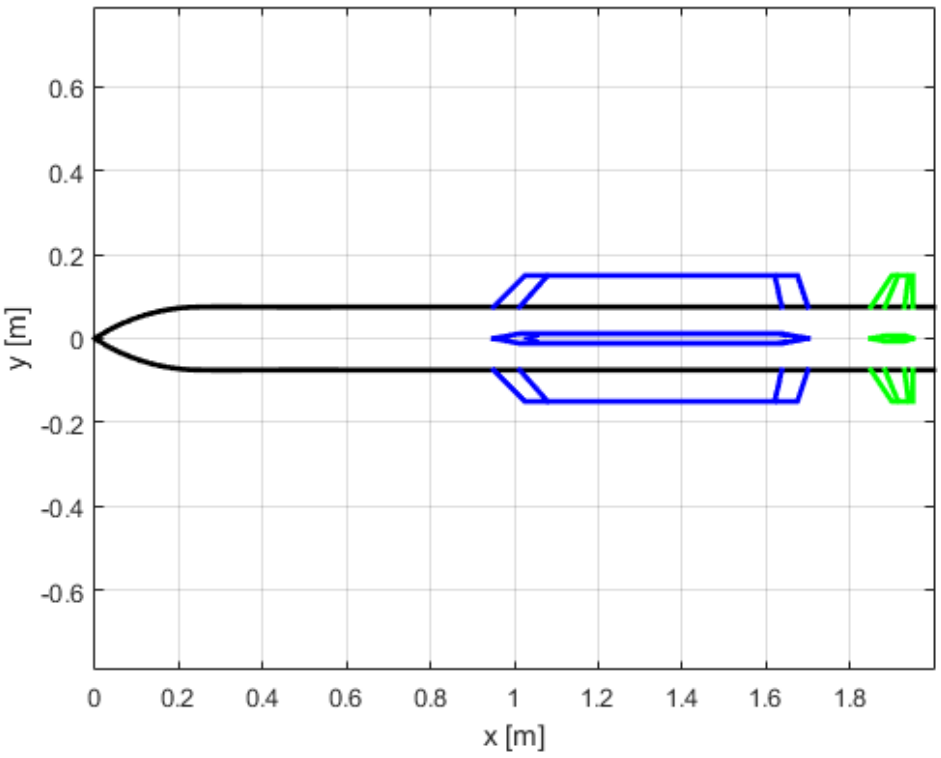

Figure 3.11: Alternative 2 Missile Geometry

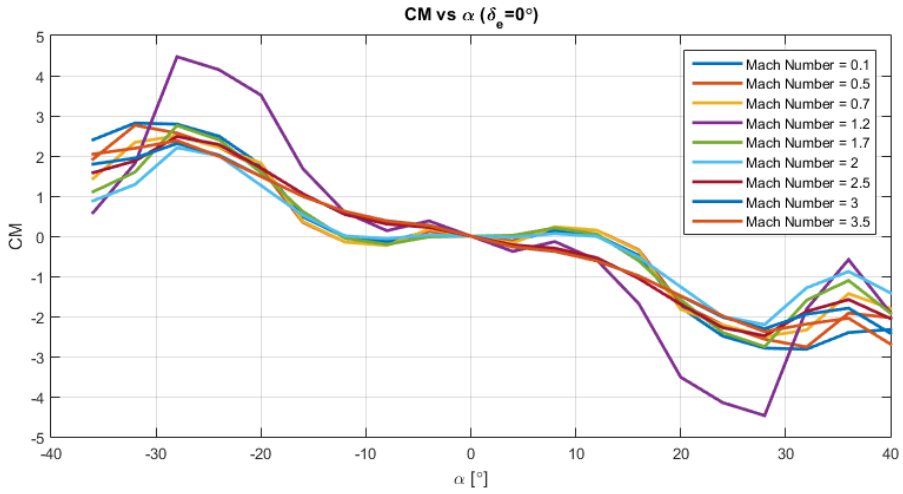

Figure 3.12: Alternative 2 Pitching Moment Coefficient @ $X_{cg} = 1m$

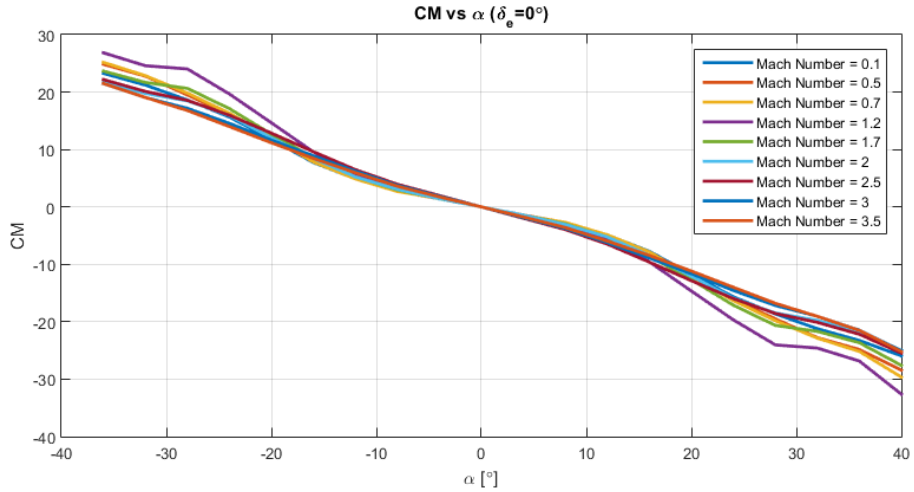

Figure 3.13: Alternative 2 Pitching Moment Coefficient @ $X_{cg} = 0.75m$

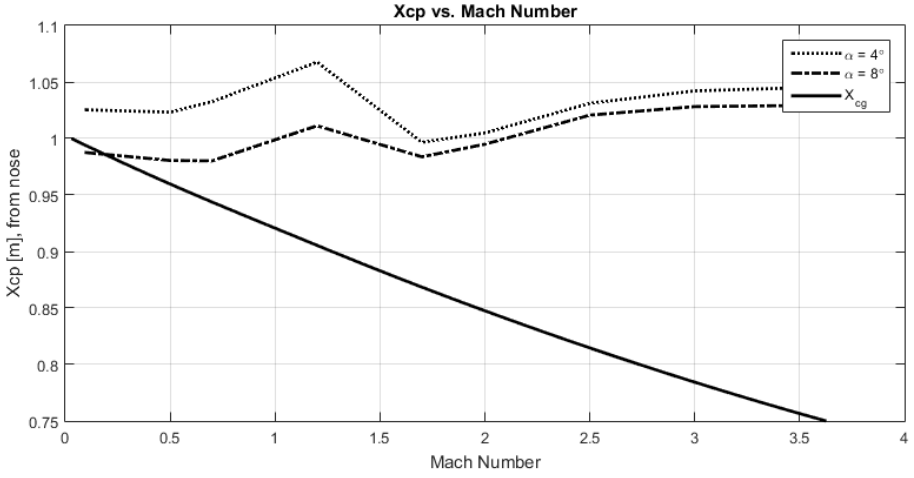

Figure 3.14: Alternative 2 X_{cp} and X_{cg} vs Mach Number

3.3 Lateral Thrusters

Lateral thrusters are devices that are placed on the missile body such that they apply a force on the body in the lateral directions. These forces usually generate a moment around the center of gravity and can be used to execute maneuvers.

There are several kinds of methods to generate lateral thrust. One is to use the main engine exhaust gas. During main engine burn, some of high pressure gases in the main engine is expelled from the side of the missile thus causing a reaction force on the missile. Since this method uses the main engine, high thrust values can be obtained, however much like thrust vector control (TVC) this system necessitates the main engine burning so that it can operate.

Lateral thrusters chosen for this work use bi propellant or mono propellants to generate force at desired times. More information about the system can be found in Appendix C. They are controlled in on-off fashion. Considering the fact that aerodynamic fins need sufficient dynamic pressure to work, in low dynamic pressure conditions (e.g., beginning of launch, stall conditions) thrusters become more effective at controlling the missile. Figure 3.15 shows an missile with lateral thrusters placed at the aft.

Thrusters are placed at the most rearward position they can be placed in order to increase the moment arm. They can be placed forward of the center of mass, however interference of thruster jet with the flow around the missile body causes challenging problems.

Figure 3.16 shows position of the thruster forces acting on the body. "X" means that the force is towards paper. Numbering convention is same as shown in Figure 2.3.

In order to create a pitching moment in positive direction (pitch-up) thruster 1 is fired, in negative direction thruster 2 is fired. Similarly thrusters 3 and 4 are fired in order to create yawing moment.

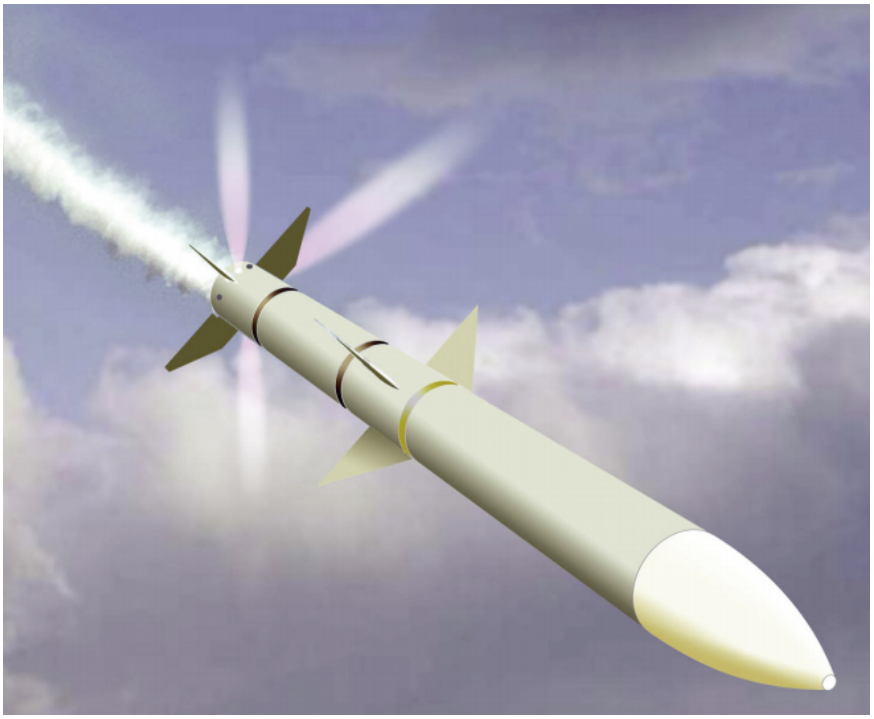

Figure 3.15: Missile with Lateral Thrusters [7]

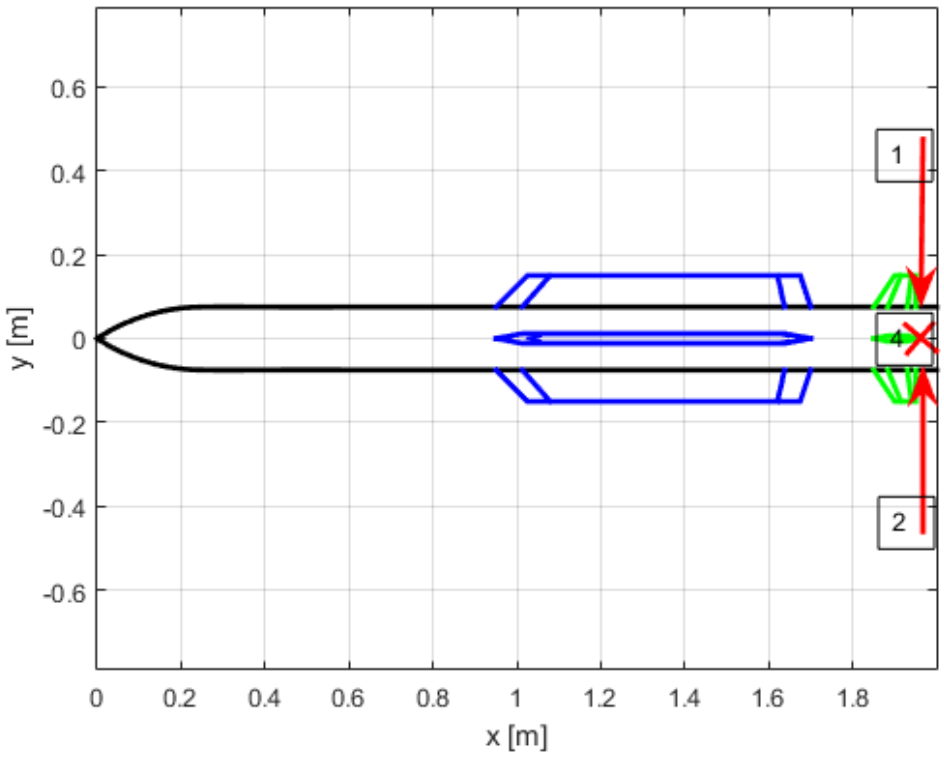

Figure 3.16: Lateral Thruster Locations

CHAPTER 4

CONTROLLER DESIGN AND GUIDANCE

Angle controller and acceleration controllers are considered. Acceleration autopilots are particularly useful for terminal guidance phase of the flight, since many terminal guidance law produce acceleration commands. Angle autopilots are suitable for controlling the missile attitude at launch and at stall conditions.

There are two actuators in the missile, one is aerodynamic fins and the other is the lateral thrusters. For pitch and yaw channels two actuators can be used separately, however roll channel can only be controlled with aerodynamic fins as the thrusters do not generate any moment about the X_B axis.

A two loop angle controller and LQR type acceleration controller are designed. LQR angle controller performed worse than two loop controller, hence two loop is chosen. LQR acceleration controller's performance is sufficient; therefore more robust controller types such as two loop or three loop is not considered for the acceleration autopilot. In addition MIMO controller design utilizing both actuators (aerodynamic fins and lateral thrusters) is examined; whereas its performance is unfavorable even in linear domain.

Controller design is done in the linear domain by linearizing the missile dynamics around an equilibrium point. Equilibrium points are defined at different Mach numbers, center of mass positions and angle of attacks, and controllers are designed at these points. In non linear simulations, controller gains are interpolated using look up tables using Mach number and center of mass.

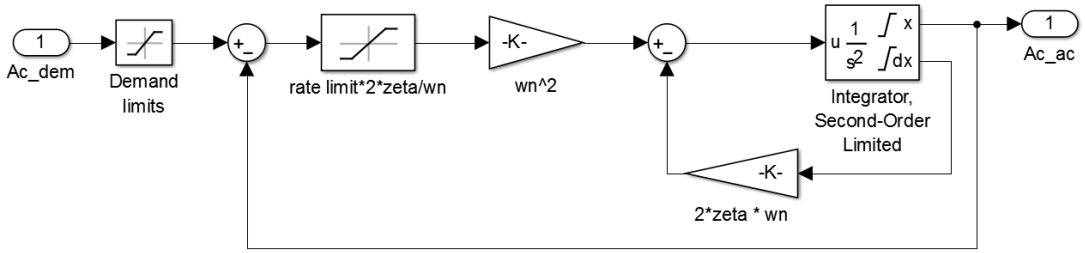

Figure 4.1: Second Order Nonlinear Actuator Model

4.1 Actuator Models

Aerodynamic control fins are generally modeled as a second order linear transfer functions with saturations on angular speed and angle (Figure 4.1). In controller design it is assumed as a second order linear delay transfer function with the natural frequency (ω_n) and damping ratio (ζ) given in Eq. (4.1)

$$\begin{aligned} G_{fin} &= \frac{\omega_n^2}{s^2 + 2\zeta\omega_n s + \omega_n^2} \\ \omega_n &= 50Hz \\ \zeta &= 0.7 \\ \delta_{max} &= 20^\circ \\ \dot{\delta}_{max} &= 300^\circ \end{aligned} \tag{4.1}$$

Thrusters are modeled as first order linear delay systems. Thruster command signal, which is 0 or 1 goes through the first order delay and then multiplied with the nominal thruster force value. In controller design it is assumed linear (Eq. (4.2)).

$$\begin{aligned} G_{thr} &= \frac{\tau}{s + \tau} \\ \tau &= 200 \end{aligned} \tag{4.2}$$

Step response and Bode diagrams of the actuators are given in Figures 4.2 and 4.3, respectively.

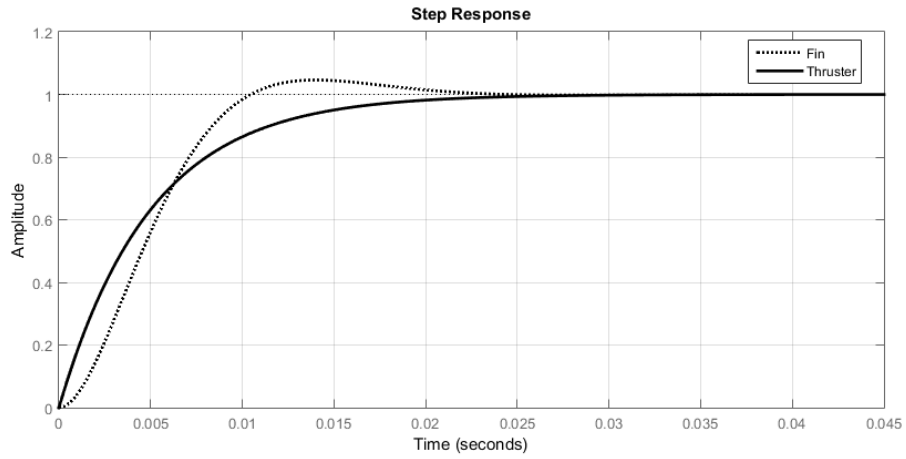

Figure 4.2: Step Reponse of Actuators

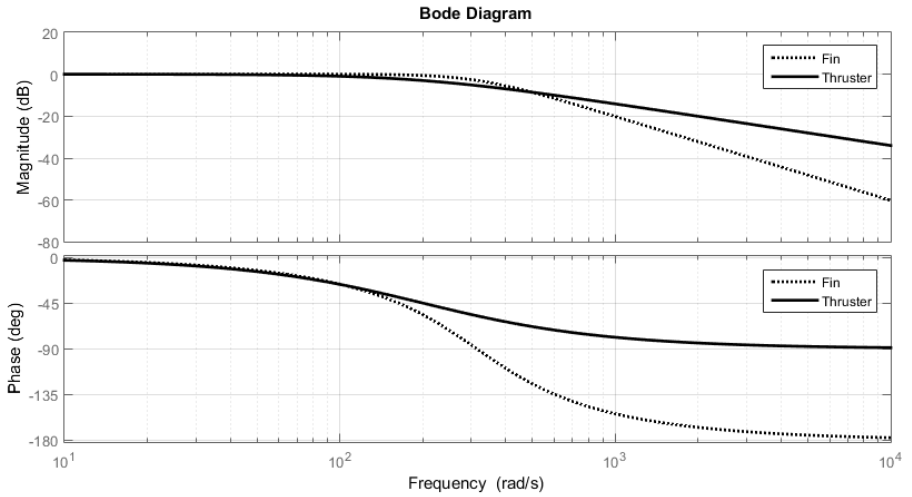

Figure 4.3: Bode of Actuators

4.2 Linearization

In general missile dynamics can be written as:

$$\dot{\bar{x}} = f(\bar{x}, \bar{u}, t) \tag{4.3}$$

where $\dot{\bar{x}}$ is the states defining the missile dynamics, $\bar{u}$ is the input, t is the time and f is the nonlinear differential equation function of the missile dynamics. In order to design a controller in linear domain, linear state equation should be written as:

$$\begin{aligned} \dot{\bar{x}} &= A\bar{x} + B\bar{u} \\ \bar{y} &= C\bar{x} \end{aligned} \tag{4.4}$$

where $\bar{x} \in R^n$, $\bar{u} \in R^m$, $A \in R^{n \times n}$ and $B \in R^{n \times m}$

Linear velocity and angular velocity equations and Euler angle equations are linearized around an equilibrium point using small perturbations. There are also some assumptions that decouple the three axes. Moreover, aerodynamic force and moment functions are nonlinear as well. Nonlinear equations of motion are derived in Chapter 2 and given in Eq. (4.5).

First, nonlinearities resulting from structure of the equations of motion are eliminated by decoupling pitch, yaw and roll channels. The missile in this study is an axisymmetrical one and it executes skid to turn maneuvers, i.e., roll of the missile is always at zero degrees. Hence the first assumption is $p = 0$ and $\phi = 0$. To decouple pitch and yaw channels following is used: when considering pitching motion, no motion in yaw plane is assumed and when considering yawing motion, no motion in pitch plane is assumed. Hence, $r = 0$ when $q \neq 0$ and vice versa. For roll channel both pitch and yaw motion is assumed to be zero, i.e., $p = r = 0$.

$$
\begin{aligned}
\dot{u} &= \frac{F_x}{m} + vr - wq \\
\dot{v} &= \frac{F_y}{m} - ur + wp \\
\dot{w} &= \frac{F_z}{m} + uq - vp
\end{aligned}
$$

$$
\begin{aligned}
\dot{p} &= \frac{\sum M_x + I_{xz}\dot{r} + I_{xz}pq + (I_{yy} - I_{zz})rq}{I_{xx}} \\
\dot{q} &= \frac{\sum M_y + (I_{zz} - I_{xx})pr + I_{xz}(r^2 - p^2)}{I_{yy}} \\
\dot{r} &= \frac{\sum M_z + I_{xz}\dot{p} + (I_{xx} - I_{yy})pq - I_{xz}qr}{I_{zz}}
\end{aligned}
\tag{4.5}
$$

$$
\begin{aligned}
\dot{\phi} &= p + qs\phi t\theta + rc\phi t\theta \\
\dot{\theta} &= qc\phi - rs\phi \\
\dot{\psi} &= q\frac{s\phi}{c\theta} + r\frac{c\phi}{c\theta}
\end{aligned}
$$

Eq. (4.6) is the roll dynamics, Eq. (4.7) is the pitch dynamics and Eq. (4.8) is the yaw dynamics after applying the assumptions.

$$
\begin{aligned}
\dot{p} &= \frac{\sum M_x}{I_{xx}} \\
\dot{\phi} &= p
\end{aligned}
\tag{4.6}
$$

$$
\begin{aligned}
\dot{u} &= \frac{F_x}{m} - wq \\
\dot{w} &= \frac{F_z}{m} + uq \\
\dot{q} &= \frac{M_y}{I_{yy}} \\
\dot{\theta} &= q
\end{aligned}
\tag{4.7}
$$

$$
\begin{aligned}
\dot{u} &= \frac{F_x}{m} + vr \\
\dot{v} &= \frac{F_y}{m} - ur \\
\dot{r} &= \frac{M_z}{I_{zz}} \\
\dot{\psi} &= r\frac{1}{cos(\theta)}
\end{aligned}
\tag{4.8}
$$

There are products of u with angular velocities in these equations. The velocity component along X_B (u) is actually not controllable. Aerodynamic fins or lateral thrusters cannot affect F_x and main engine is not throttable. Therefore, u is assumed to be constant and equal to the airspeed of the missile, i.e., $u_0 = V_\infty$. $\dot{u}$ equation is dropped and u is treated as a constant, u_0, in other equations. Then pitch dynamics become: (note that for the remaining of linearization process yaw dynamics is not written again since its structure is same as pitch dynamics)

$$
\begin{aligned}
\dot{w} &= \frac{F_z}{m} + u_0 q \\
\dot{q} &= \frac{M_y}{I_{yy}} \\
\dot{\theta} &= q
\end{aligned}
\tag{4.9}
$$

Now aerodynamic force and moment should be linearized. In this linearization process equilibrium point becomes important. For aircrafts, this equilibrium also called as trim point. In general trim state (point) is defined as point at which the derivative of the state is equal to zero:

$$
0 = f(\bar{x}_{eq}, \bar{u}_{eq}, t) \tag{4.10}
$$

where $\bar{x}_{eq}$ denotes the equilibrium state and $\bar{u}_{eq}$ denotes the equilibrium input. The missile is said to be trimmed when the pitching moment is equal to zero. This condition corresponds to specific values of $w = w_0$ and $q = q_0$. As defined in Chapter 2, angle of attack is defined as $arctan(\frac{w}{u})$; hence, w_0 corresponds to an angle of

attack value. Linearization of aerodynamic forces and moments are done by linear approximation at the equilibrium point and small perturbation theory.

Define perturbed states as:

$$\begin{aligned} q &= q_0 + \Delta q \\ w &= w_0 + \Delta w \end{aligned} \tag{4.11}$$

then aerodynamic force (F_z) can be written as (same is true for aerodynamic moment):

$$F_z(M, \alpha, q, \delta_e) = F_z(M_0, \alpha_0, q_0, \delta_{e_0}) + \Delta F_z(M_0, \alpha_0, \Delta\alpha, q_0, \Delta q, \delta_{e_0}, \Delta\delta_e) \tag{4.12}$$

Then state equations become:

$$\begin{aligned} \dot{w_0} + \dot{\Delta w} &= \frac{F_{z_0}}{m} + \frac{\Delta F_z}{m} + u_0(q_0 + \Delta q) \\ \dot{q_0} + \dot{\Delta q} &= \frac{M_{y_0}}{I_{yy}} + \frac{\Delta M_y}{I_{yy}} \end{aligned} \tag{4.13}$$

As discussed above at trim condition $M_y = 0$ and $\dot{w_0} = \frac{F_{z_0}}{m} + u_0 q_0 = 0$; hence equations reduce to:

$$\begin{aligned} \dot{\Delta w} &= \frac{\Delta F_z}{m} + u_0 \Delta q \\ \dot{\Delta q} &= \frac{\Delta M_y}{I_{yy}} \end{aligned} \tag{4.14}$$

After applying linear approximation to the coefficients:

$$\begin{aligned} F_z(M, \alpha, q, \delta_e) = F_z(M_0, \alpha_0, q_0, \delta_{e_0}) + QS(&\frac{dC_Z(M_0, \alpha_0, \delta_{e_0})}{d\alpha}\Delta\alpha \\ &+ \frac{dC_Z(M_0, \alpha_0, \delta_{e_0})}{d\delta_e}\Delta\delta_e) + QSC_{Z_q}(M_0)\Delta q\frac{d}{2V_\infty} \end{aligned} \tag{4.15}$$

(Note that $C_{Z_{\dot{\alpha}}}$ term is ignored, since it is very small relative to the other terms.)

where $\Delta\alpha$, $\Delta\delta_e$ and Δq are the small deviations from the equilibrium point. One last assumption is needed in order to write angle of attack in terms of state variables. Since $\Delta\alpha$ is small $\arctan(\frac{\Delta w}{u_0})$ is approximated as $\frac{\Delta w}{u_0}$. Then overall linear equation for pitch plane becomes:

$$\begin{aligned}\dot{\Delta w} &= QS\frac{dC_Z}{d\alpha}\frac{\Delta w}{mu_0} + (QSC_{Z_q}\frac{d}{m2u_0} + u_0)\Delta q + QS\frac{dC_Z}{d\delta_e}\frac{\Delta\delta_e}{m} \\ \dot{\Delta q} &= QSd\frac{dC_M}{d\alpha}\frac{\Delta w}{I_{yy}u_0} + QSdC_{M_q}\Delta q\frac{d}{I_{yy}2u_0} + QSd\frac{dC_M}{d\delta_e}\frac{\Delta\delta_e}{I_{yy}}\end{aligned} \tag{4.16}$$

Note that all partial differentials are evaluated at the trim point $w = w_0$, $q = q_0$, $\delta_e = \delta_{e_0}$. In state space form equation becomes:

$$\begin{bmatrix}\dot{\Delta w} \\ \dot{\Delta q}\end{bmatrix} = \begin{bmatrix}QS\frac{dC_Z}{d\alpha}\frac{1}{mu_0} & QSC_{Z_q}\frac{d}{m2u_0} + u_0 \\ QSd\frac{dC_M}{d\alpha}\frac{1}{I_{yy}u_0} & QSdC_{M_q}\frac{d}{I_{yy}2u_0}\end{bmatrix}\begin{bmatrix}\Delta w \\ \Delta q\end{bmatrix} + \begin{bmatrix}QS\frac{dC_Z}{d\delta_e} \\ QSd\frac{dC_M}{d\delta_e}\frac{1}{I_{yy}}\end{bmatrix}\Delta\delta_e \tag{4.17}$$

By similar linearization process, roll linear model can be obtained as:

$$\dot{p} = QSdC_{L_p}\frac{d}{I_{xx}u_0}p + QSd\frac{dC_L}{d\delta_a}\delta_a \tag{4.18}$$

Up until now only aerodynamic actuators are considered. Lateral thruster should also be included. Lateral thruster apply constant force whenever they are switched on. For linear analysis they are assumed to be completely linear, that is, any thrust value can be generated from a thruster. Since they are at the aft of the missile they also generate a moment around the center of mass. Then overall linear pitch dynamics become:

$$\begin{aligned}\begin{bmatrix}\dot{\Delta w} \\ \dot{\Delta q}\end{bmatrix} &= \begin{bmatrix}QS\frac{dC_Z}{d\alpha}\frac{1}{mu_0} & QSC_{Z_q}\frac{d}{m2u_0} + u_0 \\ QSd\frac{dC_M}{d\alpha}\frac{1}{I_{yy}u_0} & QSdC_{M_q}\frac{d}{I_{yy}2u_0}\end{bmatrix}\begin{bmatrix}\Delta w \\ \Delta q\end{bmatrix} \\ &+ \begin{bmatrix}QS\frac{dC_Z}{d\delta_e} & \frac{1}{m} \\ QSd\frac{dC_M}{d\delta_e}\frac{1}{I_{yy}} & \frac{(l_m - X_{cg})}{I_{yy}}\end{bmatrix}\begin{bmatrix}\Delta\delta_e \\ F_{thr}\end{bmatrix}\end{aligned} \tag{4.19}$$

Controller design with lateral thrusters include an additional modulator element to convert controllers force demand to proper on-off signals. This topic is discussed in detail in the following sections.

Note that here partial derivation notation is used; however, aerodynamic coefficients are obtained as tabulated data from Missile DATCOM; hence, in order to obtain these partial derivatives from table data, numerical method is used.

In literature, many controller designs assume that α is zero. Therefore they use the one equilibrium point of $\alpha = 0$, $q = 0$, $\delta_e = 0$. Here trim points at which angle of attack is non-zero is also considered. However nonlinear simulations showed that controllers designed at $\alpha = 0$ condition also performed sufficiently well in high angles of attack. Therefore, controllers are designed at $\alpha = 0$ trim point in order to keep design space small.

Assumptions made in this chapter are not completely correct; pitch, yaw and roll channels are coupled through equations of motion and aerodynamics, and the missile angle of attack value is not around zero all the time; hence, there is considerable modeling error. However, the assumptions simplify the linear analysis and controller design. In addition, results of nonlinear simulations show that controller robustness is able to tolerate these modeling mistakes.

4.3 Linear Analysis

In this section linear analysis of the dynamics is presented at different trim points. In addition, linear models for aerodynamic fin and thruster are added to the dynamics. Linear actuator dynamics can be written as:

$$\begin{aligned} \ddot{\delta} &= -\omega_n^2 \delta - 2\zeta\omega_n \dot{\delta} + \omega_n^2 \delta_{com} \\ \dot{F_{thr}} &= -\tau F_{thr} + \tau F_{thr_{com}} \end{aligned} \tag{4.20}$$

where "com" subscript means commanded value. Adding actuator dynamics to the Eq. (4.19):

$$\dot{\bar{x}} = \begin{bmatrix} QS\frac{dC_Z}{d\alpha}\frac{1}{mu_0} & QSC_{Z_q}\frac{d}{m2u_0} + u_0 & QS\frac{dC_Z}{d\delta_e} & 0 & \frac{1}{m} \\ QSd\frac{dC_M}{d\alpha}\frac{1}{I_{yy}u_0} & QSdC_{M_q}\frac{d}{I_{yy}2u_0} & QSd\frac{dC_M}{d\delta_e}\frac{1}{I_{yy}} & 0 & \frac{(l_m - X_{cg})}{I_{yy}} \\ 0 & 0 & 0 & 1 & 0 \\ 0 & 0 & -\omega_n^2 & -2\zeta\omega_n & 0 \\ 0 & 0 & 0 & 0 & -\tau \end{bmatrix} \begin{bmatrix} \Delta w \\ \Delta q \\ \Delta\delta_e \\ \Delta\dot{\delta}_e \\ F_{thr} \end{bmatrix} + \begin{bmatrix} 0 & 0 \\ 0 & 0 \\ 0 & 0 \\ \omega_n^2 & 0 \\ 0 & \tau \end{bmatrix} \begin{bmatrix} \Delta\delta_e \\ F_{thr} \end{bmatrix} \tag{4.21}$$

In addition define the output as:

$$\begin{bmatrix} \Delta w \\ \Delta q \\ \Delta\delta_e \\ \Delta\dot{\delta}_e \\ F_{thr} \\ a_z \\ \alpha \end{bmatrix} = \begin{bmatrix} 1 & 0 & 0 & 0 & 0 \\ 0 & 1 & 0 & 0 & 0 \\ 0 & 0 & 1 & 0 & 0 \\ 0 & 0 & 0 & 1 & 0 \\ 0 & 0 & 0 & 0 & 1 \\ QS\frac{dC_Z}{d\alpha}\frac{1}{mu_0} & QSC_{Z_q}\frac{d}{m2u_0} & QS\frac{dC_Z}{d\delta_e} & 0 & \frac{1}{m} \\ \frac{1}{u_0} & 0 & 0 & 0 & 0 \end{bmatrix} \begin{bmatrix} \Delta w \\ \Delta q \\ \Delta\delta_e \\ \Delta\dot{\delta}_e \\ F_{thr} \\ a_z \\ \alpha \end{bmatrix} \tag{4.22}$$

where a_z is the acceleration in the Z_B direction, calculated with F_z/m.

For a numerical example the following design point is chosen:

$$\begin{aligned} altitude &= 1000m \\ Mach &= 0.5 \\ \alpha &= 0^\circ \\ \beta &= 0^\circ \\ X_{cg} &= 0.96m \end{aligned} \tag{4.23}$$

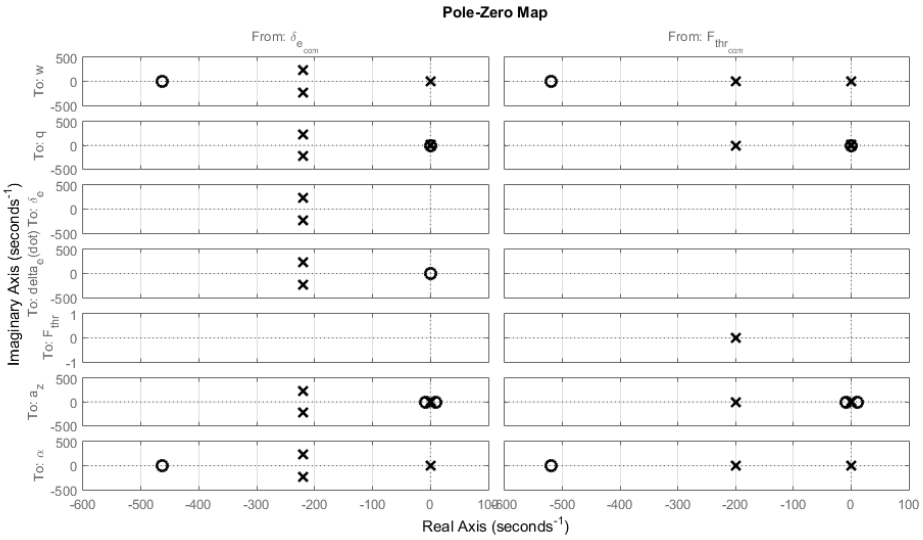

Figure 4.4: Pole Zero Map

A, B and C matrices then become:

$$A = \begin{bmatrix} -0.20 & 167.88 & -9.31 & 0 & 0.01 \\ -0.04 & -0.08 & -25.72 & 0 & 0.03 \\ 0 & 0 & 0 & 1 & 0 \\ 0 & 0 & -98696 & -439.82 & 0 \\ 0 & 0 & 0 & 0 & -200 \end{bmatrix}$$

$$B = \begin{bmatrix} 0 & 0 \\ 0 & 0 \\ 0 & 0 \\ 98696 & 0 \\ 0 & 200 \end{bmatrix} \tag{4.24}$$

$$C = \begin{bmatrix} 1 & 0 & 0 & 0 & 0 \\ 0 & 1 & 0 & 0 & 0 \\ 0 & 0 & 1 & 0 & 0 \\ 0 & 0 & 0 & 1 & 0 \\ -0.20 & -0.33 & -9.31 & 0 & 0.01 \\ -0.01 & 0 & 0 & 0 & 0 \end{bmatrix} \tag{4.25}$$

Figure 4.4 shows the pole zero map of transfer functions between each input and

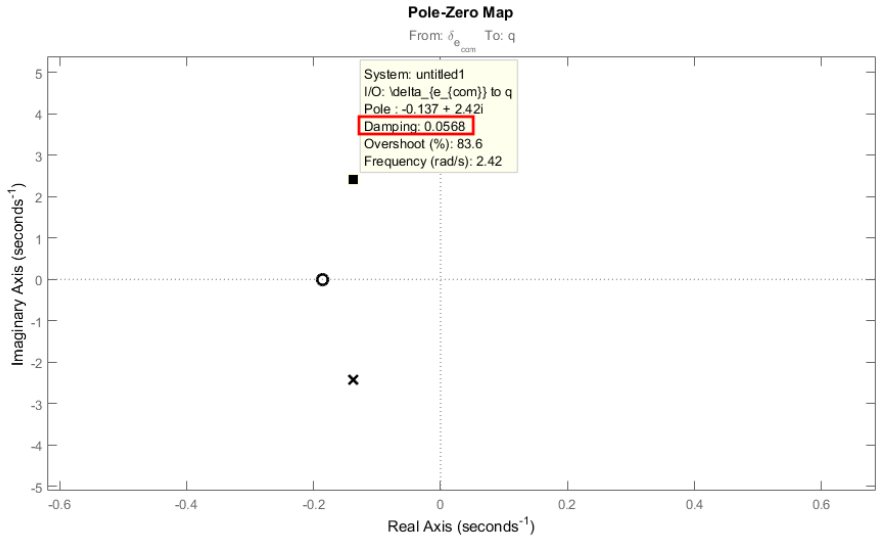

Figure 4.5: Pole Zero Map - $\frac{q}{\delta_e}$

output. One interesting point to note here is the low damping system poles of q dynamics, which is shown more clearly in Figure 4.5. This is a common occurrence in aircrafts; hence, damping of q dynamics is increased by introducing inner loops to the conventional feedback designs. Some designs contains up to 4 loops in controller design. In some cases α is also added as a feedback loop [8]. Although this approach may result in better controllers, in design phase checking the stability parameters such as gain and phase margin becomes more complicated when there are many loops. In [23], there is an open loop definition for a multi loop control systems.

Figure 4.6 shows the response of the system to the initial state $\bar{x}_0 = [1, 1, 0, 0, 0]^T$. Again low damping characteristics of the q dynamics is apparent.

At the same design point, trim angle of attack value is changed from 0° to 20° to observe the differences. The main difference is in the first two rows of the first column which are the terms depending on derivative with respect to α. As seen from the eigenvalues of the matrix A (Eq. (4.26)) system is more stable at $\alpha = 20^\circ$; hence, the controller designed for $\alpha = 0^\circ$ case will have no problem.

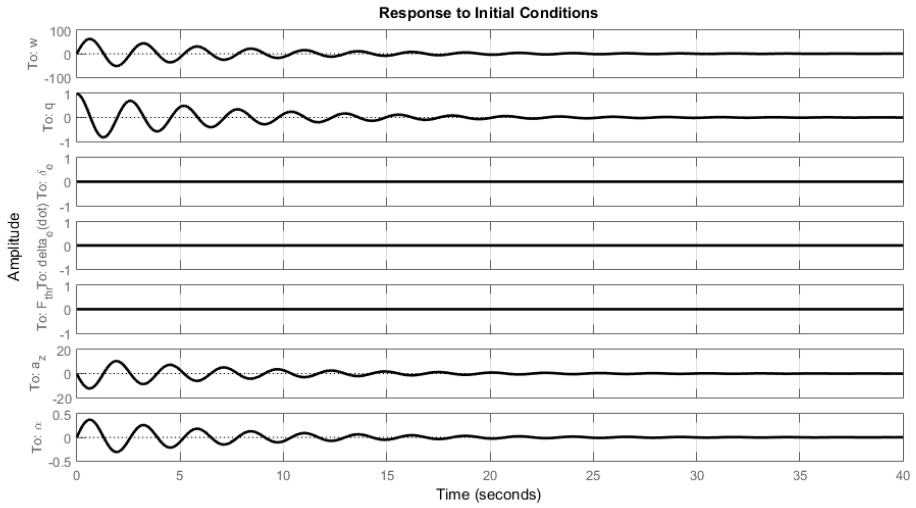

Figure 4.6: Initial Response

$$
\begin{aligned}
A_{\alpha=0} &= \begin{bmatrix} -0.20 & 167.88 & -9.31 & 0 & 0.01 \\ -0.04 & -0.08 & -25.72 & 0 & 0.03 \\ 0 & 0 & 0 & 1 & 0 \\ 0 & 0 & -98696 & -439.82 & 0 \\ 0 & 0 & 0 & 0 & -200 \end{bmatrix} \\
\lambda_{\alpha=0} &= \begin{bmatrix} -0.14 + 2.42i \\ -0.14 - 2.42i \\ -219.91 + 224.35i \\ -219.91 - 224.35i \\ -200 + 0i \end{bmatrix} \\
A_{\alpha=20} &= \begin{bmatrix} -0.52 & 157.64 & -10.11 & 0 & 0.01 \\ -0.17 & -0.07 & -27.93 & 0 & 0.03 \\ 0 & 0 & 0 & 1 & 0 \\ 0 & 0 & -98696 & -439.82 & 0 \\ 0 & 0 & 0 & 0 & -200 \end{bmatrix} \\
\lambda_{\alpha=20} &= \begin{bmatrix} -0.29 + 5.23i \\ -0.29 - 5.23i \\ -219.91 + 224.35i \\ -219.91 - 224.35i \\ -200 + 0i \end{bmatrix}
\end{aligned}
\tag{4.26}
$$

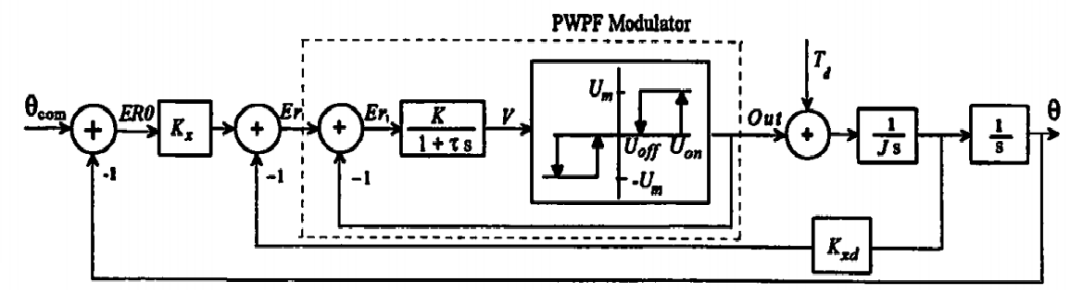

Figure 4.7: Pulse Width Pulse Frequency Modulator (PWPF) [10]

4.4 Thrust Modulator

Lateral thrusters have constant force value and can only be operated as on-off, as mentioned earlier. In linear analysis and controller design they are treated as linear devices. Therefore, a controller designed with the thrusters will demand any force value according to the error input. There must be some algorithm to convert these force demands into proper on-off (1-0) signal. These algorithms are called thrust modulators and placed between controller output and actuator input.

Figure 4.7 shows a modulator called Pulse Width Pulse Frequency (PWPF) modulator, that changes the duration and frequency of the activation signal of the thruster. It employs a Schmitt trigger with a hysteresis loop, a first order filter and a feedback loop. The characteristics of the modulator is adjusted by the Schmitt trigger and filter parameters. Because of the non-linear thruster actuator, error of a controller will never be zero, but it will oscillate around zero. The modulator parameters are also responsible for the characteristics of the oscillation. Figure 4.8 shows how PWPF modulator generates on-off signal from the input controller signal.

On and off times of the modulator are given in [10] as:

$$\begin{aligned} t_{on} &= \tau \frac{U_{on} - U_{off}}{KU_m - KIn + U_{on}} \\ t_{off} &= \tau \frac{U_{on} - U_{off}}{KIn - U_{off}} \end{aligned} \tag{4.27}$$

In this study PWPF parameters are chosen as shown in Eq. (4.28):

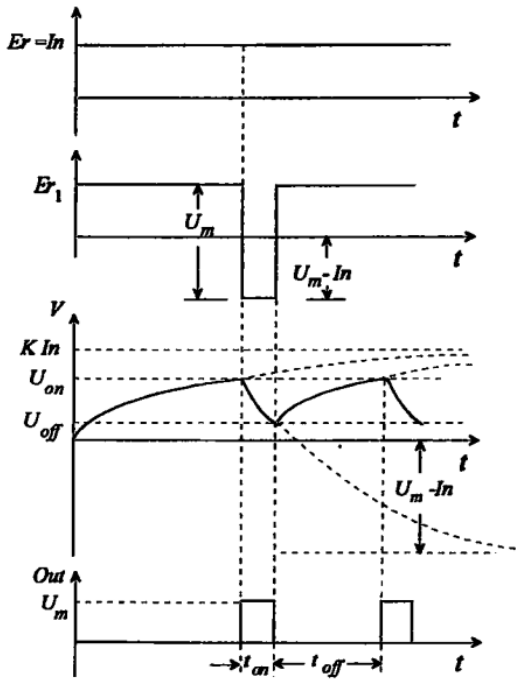

Figure 4.8: Time Behavior of PWPF Modulator [10]

$$\begin{aligned} \tau &= 0.1 \\ U_{on} &= 0.8F_{thr_{nominal}} \\ U_{off} &= 0.2F_{thr_{nominal}} \end{aligned} \tag{4.28}$$

4.5 Angle Controller

Controlling Euler angles of the missile is particularly useful in low speed conditions such as beginning of launch. Since there is not enough dynamic pressure on the missile, acceleration controllers are not convenient. A two loop angle controller is designed in all three axes to control roll (ϕ), pitch (θ) and yaw (ψ). The inner loop is introduced in order to increase the damping of the q (similarly for p and r) dynamics and to have a better performance on the outer angle loop. General structure of the two loop angle controller is shown in Figure 4.9. Plant transfer function is the transfer function between the actuator (fins or thrusters) and the angular velocity including actuator dynamics. Saturation on the error is placed in order to limit speed at which the aerodynamic fins move. As discussed in Section 4.1 fin actuators have nonlineari-

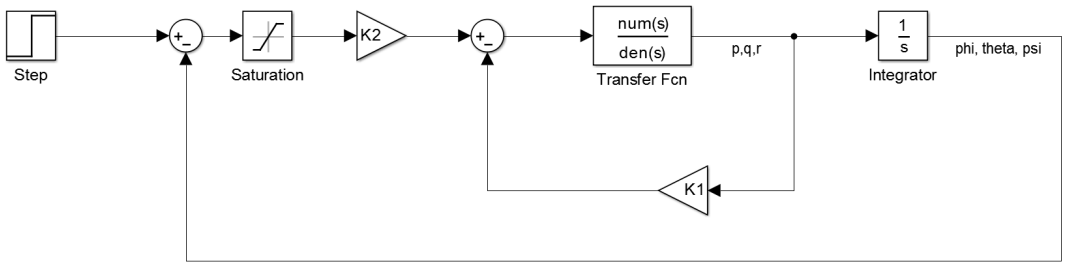

Figure 4.9: Two Loop Angle Controller Structure

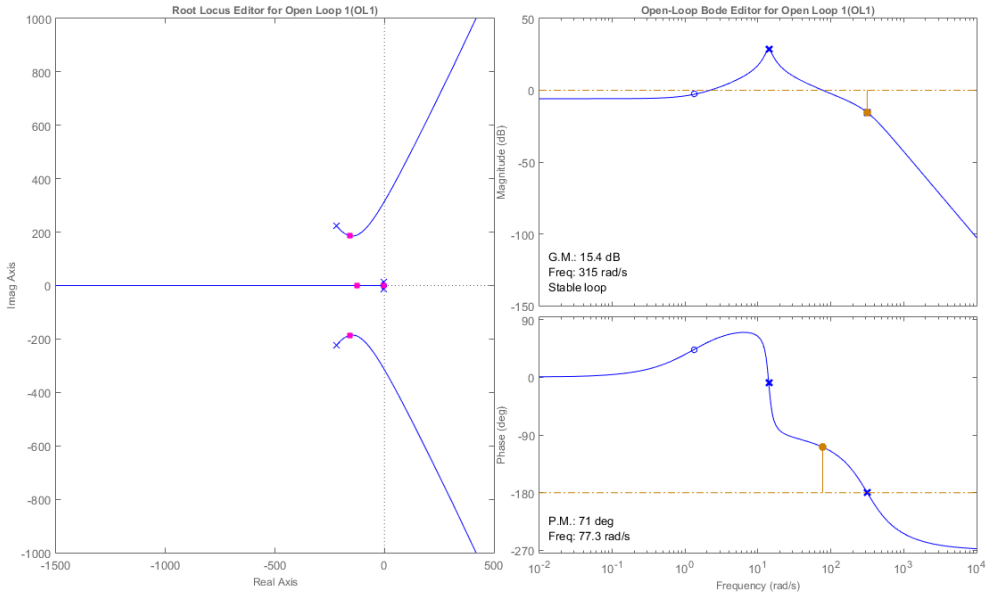

Figure 4.10: Inner Loop Properties

ties in the form of maximum deflection (δ_{max}) and maximum deflection speed ($\dot{\delta}_{max}$). Exceeding these limits can introduce instability to the system; therefore, reference input demand is limited accordingly.

"K1" gain is determined by considering only the inner loop. Values for transfer functions are obtained from the A matrix given before.

K1 is chosen to have a 15 dB gain margin in the inner loop. This constraint also damps the inner loop sufficiently. Figure 4.10 shows inner loop properties after compensation.

After closing the inner loop, K2 is chosen in the same manner, 20 dB gain margin is

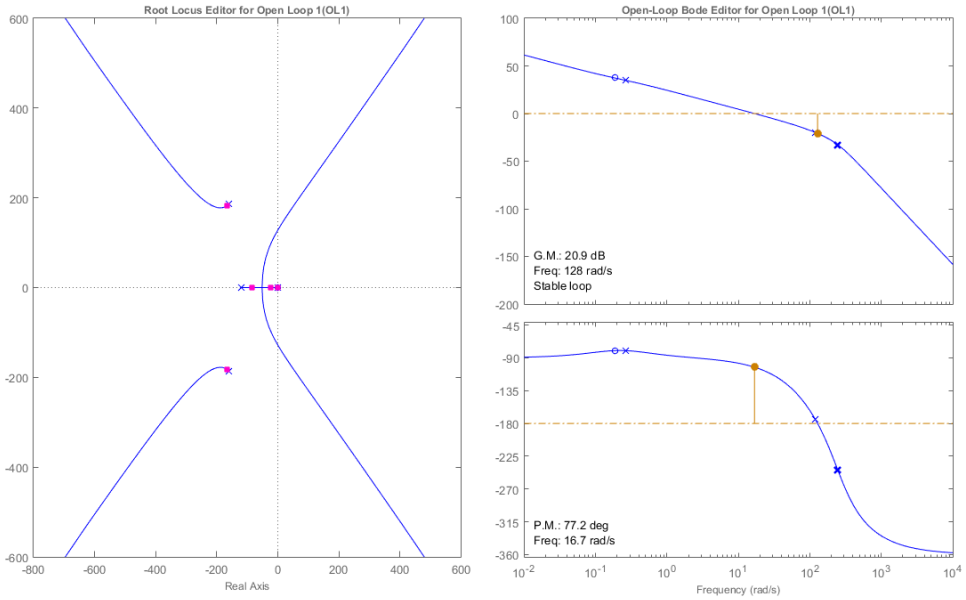

Figure 4.11: Outer Loop Properties

set for outer loop. Figure 4.11 shows the outer loop properties after compensation. Figure 4.12 shows the step response of the overall closed loop system.

Mach number and center of gravity position are the main factors in missile dynamics, therefore controllers are designed at different Mach numbers and center of gravity positions. Eq. (4.29) indicates the design space of controllers.

$$\begin{aligned} M &= \begin{bmatrix} 0.2 & 0.5 & 0.8 & 1.1 & 1.5 & 2.5 & 3.2 \end{bmatrix} \\ X_{cg} &= \begin{bmatrix} 0.75 & 0.8125 & 0.875 & 0.9375 & 1 \end{bmatrix} \end{aligned} \tag{4.29}$$

$7Mnumbers \times 5X_{cg}positions = 35$ controller designs are done. Figure 4.13 shows the ramp response of the output and Figure 4.14 shows the state response of the 35 designs. Note that in Figure 4.14 δ and $\dot{\delta}$ are limited to the nonlinear actuator values by limiting the ramp slope. This slope limit is then used to keep the actuator in the linear region.

The example discussed here is the angle controller for the pitch axis. Same design methodology is applied in the other (yaw, roll) axes. However there is one important thing to note here. Yaw dynamics is slightly different than pitch dynamics. In Section

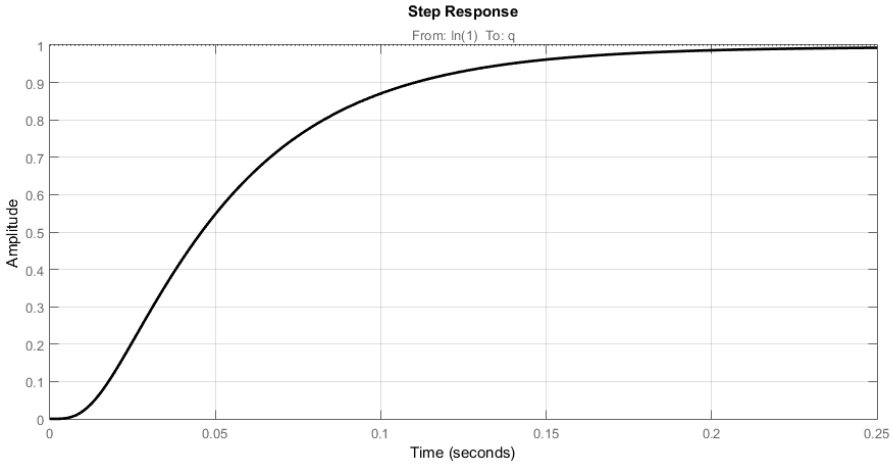

Figure 4.12: Step Response of Overall System

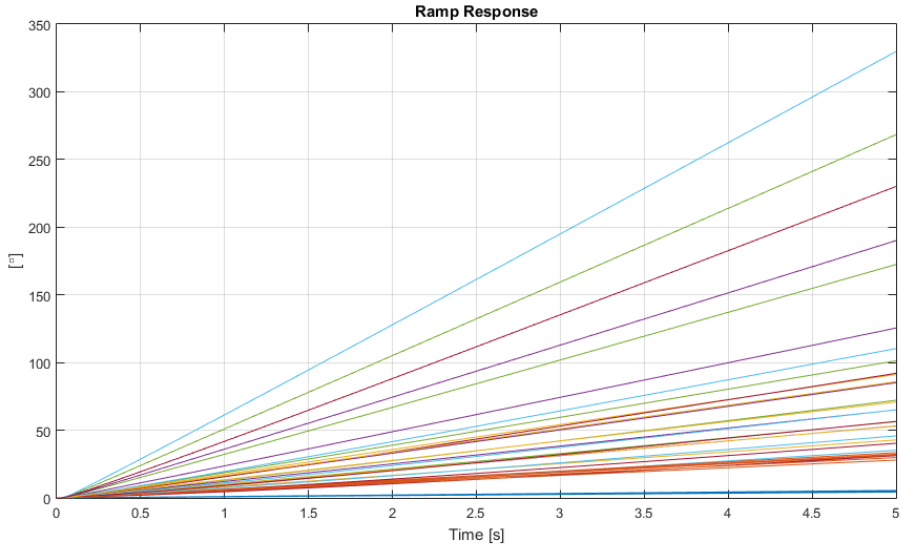

Figure 4.13: Ramp Response - Output

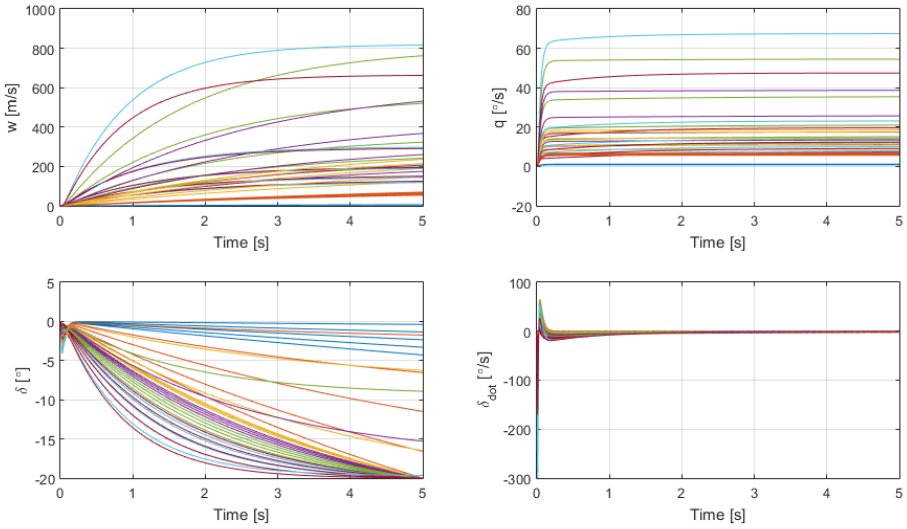

Figure 4.14: Ramp Response - States

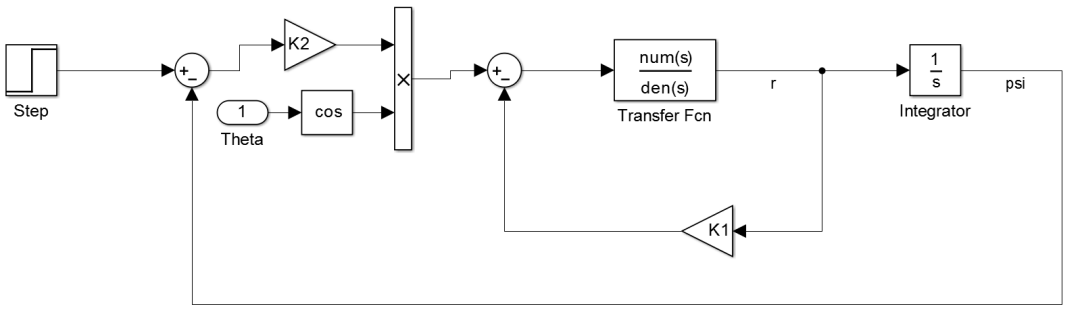

Figure 4.15: Two Loop Structure for Yaw Plane

4.2, in Eq. (4.7) $\dot{\psi}$ is given as:

$$\dot{\psi} = r\frac{1}{cos(\theta)} \tag{4.30}$$

Therefore, the controller structure given in Figure 4.9 is not actually valid. Because integral of r is not ψ. However solution is simple; after designing the controller according to the structure given in Figure 4.9, K2 gain is multiplied with $cos(\theta)$ to neutralize the $\frac{1}{cos(\theta)}$ term. As a result in yaw plane controller structure is as shown in Figure 4.15.

In the example above, controller is designed with aerodynamic fins. Following ex-

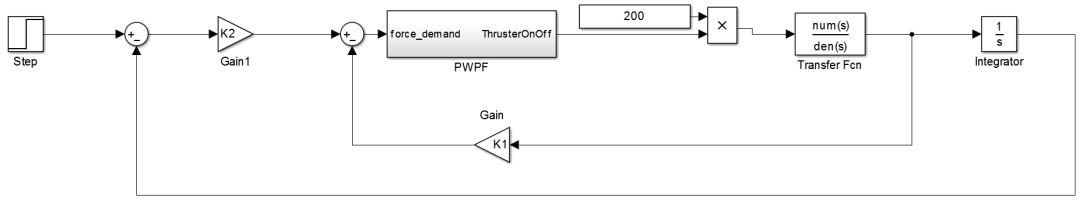

Figure 4.16: Two Loop Structure for Thrusters

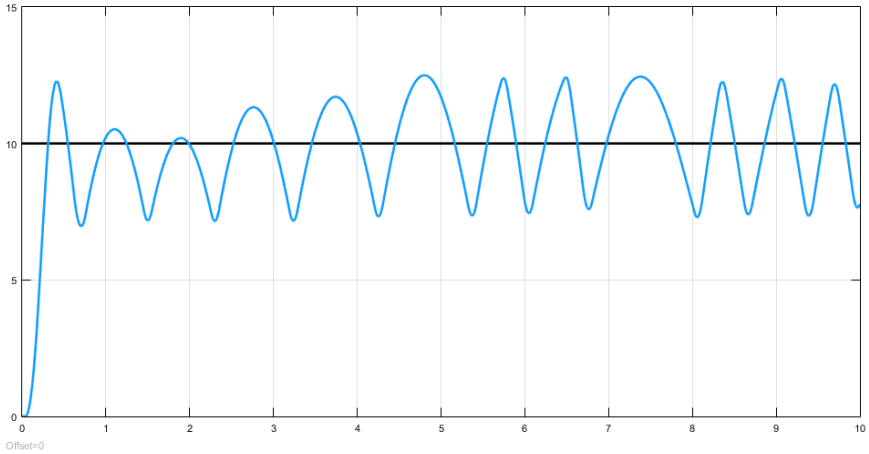

Figure 4.17: Step Response of Controller with Thruster

ample shows the same two loop controller structure with thruster. Design procedure is the same: first K1 value is chosen with 15 dB gain margin constraint and then K2 is set to make outer loop gain margin 20 dB. Again at different Mach and center of gravity values controller is designed. Figure 4.16 shows the addition of the PWPF modulator before the plant.

Note that thruster modulator outputs -1,0 or 1 here, where -1 means to turn on the thruster at the other side. Also note that thruster on-off signal is multiplied with nominal force value of 200 N. Figure 4.17 shows the controller performance under 10° step input and Figure 4.18 shows the thruster firing signal.

Similar to aerodynamic fin actuator case, at 7 Mach numbers and 5 center of gravity positions controllers are designed for thruster actuator case. Figure 4.19 shows the ramp response and Figure 4.20 shows the state response of these controllers.

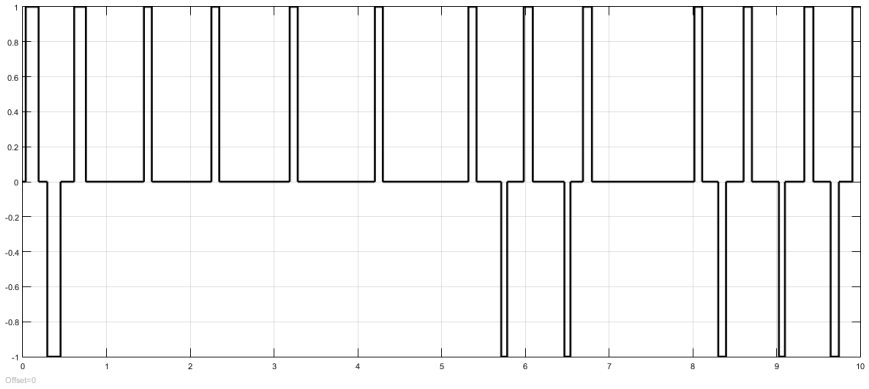

Figure 4.18: Thruster Firings Under Step Input

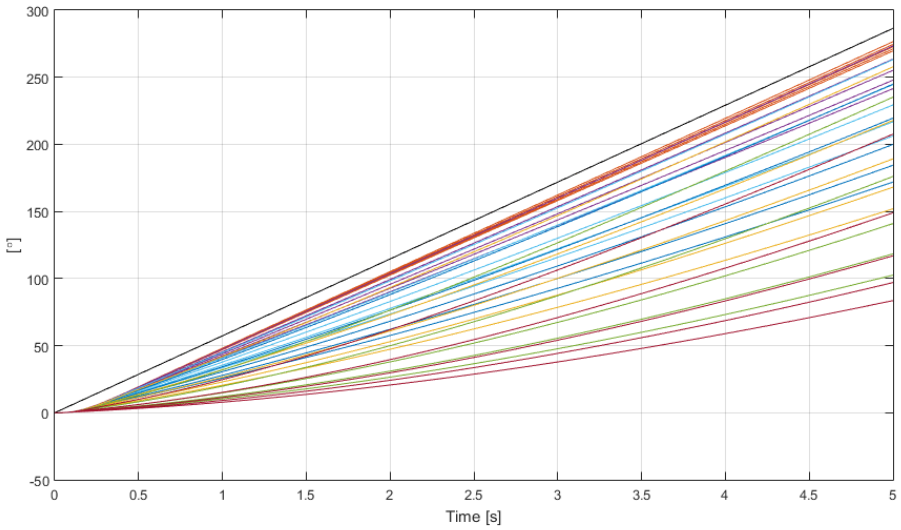

Figure 4.19: Ramp Response - Output

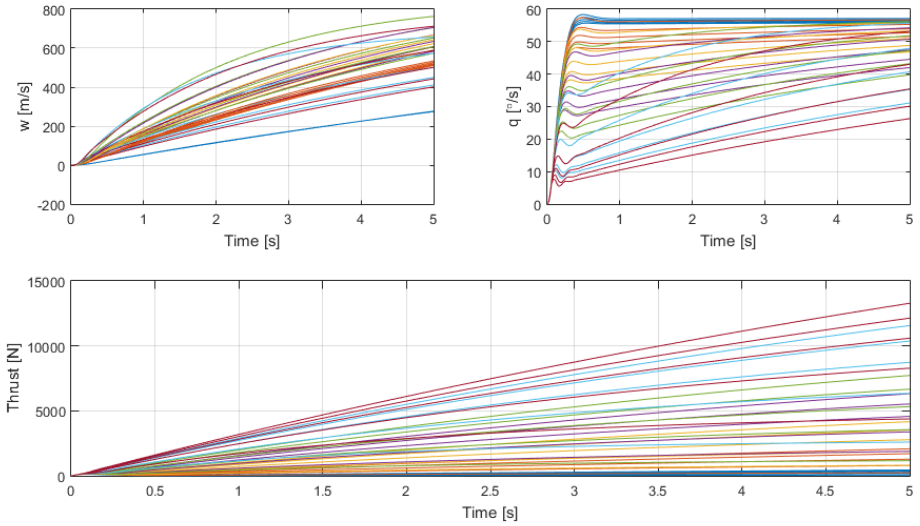

Figure 4.20: Ramp Response - States

Note that, input ramp slope is 1 for all designs in thruster case, because thruster is already a nonlinear actuator so there is no way of staying in linear region as is the case with aerodynamic fins.

4.6 Acceleration Controller

Many terminal guidance algorithms output lateral acceleration value. Thus, acceleration controllers are used at the terminal leg of the flight to realize guidance commands. Both two loop and linear quadratic regulator approach are examined.

4.6.1 Two Loop

Similar to angle controller case, inner loop is to increase damping and the outer loop is to track acceleration commands. Figure 4.21 shows the two loop acceleration structure. For design example following conditions are chosen:

$$
\begin{aligned}
altitude &= 1000m \\
Mach &= 2.5 \\
\alpha &= 0^\circ \\
\beta &= 0^\circ \\
X_{cg} &= 0.75m
\end{aligned}
\tag{4.31}
$$

Considering the flight phase the acceleration controller works, 2.5 Mach and center of gravity position after burnout is chosen. At this design point system matrices become as shown in Eq. (4.32).

Design methodology is similar to two loop angle controller. One difference is the integrator in the outer loop. In angle controller case the plant already has an integrator; hence outer loop steady state properties was satisfactory. However in acceleration plant there is no integrator, therefore outer loop controller is designed with integrator.

$$
\begin{aligned}
A &= \begin{bmatrix} -2.23 & 838.31 & -183.18 & 0 & 0.02 \\ -1.87 & -4.09 & -636.93 & 0 & 0.07 \\ 0 & 0 & 0 & 1 & 0 \\ 0 & 0 & -98696 & -439.82 & 0 \\ 0 & 0 & 0 & 0 & -200 \end{bmatrix} \\
B &= \begin{bmatrix} 0 & 0 \\ 0 & 0 \\ 0 & 0 \\ 98696 & 0 \\ 0 & 200 \end{bmatrix} \\
C &= \begin{bmatrix} -2.23 & -2.77 & -183.18 & 0 & 0.02 \end{bmatrix}
\end{aligned}
\tag{4.32}
$$

K1 is determined with a constraint of 15 dB gain margin for inner loop. Figure 4.22 shows the inner loop properties. K2 is set after closing the inner loop with K1. As seen from the root locus in Figure 4.23, acceleration plant has a right half plane zero, hence undershoot is observed in the step response. While determining K2, undershoot

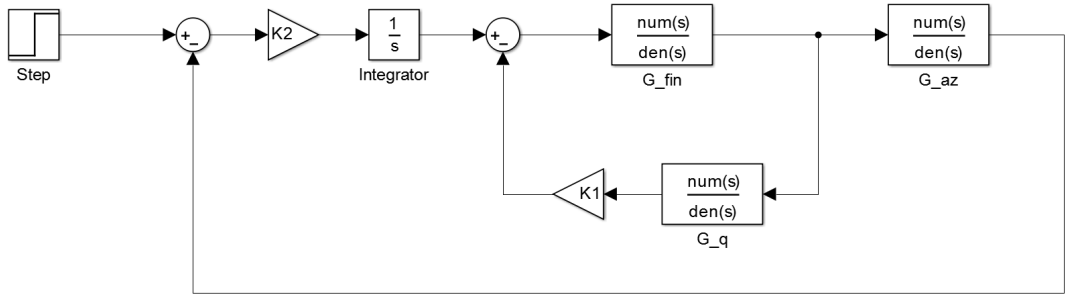

Figure 4.21: Two Loop Acceleration Controller Structure

percentage is also considered. Figure 4.24 shows the step response of the overall closed loop system.

4.6.2 LQR

LQR is also considered for acceleration tracking. Its performance is very close to the two loop structure and in the simulations LQR is used as acceleration controller.

LQR is a special case of state feedback controller in which the gain matrix minimizes a quadratic cost function including weighted sums of state and input energy (Eq. (4.33)).

$$J = \int_0^\infty (\bar{x}^T Q \bar{x} + \bar{u}^T R \bar{u}) dt \tag{4.33}$$

The feedback control law that minimizes the value of the cost is:

$$\bar{u} = K\bar{x} \tag{4.34}$$

where K is given by:

$$K = R^{-1} B^T P \tag{4.35}$$

and P is found by solving the continuous time algebraic Riccati equation:

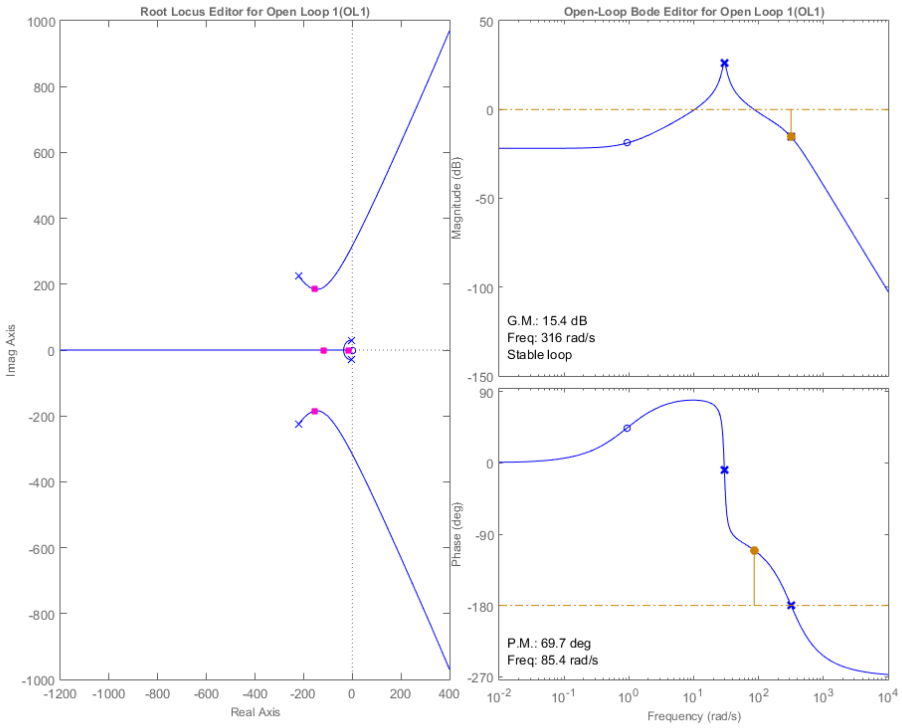

Figure 4.22: Inner Loop Properties

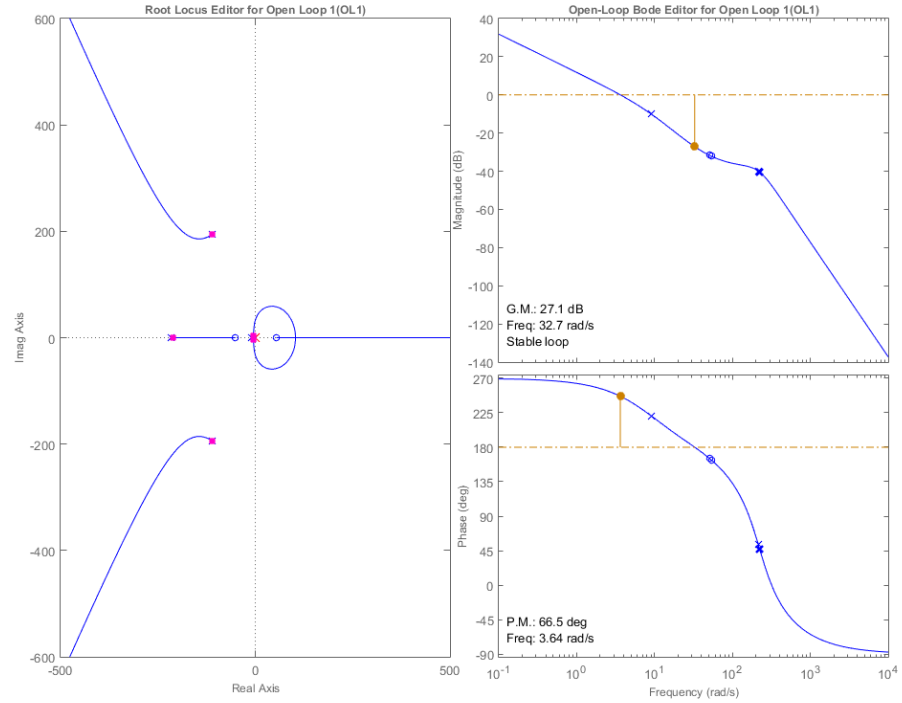

Figure 4.23: Outer Loop Properties

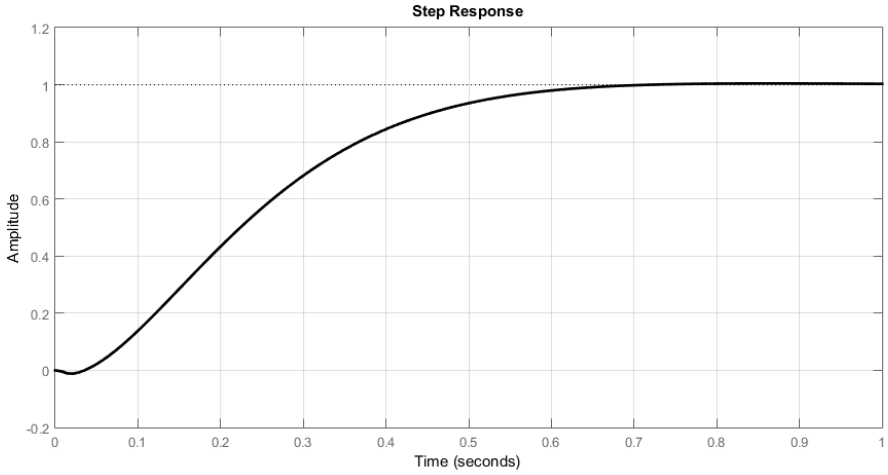

Figure 4.24: Step Response of Overall System

$$A^T P + PA - PBR^{-1}B^T P + Q = 0 \tag{4.36}$$

LQR is a state regulator, i.e., it tries to keep the state at the origin. In order to perform tracking some rearrangements are necessary which are given in [15]. For plants that have no integrator states are redefined to include the tracking error as a new state.

$$\begin{aligned} \dot{\bar{x}} &= A\bar{x} + B\bar{u} \\ y &= C\bar{x} \\ \bar{u} &= -K\bar{x} + k_I\xi \\ \dot{\xi} &= r - y = r - C\bar{x} \end{aligned} \tag{4.37}$$

where r is the reference to be tracked and $\dot{\xi}$ is the error. Define the new state as shown in Eq. (4.38)

$$\begin{aligned} \bar{x}(t) - x(\infty) &= \bar{x}_e(t) \\ \xi(t) - \xi(\infty) &= \xi_e(t) \\ \bar{u}(t) &= u_e(t) \end{aligned} \tag{4.38}$$

Then state equation becomes:

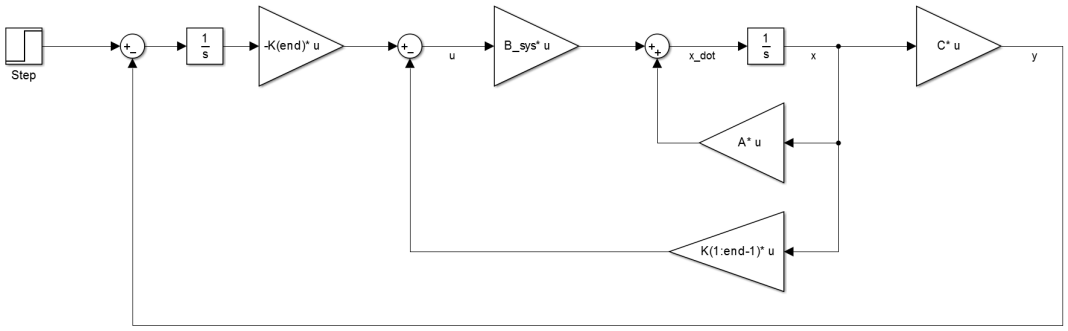

Figure 4.25: Linear Quadratic Tracker

$$\begin{bmatrix} \dot{\bar{x}}_e \\ \dot{\xi}_e \end{bmatrix} = \begin{bmatrix} A & 0 \\ -C & 0 \end{bmatrix} + \begin{bmatrix} B \\ 0 \end{bmatrix} \bar{u}_e \tag{4.39}$$

According to new state definition, $\bar{x}_e \rightarrow 0$, and $\xi_e \rightarrow 0$ means output is following the reference. Therefore, designing a state regulator for the system in Eq. (4.39) will result in a tracker for the original system. To be able to design a state feedback regulator for the system in Eq. (4.39), new state and input matrix pair should be controllable. Also full state information is assumed to be available. Eq. (4.40) shows the controllability matrix for the example case. As it is full rank, system is controllable so that poles of the closed loop system can be placed anywhere. At other design points system is also controllable. Figure 4.25 shows the linear quadratic tracker structure.

$$\begin{aligned} M &= \begin{bmatrix} B & AB & A^2B & A^3B \end{bmatrix} \\ M &= \begin{bmatrix} 0 & 0 & -1.01e+7 & -2.51e+10 & 1.21e+13 \\ 0 & 0 & -3.52e+7 & 1.56e+10 & -3.34e+12 \\ 0 & 98696 & -4.34e+7 & 9.35e+9 & 1.71e+11 \\ 98696 & -4.34e+7 & 9.35e+9 & 1.71e+11 & -9.98e+14 \\ 0 & 0 & 1.01e+7 & -4.52e+9 & 9.52e+11 \end{bmatrix} \\ rank(M) &= 5 \end{aligned} \tag{4.40}$$

In this design Q and R cost matrices as chosen as in Eq. (4.41):

$$Q = \begin{bmatrix} 1 & 0 & 0 & 0 & 0 \\ 0 & 1 & 0 & 0 & 0 \\ 0 & 0 & 1 & 0 & 0 \\ 0 & 0 & 0 & 1 & 0 \\ 0 & 0 & 0 & 0 & 30 \end{bmatrix} \qquad (4.41)$$

$$R = 1$$

The last term on Q matrix ($Q(5,5)$) is the penalty on the reference tracking error. It directly relates to the system speed. Choosing $Q = C^T C$ is a common way of designing LQR controllers; however in this case Q chosen above performed better. Gain matrix, K, is then calculated with the selected Q and R matrices (Eq. (4.42)).

$$K = \begin{bmatrix} -0.75 & -24.10 & 126.44 & 0.99 & -5.48 \end{bmatrix} \qquad (4.42)$$

Closed loop step response is shown in Figure 4.26 and Figure 4.27 shows the state response. Note that for acceleration controller, design points are chosen as: $M = [1.1, 1.5, 2.5, 3.2]$ and $X_{cg} = 0.75m$, because at other conditions acceleration controller will not be used. Also note that step input magnitude is limited according to δ_{max} and $\dot{\delta}_{max}$ values of the aerodynamic fin actuators.

From Figure 4.26, it is seen that, speed of the closed loop system is different at different Mach values, even though state and input penalty matrices are the same for all design points. That is because of the fact that at high Mach values dynamic pressure is higher and aerodynamics fins are more effective on the missile.

Lateral thrusters are not considered for acceleration controllers because at high speeds missile is stable. Hence, large moments are required to trim the missile at high angle of attack values. 200 N thrusters become inadequate to supply that moments. Therefore, only aerodynamic fins are considered for acceleration controller.

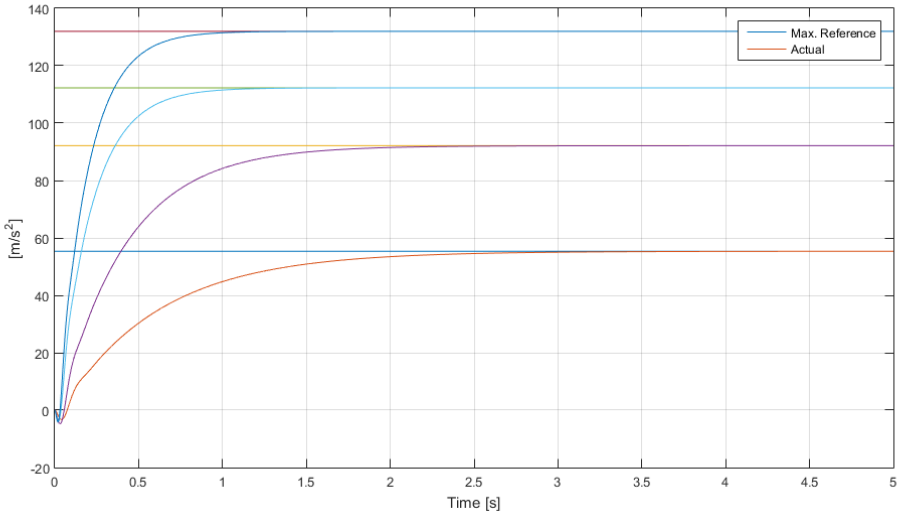

Figure 4.26: Step Response - Output

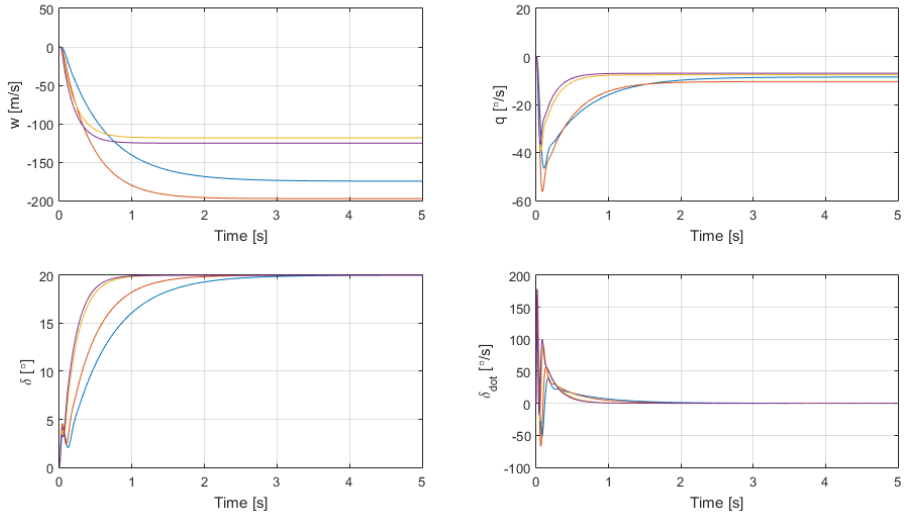

Figure 4.27: Step Response - States

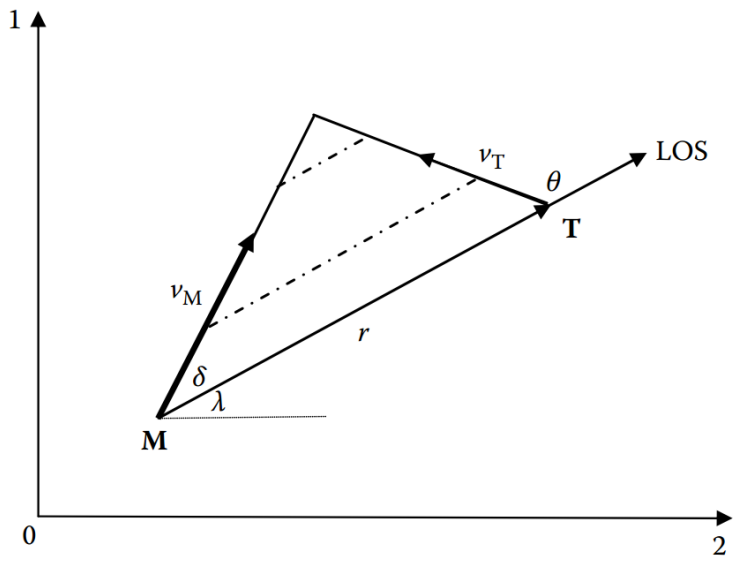

Figure 4.28: Missile and Target Engagement Geometry [22]

4.7 Guidance

In this study, the focus is on the initial turn maneuvers of the missile. These maneuver are realized through the angle controller and the reference angle values for the maneuvers are simply the desired missile attitude angle values. Therefore, there is not a formal guidance rule for the initial flight phase. For the terminal guidance, proportional navigation guidance (PNG) is used. In proportional navigation aim is to make the LOS rate zero. In Figure 4.28, M is the missile and T is the target. λ denotes the line of sight angle.

PNG rule is given as:

$$\vec{a_{zcom}} = N\dot{\vec{\lambda}} \times \vec{V_{cl}} \tag{4.43}$$

where $\vec{a_{zcom}}$ is the acceleration command, N is PNG gain, $\dot{\vec{\lambda}}$ is line of sight (LOS) rate and $\vec{V_{cl}}$ is the relative velocity of the target with respect to the missile. LOS angle (λ) is the angle between horizontal plane and the missil-to-target line. PNG gain, N, affects the trajectory shape to the target. In simulations it is taken as 2. For targets at different ranges or moving targets, PNG gain can be adjusted to increase the performance.

CHAPTER 5

MANEUVER SIMULATIONS

The differential equations of motion, derived in Chapter 2, are realized in MATLAB SIMULINK environment and built-in numerical solver "Runge-Kutta4" is used with 1 ms of step size. Considering the missile dynamics 1 ms is small enough to study the motion of the missile. Atmosphere and gravity are modeled as analytical functions; however, the missile aerodynamics are modeled by tabulating the coefficients and then using built-in look-up tables that perform linear interpolation. Gravity only depends on the Z position of the missile in the inertial frame, i.e., a flat Earth is assumed. Moreover, the equations of motion are derived with the assumption that the missile body is rigid; therefore, there is no elastic effects in the simulations.

5.1 Trim Point and Agility Simulation

In this section, the relationship with between stability and agility is demonstrated in the nonlinear simulation. Typical missile and Alternative 1 missile, discussed in Chapter 3, are simulated with the acceleration controller and the resulting angle of attack, lateral acceleration and the fin deflection angles are compared. In the simulation, the missile starts with the initial speed of 2.5 Mach, at an altitude of 1000 m, in vertical attitude and executes a pull-up maneuver, i.e., accelerating in the $-Z_B$ direction. 100 m/s^2 of acceleration is commanded in the $-Z_B$ direction. Figure 5.1 depicts the maneuver.

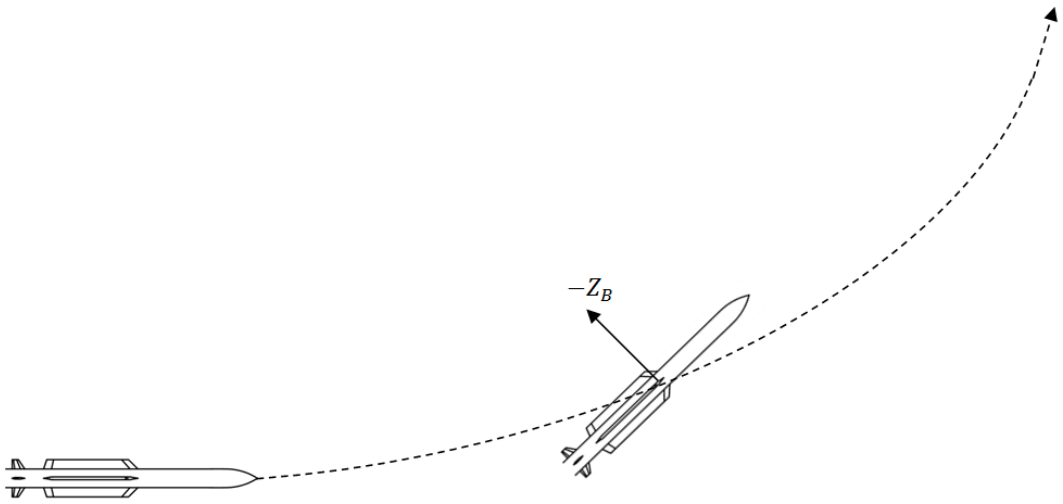

Figure 5.1: Trim Point Comparison Maneuver

Figure 5.2 shows the acceleration, angle of attack and fin deflection values for typical and Alternative 1 missile configurations. As it can be seen from the figure, Alternative 1 missile, which is designed to be agile after the main engine burnout, can execute the maneuver with less fin deflection angle. Note that the deflection sign is different in the two cases. That is because alternative 1 missile is slightly unstable in this flight condition; whereas typical missile is very stable. Since the moment caused by angle of attack changes sign with the stability, the balancing moment coming from the fins also changes sign.

5.2 Vertical Launch to Horizontal Maneuver

Vertical launch is a concept used mainly in naval ships. It increases the missile loading capacity of the canisters and also decreases pre-launch works such as directing the canister to the target. However, in vertical launch, there needs to be a pitch over maneuver to the target unlike missiles fired in target azimuth. This maneuver should be completed as early as possible as it will cause decrease in missile burnout speed and increase in altitude. Flying below a certain altitude is usually a requirement for anti-ship missiles in order to keep the missile off the target's radar. The maneuver can be illustrated as shown in Figure 5.3.

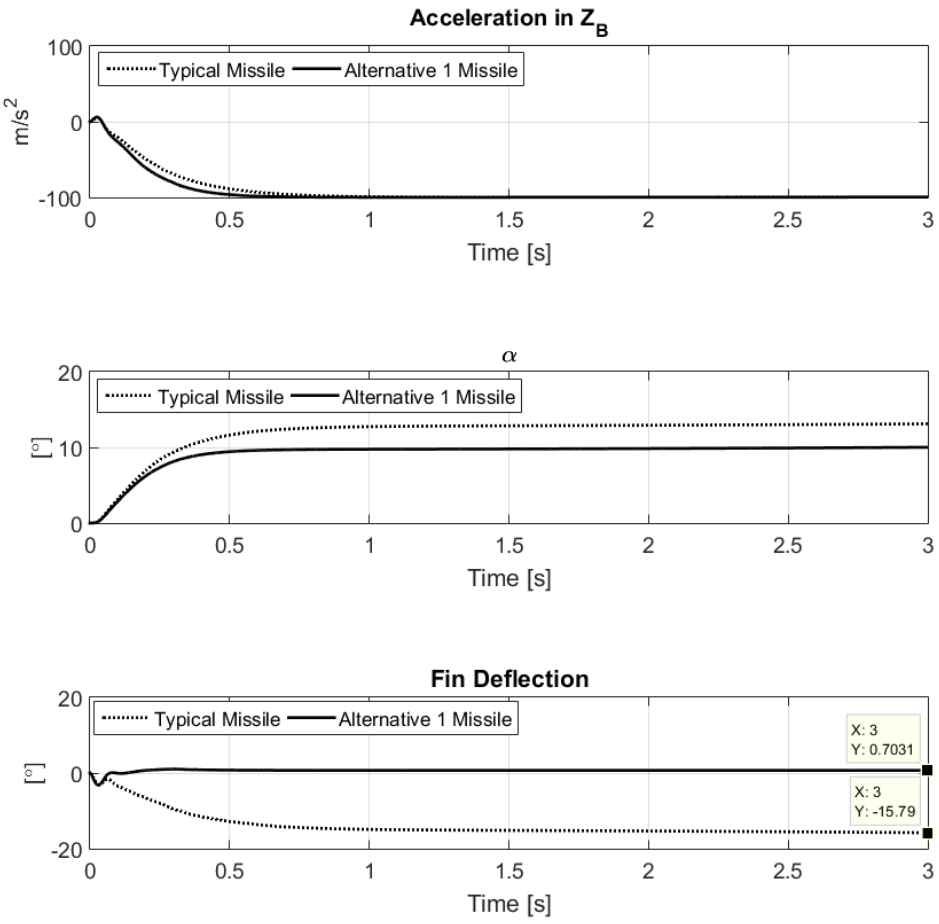

Figure 5.2: a_z - α - δ

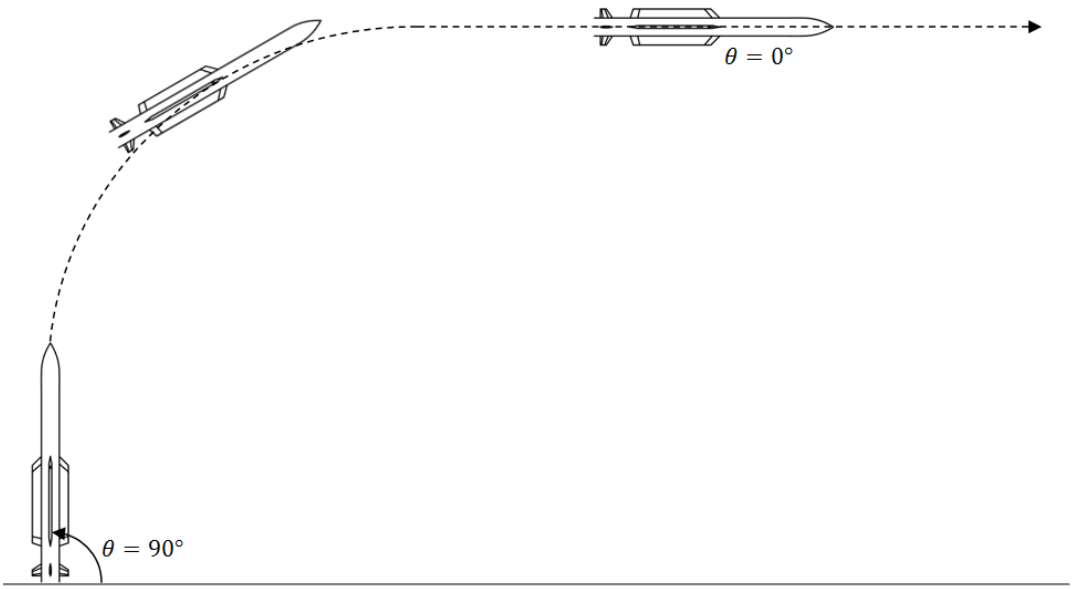

Figure 5.3: Vertical Launch to Horizontal Maneuver

In this maneuver the missile is launch with $\theta = 90°$ and $\theta_{ref} = 0°$ is requested from the angle controller.

Here three cases are presented. In the first case typical missile aerodynamics is used to turn over the missile using only aerodynamic fins. In the second case more agile geometry (Alternative 2) is considered, again using only aerodynamic fins. In the third case agile missile is turned over with the lateral thrusters. Performance of three cases are then compared.

Figure 5.4 shows the θ of three cases. As seen from the figure, agile missile performs better than typical missile and thruster performs better than aerodynamic control. Figure 5.5 shows the trajectory of the missile in $X-Z$ plane, it can also be interpreted as altitude versus downrange.

As seen from Figure 5.5 the case with thruster control performs the best in terms of turn radius and final altitude. Also note that in the aerodynamic case even though fin deflection (Figure 5.7) is at maximum, because of low dynamic pressure it is not as effective as the thrusters. q and α for the aerodynamic control cases have large oscillations. This behavior is a result of aerodynamic fin actuators working in their

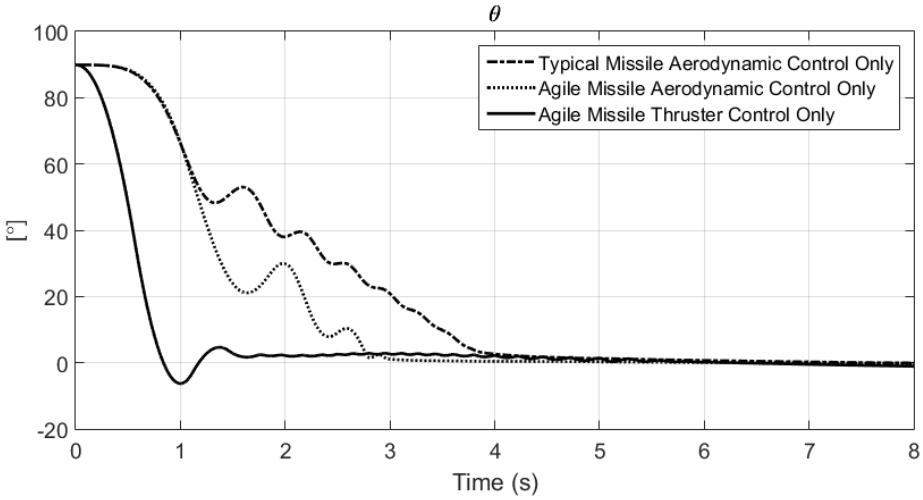

Figure 5.4: Vertical Launch to Horizontal Maneuver - θ

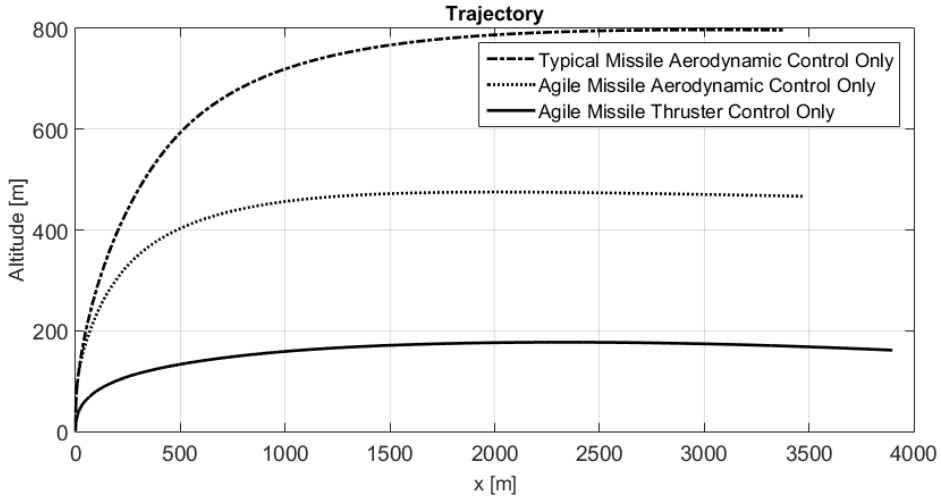

Figure 5.5: Vertical Launch to Horizontal Maneuver - $Trajectory$

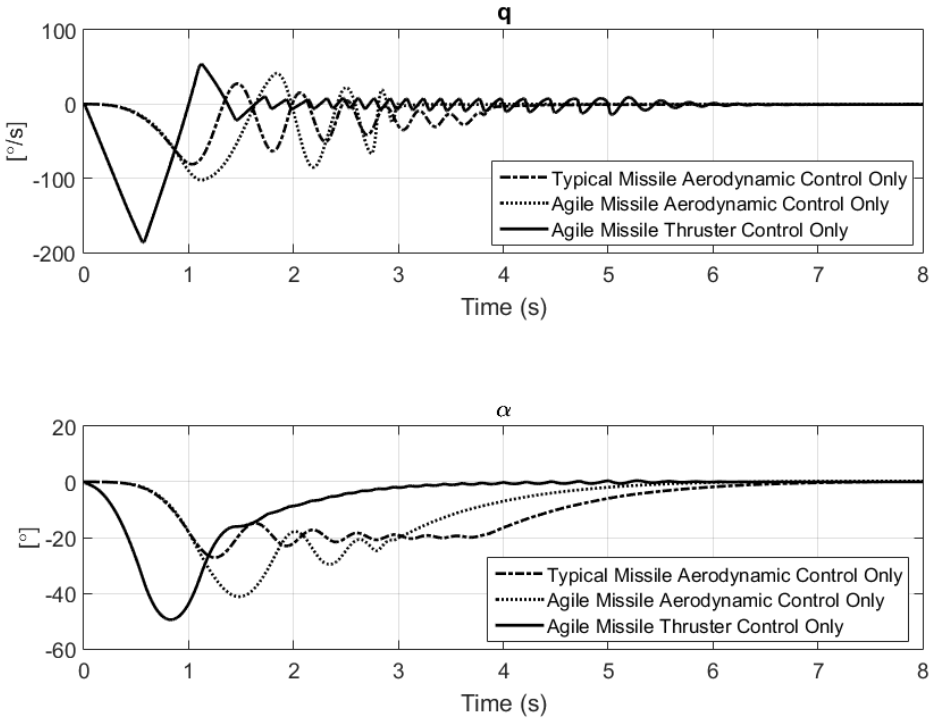

Figure 5.6: Vertical Launch to Horizontal Maneuver - $q - \alpha$

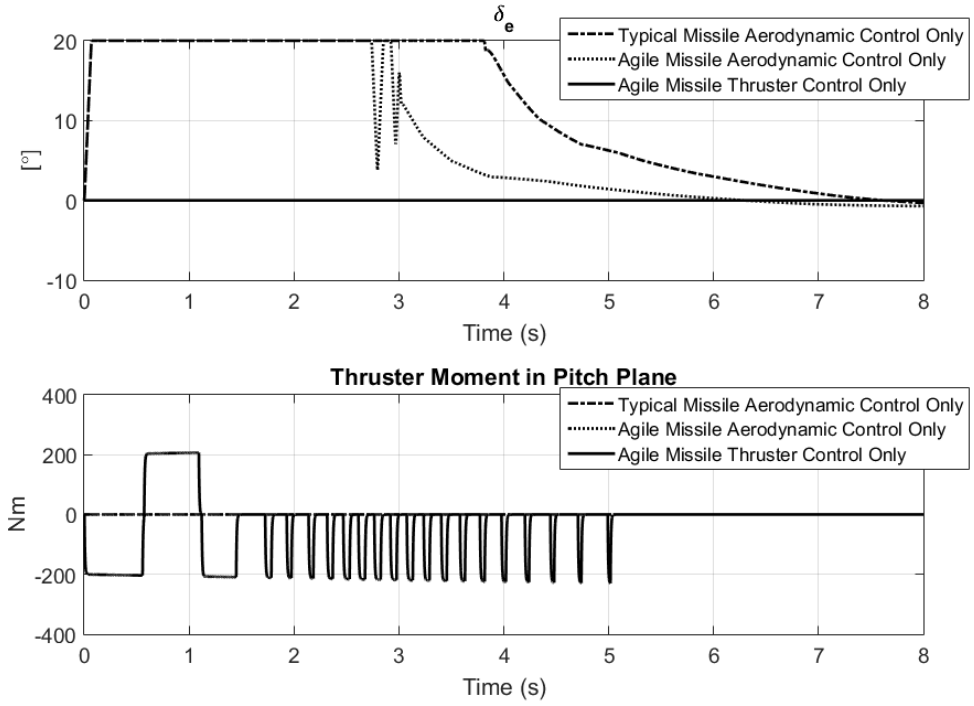

Figure 5.7: Vertical Launch to Horizontal Maneuver - δ_e - Thruster Moments

nonlinear region, so that they are not able to properly stabilize the system. The limits on the reference tracking error of the controller can be increased in order to force fin actuators to the linear region; however in that case system will slow down and the turnover performance will worsen. Oscillation is also present in the thruster controlled case; whereas they are much smaller in amplitude compared to the other cases. This response is again because of the nonlinear nature of the actuator. As mentioned in the previous chapters, thrusters operate in on-off fashion; therefore, output of the thruster controller will always oscillate around the reference input. Figure 5.7 shows the thruster moments. Note that positive moment is created by thruster 1 and negative moment is created by thruster 2.

5.3 Airborne Launch 180° Maneuver

This maneuver is thought as a launch from an aircraft flying at a speed of 0.8 Mach. The aim is to quickly reverse the direction of the missile 180° in order to engage targets behind the aircraft. Two cases are examined. In the first case the missile immediately ignites the main engine and executes the maneuver with aerodynamic fins, as thrusters are not effective for a speed of 0.8 Mach and accelerating. In the second case, the missile does not ignites the main engine immediately but still begins to execute the maneuver with its initial speed. At some point angle of attack exceeds 40° and speed drops below 200 m/s. At these conditions the missile is assumed to be stalled, i.e., aerodynamics no longer work. This is modeled as nulling the aerodynamic moments and applying only stall drag force on the missile. A drag coefficient of 2.5 is chosen for stall conditions and the force is applied in the body axes according to the angle of attack. In the simulations the missile is launched with a initial speed of 0.8 Mach, horizontally ($\theta = 0°$), at an altitude of 1000 m. The maneuver is illustrated in Figure 5.8.

Figure 5.9 shows the resulting trajectory when the first case is simulated, i.e., the missile ignites the main engine immediately and executes the maneuver. Note that triangles indicate (roughly) the missile attitude and the motion direction. As seen from the figure, turn maneuver is completed at about 2500 meters, 1500 meters above the launching altitude.

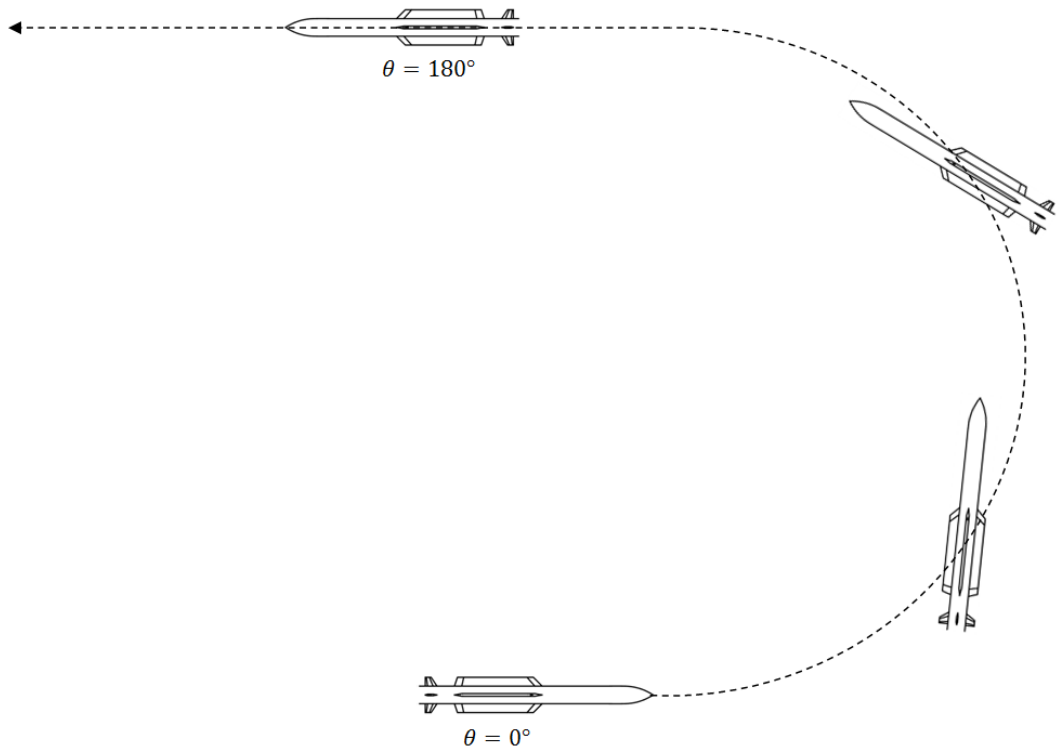

Figure 5.8: Horizontal Launch 180° Maneuver

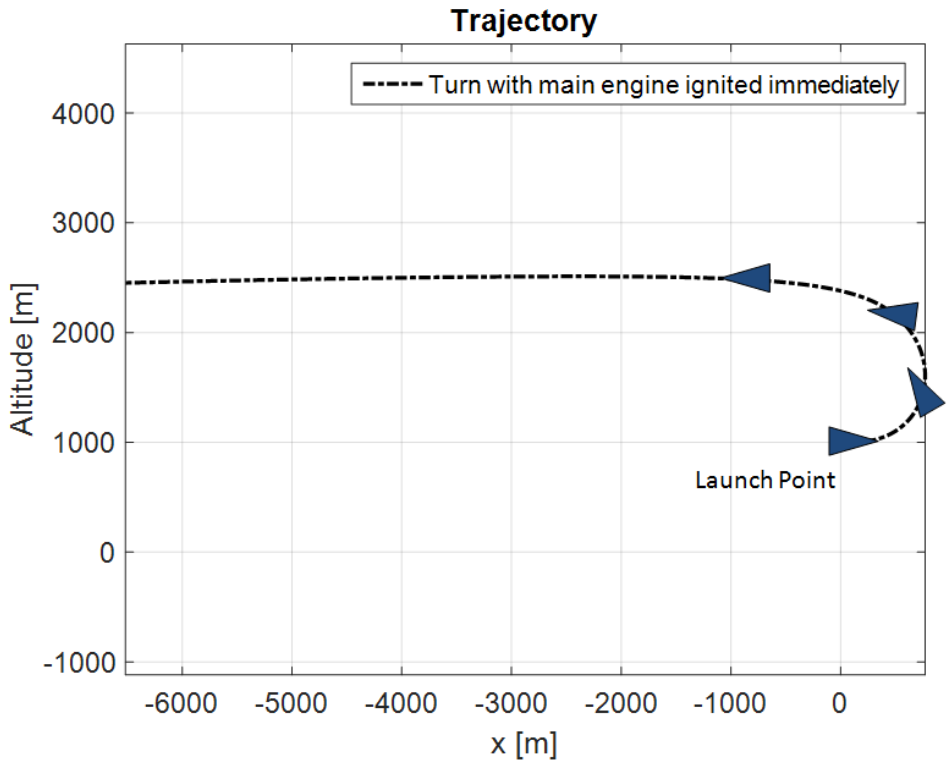

Figure 5.9: Horizontal Launch 180° Maneuver - Main Engine Ignited Immediately

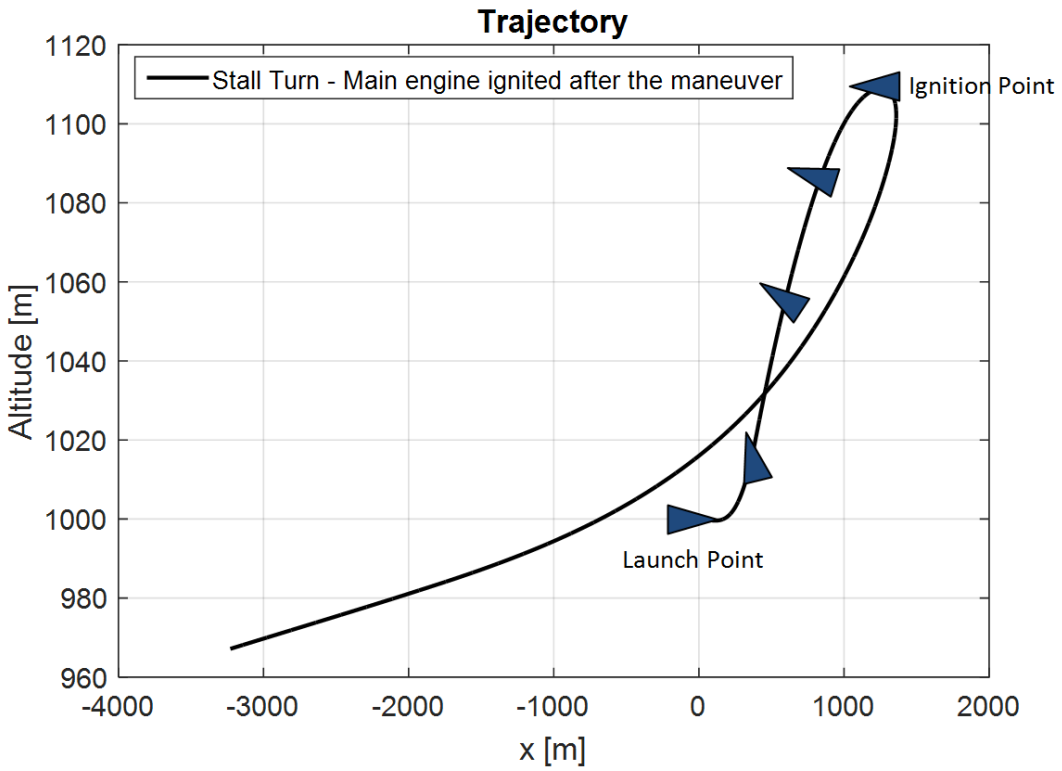

Figure 5.10: Horizontal Launch 180° Maneuver - Stall Turn

Figure 5.10 shows the trajectory when the main engine is not ignited immediately and the missile begins the turn with its initial speed. In this case, at some point missile angle of attack exceeds 40° and aerodynamic moment effects diminish but with lateral thrusters, the missile completely reverses its body while still going in the original direction, i.e., angle of attack reaches 180°. From the moment angle of attack exceeds 40° until it returns to below $40°$, thrusters are used to complete the maneuver and stabilize the missile. When the desired attitude ($\theta = 180°$) is obtained, main engine starts. For a short time missile continues to travel in the original direction because of the initial velocity, then main engine thrust nulls this velocity and the missile begins accelerating in the reverse direction. The velocity reversal can be observed from the Figure 5.12. Also note that stall turn case has a small final velocity advantage.

Note that axes of the trajectory plot in Figure 5.10 are not equally spaced in order to show the trajectory shape. Figure 5.11 shows the same plot with the axes equalized and low turn altitude is more apparent.

Figure 5.13 shows the attitude angle change over time. Both cases finished the ma-

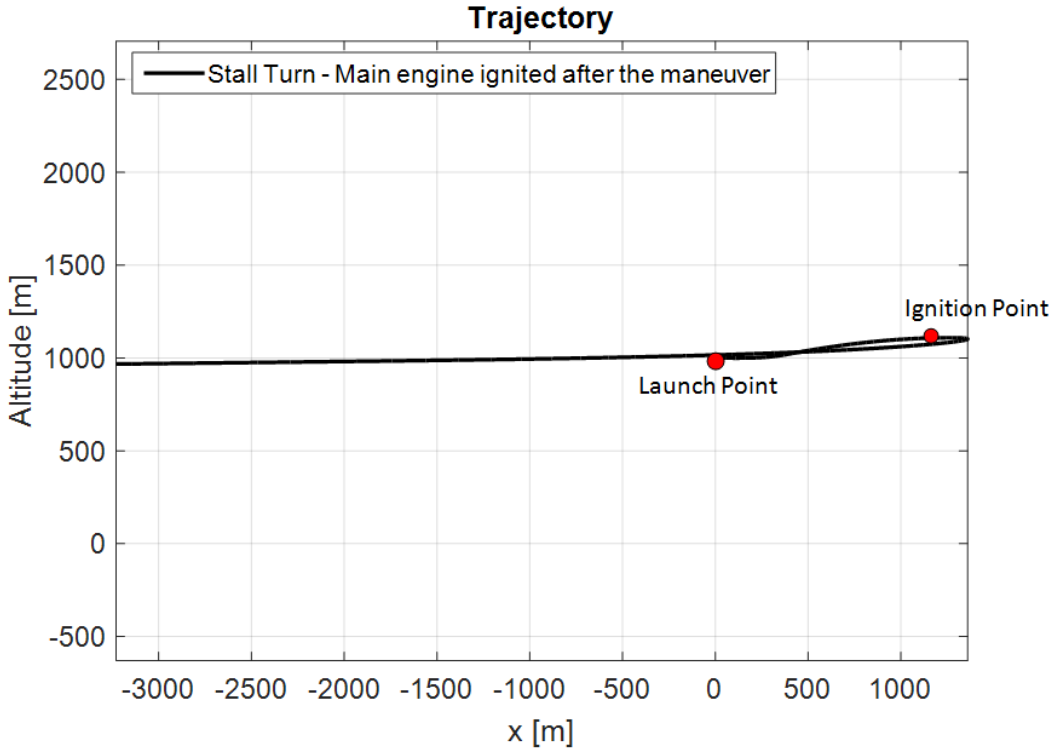

Figure 5.11: Horizontal Launch 180° Maneuver - Stall Turn (Axes Equalized)

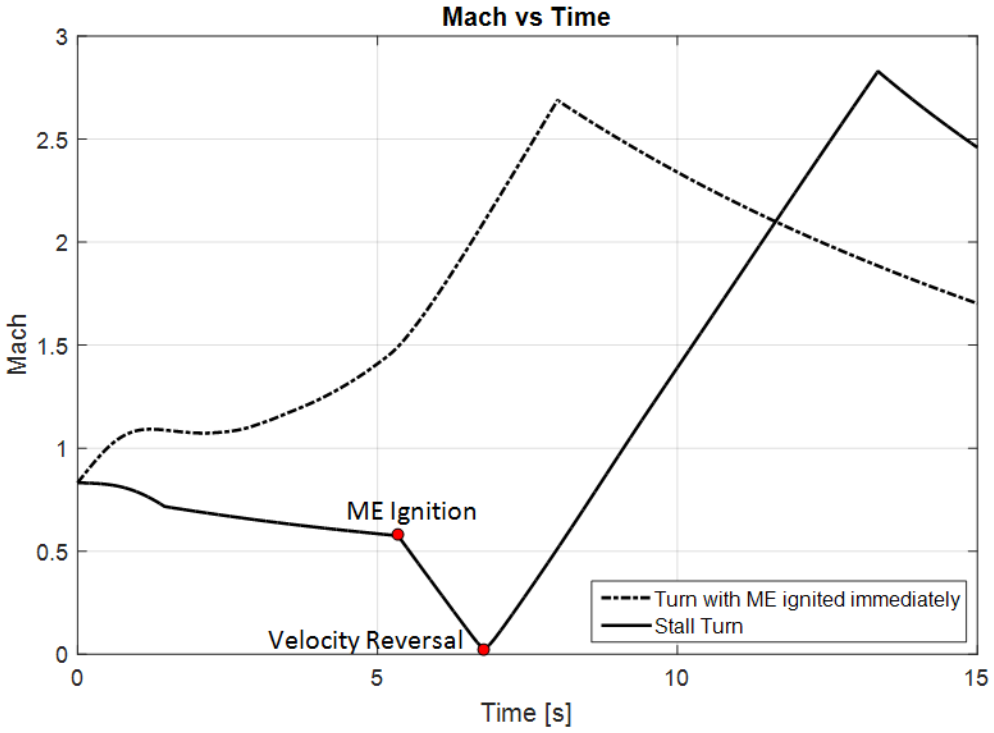

Figure 5.12: Horizontal Launch 180° Maneuver - $Mach$

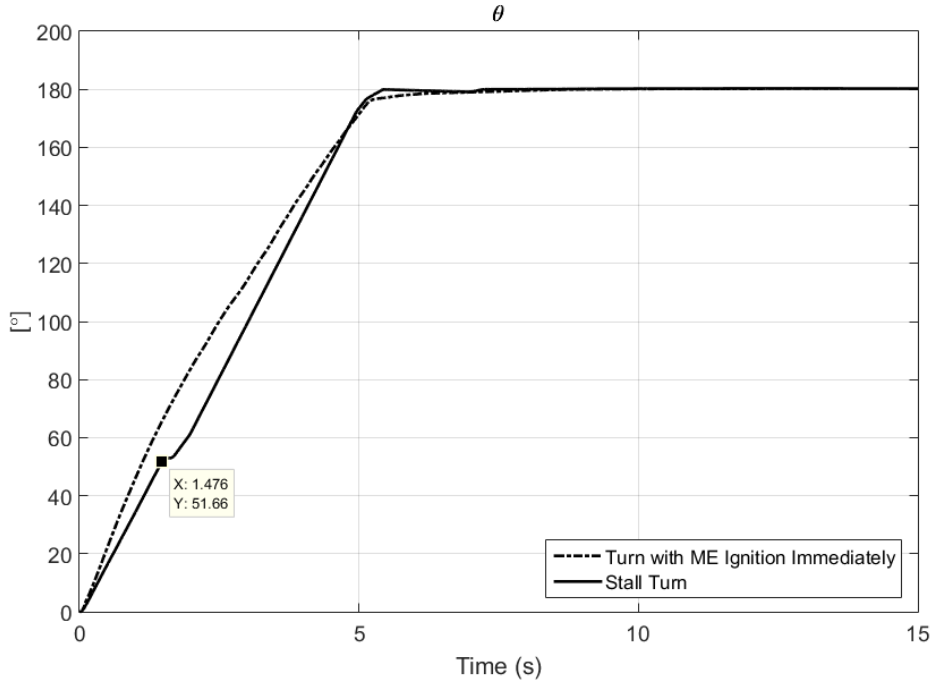

Figure 5.13: Horizontal Launch 180° Maneuver - θ

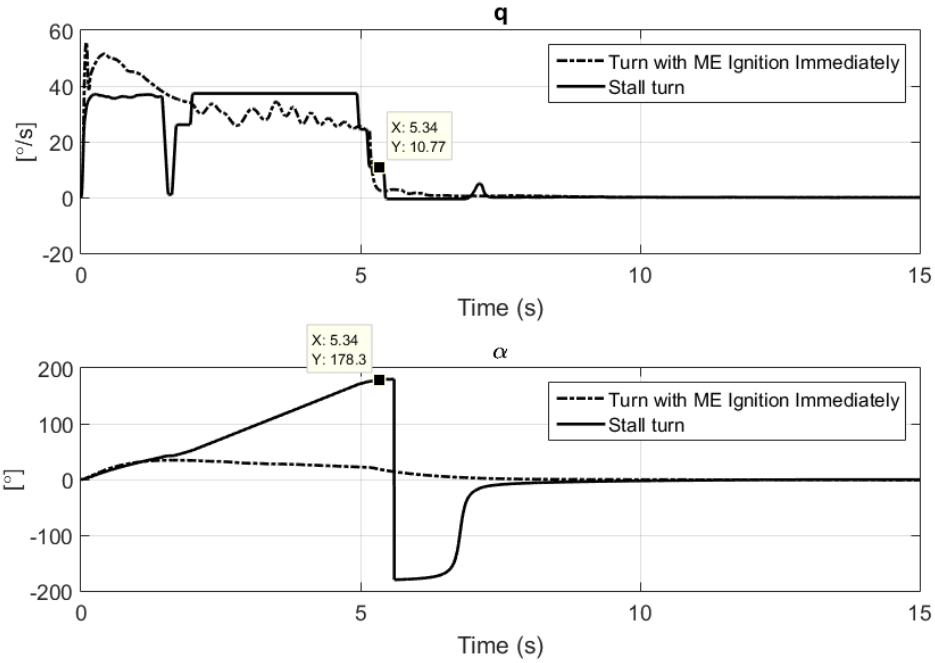

Figure 5.14: Horizontal Launch 180° Maneuver - $q - \alpha$

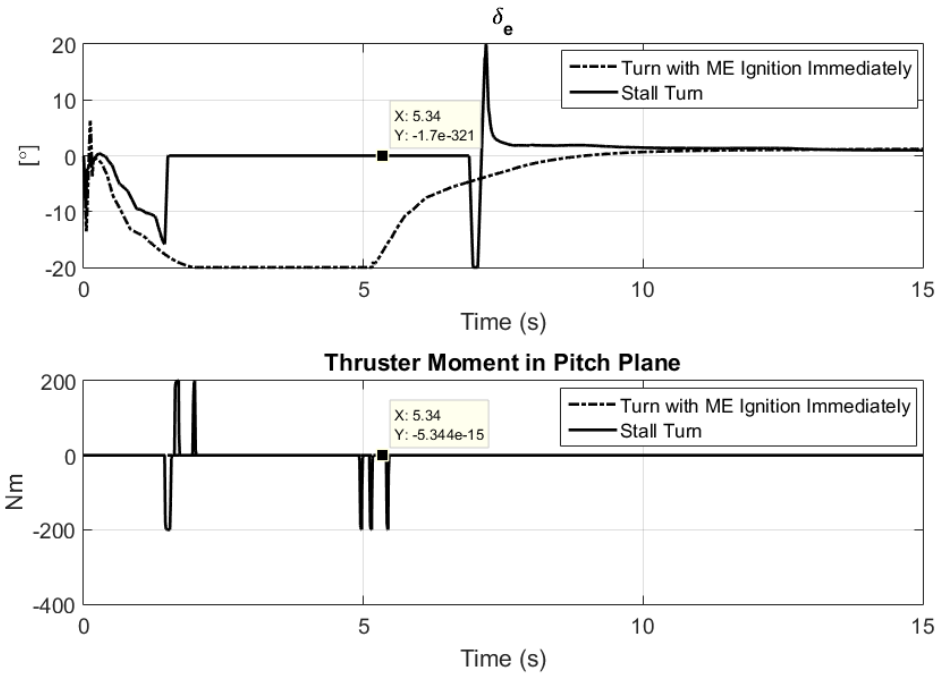

Figure 5.15: Horizontal Launch 180° Maneuver - $\delta_e - ThrusterMoments$

neuver around the same time however, in stalled case altitude of the turn is much lower.

Figure 5.14 shows the angular velocity in pitch plane and angle of attack for the two cases. For the first case (main engine is ignited immediately) angle of attack is about 30° for the duration of the maneuver. However, angle of attack reaches 180° in the second case, because main engine is not ignited at the launch and the missile stalls. Since aerodynamic moments are assumed to be zero at the stall condition, thrusters can rotate the missile to 180° attitude, hence the high values of the angle of attack. The jump in α plot around 5.5 seconds is because of purely mathematical reasons. As mentioned in Chapter 2, angle of attack is calculated with $arctan$ function whose output range is $[-\pi, +\pi]$; therefore whenever α becomes greater than 180° it jumps to negative region. Since the thruster control causes oscillation around the reference value, these jumps are expected.

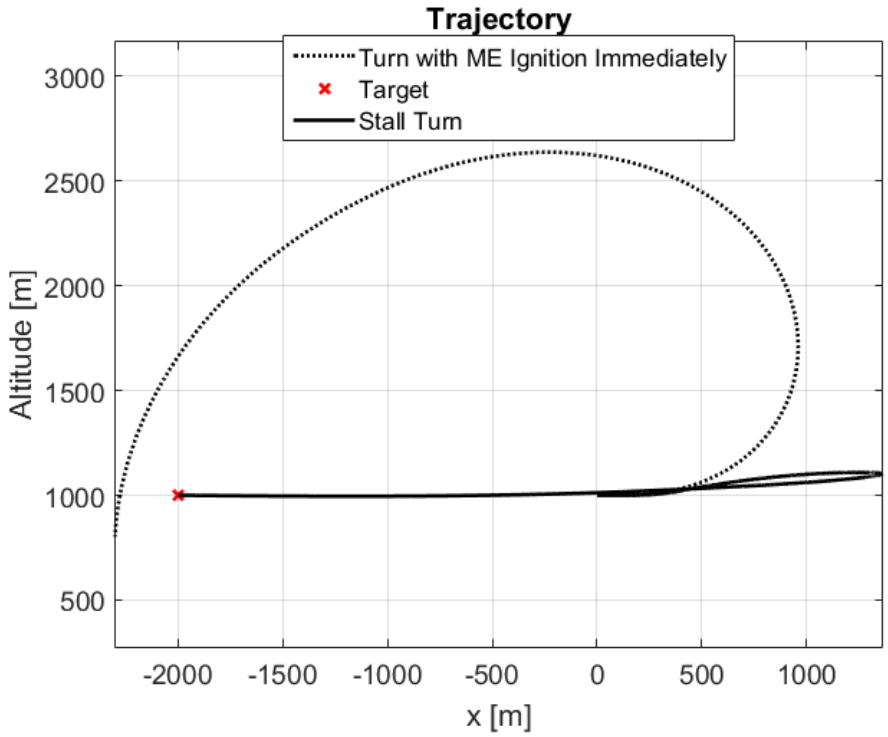

Figure 5.16: Target Engagement in Rear Hemisphere - Trajectory

5.4 Airborne Launch and Terminal Guidance

In this section, airborne launch case is considered with terminal guidance to a fixed target behind the missile launch point. Again two turn cases is simulated: one with main engine ignition immediately and the other is the stall turn. The missile starts with 0.8 Mach of speed, at an altitude of 1000 m and the target is placed at the same altitude but 2000 m behind. Apart from the terminal phase, this is the same maneuver discussed in the previous section.

In terminal guidance, following PNG rule is used as discussed in Chapter 4 Section 4.7:

$$\vec{a_{z}}_{com} = N\dot{\vec{\lambda}} \times \vec{V}_{cl} \tag{5.1}$$

Figure 5.16 shows the resulting trajectories for this scenario. For a target 2000 m behind, the missile that ignites the main engine immediately, cannot turn sharply enough to engage with the target. However, in the stall turn case after the main engine

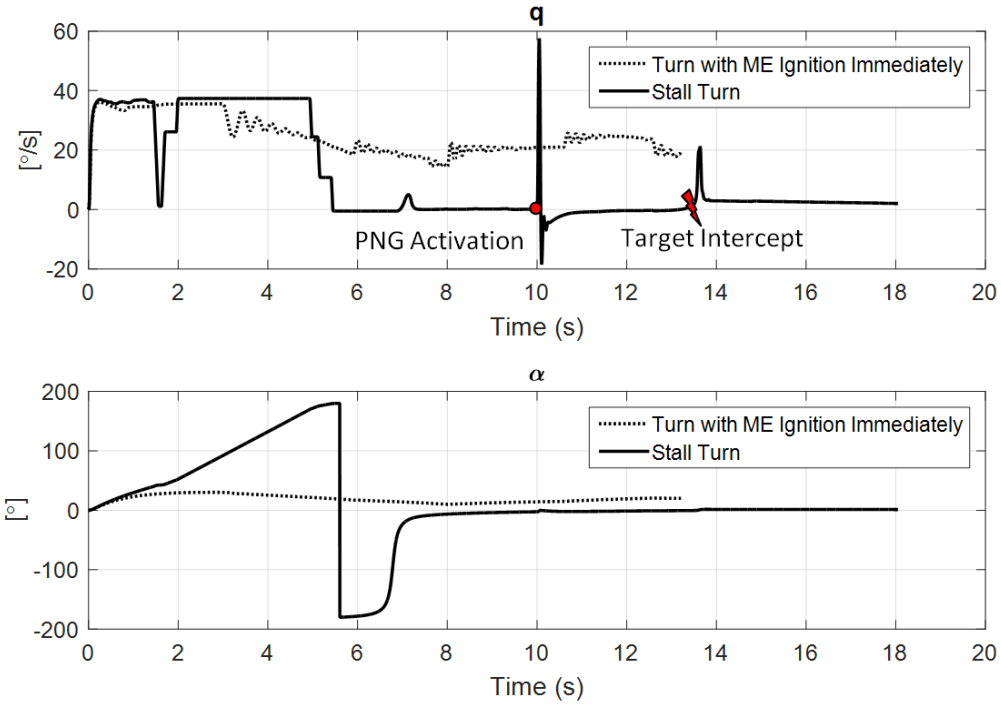

Figure 5.17: Target Engagement in Rear Hemisphere - $q - \alpha$

ignition, the missile can intercept the target.

Figure 5.17 shows the attitude rate and angle of attack values for the two cases. Note that the missile that ignites the main engine immediately is turning as quickly as possible (deflection is maximum in Figure 5.18); however, its turn rate is not enough to intercept the target.

Figure 5.19 shows the Mach number of the two cases. Note that the missile that ignites its main engine immediately, slows down as it flies at high angle of attack in order to turn quickly. Stall turn case not only turns quicker but also it shows better speed throughout its path.

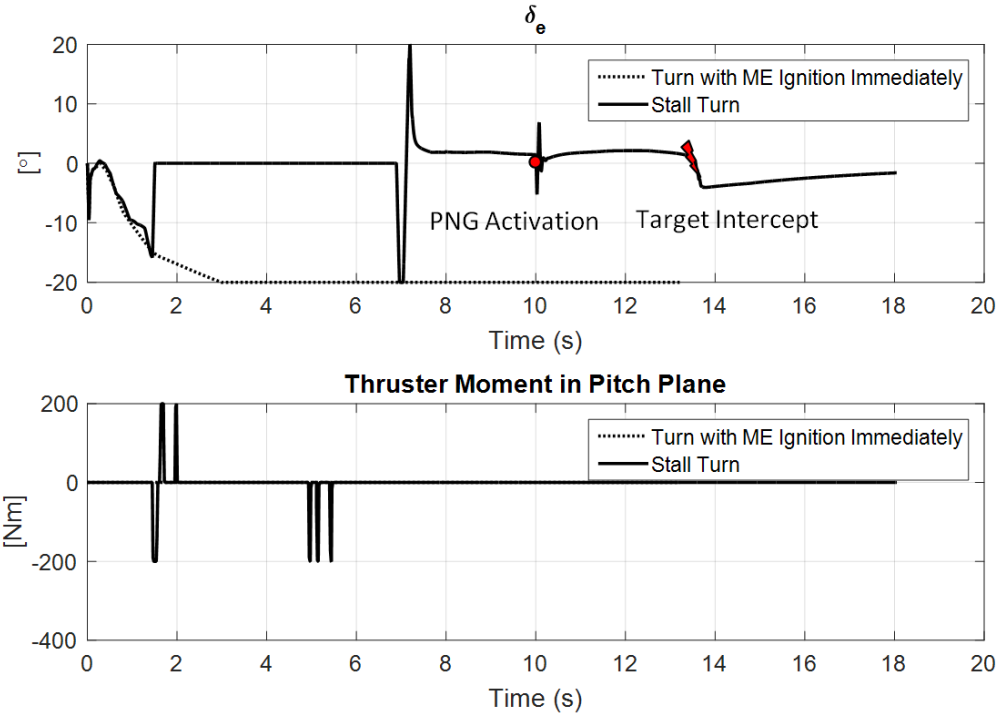

Figure 5.18: Target Engagement in Rear Hemisphere - δ_e - Thruster Moments

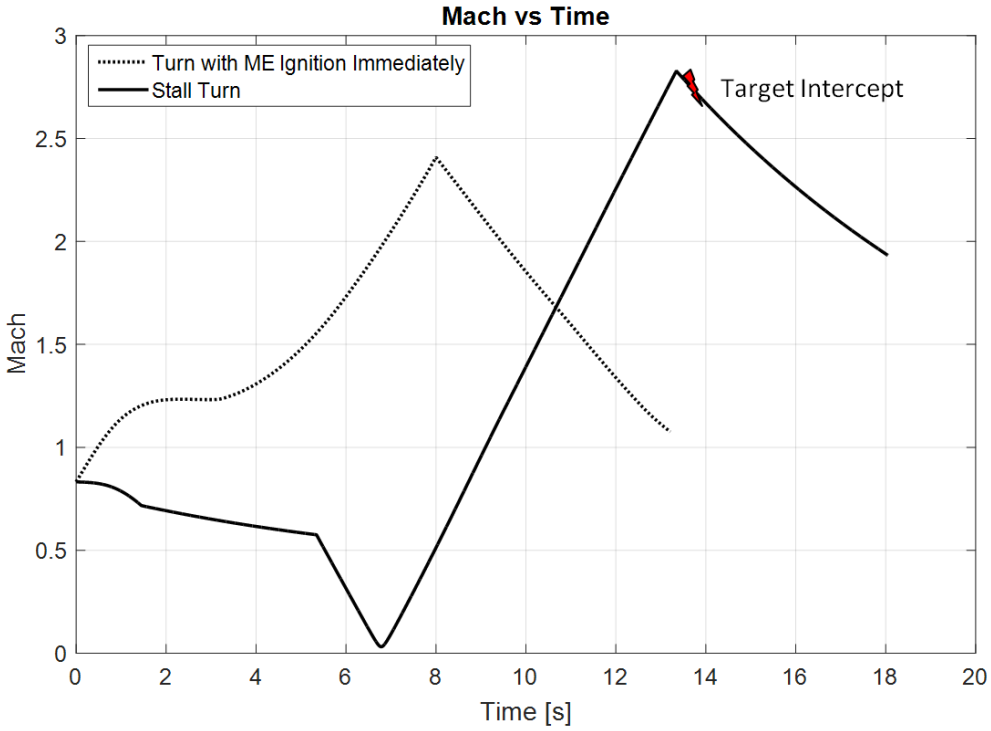

Figure 5.19: Target Engagement in Rear Hemisphere - Mach

CHAPTER 6

CONCLUSIONS AND DISCUSSIONS

In this study a tactical missile is considered. Its aerodynamic design is modified according to the stability and agility requirements of the specific maneuvers. Lateral thrusters are added to the missile in order to increase agility. Especially conditions in which the classical aerodynamic fins lose their effectiveness, thrusters are used to execute maneuvers quickly. In controller design both actuators are considered and thrust modulator algorithm is added in order to drive the thrusters in an on-off fashion. Vertical and airborne launch and quick turn maneuvers are simulated in 6 DoF environment and thruster effect is observed. In low speed and stall conditions, it is observed that lateral thrusters can be effective against the aerodynamic fins and increase the agility of the missile in these specific scenarios.

Using lateral thrusters in the endo-atmospheric conditions is an interesting concept. The force level of the thrusters discussed in this work is kept low in order to be realistic. Increasing force value can expand the flight envelope in which the effectiveness of the thrusters are considerable. Thruster control performance can be studied under uncertainties and environmental disturbances such as winds. Robustness analysis of the thruster controller is another challenging topic as the actuators are nonlinear and other nonlinearities are introduced in the controller structure (e.g., thruster modulator). Other modulation types, for instance PWM can be compared against PWPF in terms of performance and robustness. Moreover, different controller design strategies using both actuators at the same time can be studied to investigate any possible gains relative to the classical single input design.

REFERENCES

[1] A vertical launch sea wolf missile is fired from type 23 frigate hms richmond. `http://www.defenceimagery.mod.uk/`.

[2] Aerojet. *Space Shuttle ACS and Gas Generators*, 2006.

[3] Arda Aksu. Aerodynamic parameter estimation of a missile. Master's thesis, Middle East Technical University, Turkey, 2013.

[4] William B. Blake. *Missile DATCOM User's Manual - 1997 FORTFAN 90 Revision*. Air Force Research Laboratory.

[5] John H. Blakelock. *Automatic Control of Aircraft and Missiles*. John Wiley and Sons, 1991.

[6] Eugene L. Fleeman. *Tactical Missile Design*. AIAA, 2001.

[7] Honeywell. *Reaction Control Systems*, 2010.

[8] Paul B. Jackson. Overview of missile flight control systems. *Johns Hopkins APL Technical Digest*, 29(1):9–24, 2010.

[9] Yao Junkui and Qi Zaikang. Control analysis and autopilot design for static unstable missiles. In *International Conference on Electrical and Control Engineering*. IEEE, 2010.

[10] Sidi Marcel. *Spacecraft Dynamics and Control*. Cambridge University Press, 1997.

[11] MBDA Missile Systems. *Vertical Launch MICA*, 2015.

[12] Moog. *Monopropellant Thrusters*, 2013.

[13] Moog. *Upper Stage Engines*, 2013.

[14] John B. Nowell. Missile total and subsection weight and size estimation equations. Master's thesis, United States Naval Academy, USA, 1992.

[15] Katsuhiko Ogata. *Modern Control Engineering*. Prentice-Hall, 1997.

[16] Antti Pankkonen. Method for rapid modelling of missile aerodynamics. In *AIAA Atmospheric Flight Mechanics Conference*. AIAA, 2011.

[17] Jan Roskam. *Airplane Flight Dynamics and Automatic Flight Controls, Part I*. Design, Analysis and Research Corporation, 2001.

[18] T.J. Sooy and R.Z. Schmidt. Aerodynamic predictions, comparisons, and validations using missile datcom (97) and aeroprediction 98 (ap98). *Journal of Spacecraft and Rockets*, 42(2):257–265, March-April 2005.

[19] Raziye Tekin. Design, modeling, guidance and control of a vertical launch surface to air missile. Master's thesis, Middle East Technical University, Turkey, 2010.

[20] Ajay Thukral and Mario Innocenti. A sliding mode missile pitch autopilot synthesis for high angle of attack maneuvering. *IEEE Trans. on Control Systems Technology*, 6(3):359–371, 1998.

[21] Kevin A. Wise and David J. Broy. Agile missile dynamics and control. *Journal of Guidance, Control, and Dynamics*, 21(3):441–449, May-June 1998.

[22] Rafael Yanushevsky. *Modern Missile Guidance*. CRC Press, 2008.

[23] Paul Zarchan. *Tactical and Strategic Missile Guidance*. AIAA, 1997.

[24] Bülent Özkan. *Dynamic Modeling, Guidance, and Control of Homing Missiles*. PhD thesis, Middle East Technical University, Turkey, 2005.

APPENDIX A

MISSILE DATCOM

Missile DATCOM is a computer program that enables users to quickly estimate the aerodynamics of a wide variety of missile configurations. The program computes the aerodynamic parameters given in Table A.1 as a function of angle of attack for a given configuration.

A missile geometry and a set of flight conditions (Mach number, altitude, angle of attack, angle of side slip, aerodynamic surface deflections) are entered in order for the program to execute and compute the aerodynamic data. In a single run, Missile DATCOM is able to produce aerodynamic parameters for a set of angle of attack and a set of Mach number values.

The inputs to the program is written into "for005.dat" file. When the program is excuted, it writes output values into "for006.dat" file. However, for convenience "for004.dat" file can also be used to obtain the aerodynamic data.

Since, almost all of the parameters given in Table A.1 is a function of angle of sideslip, angle of surface deflections etc. as well as Mach number and angle of attack, the program must be run several times changing other parameters (angle of sideslip, angle of surface deflections etc.) at each run. MATLAB environment can be used to execute the program and store output values.

A.1 Obtaining Aerodynamic Parameters of Javelin ATGM

Dimensions for Javelin ATGM is taken from [3] (Figure A.1). Inputs to Missile DATCOM is explained in the following sections. Values are input according to Javelin

Table A.1: Missile DATCOM Computed Aerodynamic Parameters

C_N	Normal Force Coefficient
C_L	Lift Coefficient
C_m	Pitching Moment Coefficient
X_{cp}	Center of Pressure in calibers from the moment reference center
C_A	Axial Force Coefficient
C_D	Drag Coefficient
C_Y	Side Force Coefficient
C_n	Yawing Moment Coefficient (body axis)
C_l	Rolling Moment Coefficient (body axis)
$C_{N\alpha}$	Normal force coefficient derivative with angle of attack
$C_{m\alpha}$	Pitching moment coefficient derivative with angle of attack
$C_{y\beta}$	Side force coefficient derivative with sideslip angle
$C_{n\beta}$	Yawing moment coefficient derivative with sideslip angle (body axis)
$C_{l\beta}$	Rolling moment coefficient derivative with sideslip angle (body axis)
C_{mq}	Pitching moment coefficient derivative with pitch rate
C_{Nq}	Normal force coefficient derivative with pitch rate
C_{Aq}	Axial force coefficient derivative with pitch rate
$C_{m\dot{\alpha}}$	Pitching moment derivative with rate of change of angle of attack
$C_{N\dot{\alpha}}$	Pitching moment derivative with rate of change of angle of attack
C_{lp}	Rolling moment coefficient derivative with roll rate
C_{np}	Yawing moment coefficient derivative with roll rate
C_{Yp}	Side force coefficient derivative with roll rate
C_{lr}	Rolling moment coefficient derivative with yaw rate
C_{nr}	Yawing moment coefficient derivative with yaw rate
C_{Yr}	Side force coefficient derivative with yaw rate

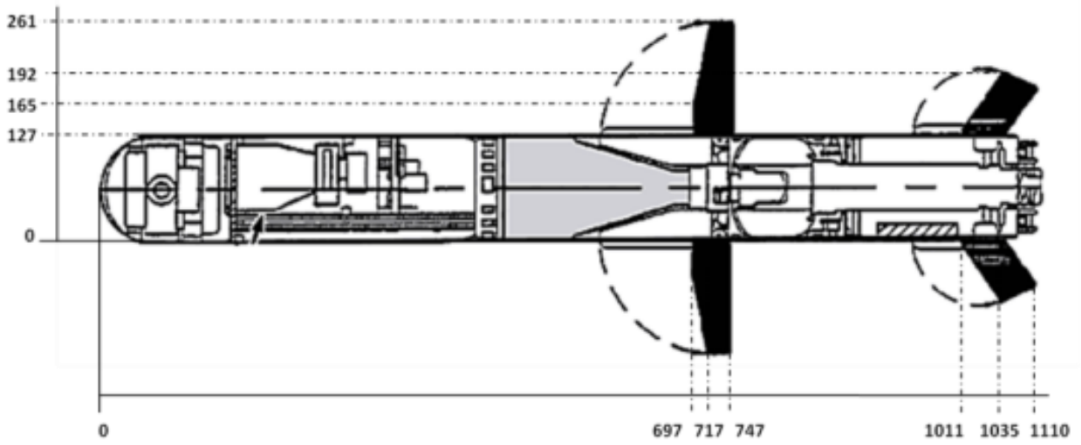

Figure A.1: Dimension (in mm) of Javelin ATGM

Table A.2: FLTCON Namelist Variable Definitions [4]

NALPHA	Number of angles of attack
ALPHA	Angle of attack
BETA	Sideslip angle
PHI	Aerodynamic roll angle
NMACH	Number of Mach numbers
MACH	Mach numbers
ALT	Altitudes

ATGM dimensions and flight regime. Sections are divided according to the DATCOM "namelist"s. The first part of the each section is taken directly from "for005.dat" file.

A.1.1 Flight Conditions

```
1  FLTCON
2  NALPHA=20.0,
3  ALPHA= 18.0, 16.0, 14.0, 12.0, 10.0, 8.0, 6.0, 4.0, 2.0,0.0,
4  ALPHA(11)=2.0,4.0,6.0,8.0,10.0,12.0,14.0,16.0,18.0,20.0,
5  BETA=0.0,
6  PHI=0.0,
7  NMACH=10.0,
8  MACH=0.1,0.2,0.3,0.4,0.5,0.6,0.7,0.8,0.9,1.0,
9  ALT=0.0,0.0,0.0,0.0,0.0,0.0,0.0,0.0,0.0,0.0,
10 END
```

DATCOM can calculate aerodynamic coefficients for a maximum of 20 angle of attacks and 20 Mach numbers in a single run. Therefore, it is reasonable to enter 20 values for each of them. Since DATCOM runs with a single side slip angle (BETA),

Table A.3: REFQ Namelist Variable Definitions [4]

SREF	Reference area
LREF	Longitudinal reference length L
LATREF	Lateral reference length
XCG	Longitudinal position of CG
ZCG	Vertical position of CG
BLAYER	Boundary layer type

while calculating aerodynamic coefficients that depend on the side slip angle, BETA value should be changed at each run. Aerodynamic roll angle value is input as zero for all runs, since Javelin ATGM is a axisymmetrical missile. Maximum altitude in Javelin's flight regime is about 160 meters. For this altitude value, properties of the atmosphere does not change much, hence altitude values (ALT) input to the DATCOM are set to zero for all Mach numbers.

A.1.2 Reference Quantities

```
1 REFQ
2 XCG=0.0,
3 END
```

Reference area and length is computed by DATCOM when a body geometry is entered. Thus, there is no need to input reference quantities here. Since Javelin has a symmetrical body, lateral reference length is equal to the reference length. DATCOM calculates the aerodynamic coefficients with respect to the center of gravity (X_{cg}). For most missiles, center of gravity changes during flight because of the fuel dumped. Hence, it is convenient to calculate coefficients with respect to the nose ($X_{cg} = 0$), and then move these coefficients to the changing center of gravity. For the sake of simplicity center of gravity is assumed to have no offset value in z-axis (Figure A.2).

Table A.4: AXIBOD Namelist Variable Definitions [4]

XO	Longitudinal coordinate of nose tip
TNOSE	Type of nose shape
LNOSE	Nose length
DNOSE	Nose diameter at base
LCENTR	Centerbody length
DCENTR	Centerbody diameter at base

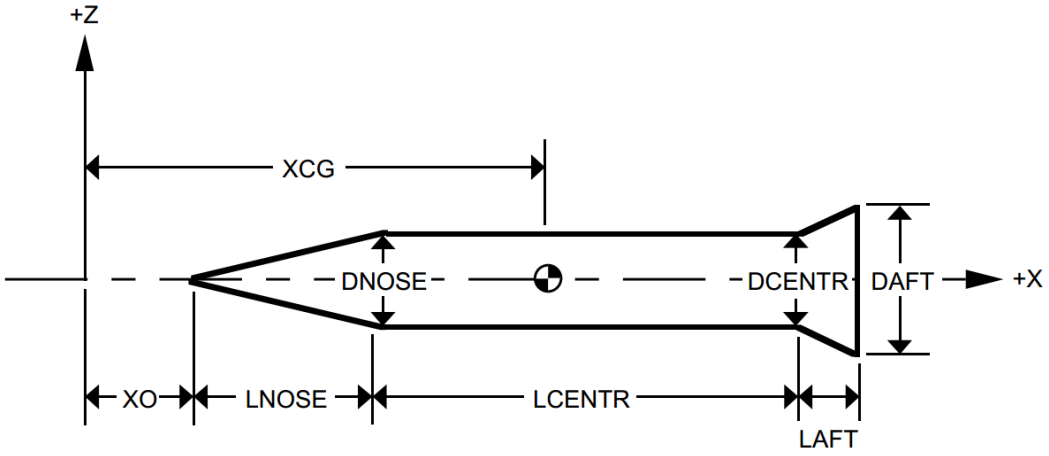

Figure A.2: AXIBOD Namelist Variables [4]

A.1.3 Axisymmetric Body Definition

```
1 AXIBOD
2 TNOSE=OGIVE,
3 LNOSE=0.0635,
4 DNOSE=0.1270,
5 LCENTR=1.0465,
6 DCENTR=0.1270,
7 END
```

XO is not entered, so DATCOM takes it as zero. It is convenient to enter XO as zero as it makes missile nose the origin in x-axis (Figure A.2). Javelin has a half spherical nose. Therefore, nose shape is chosen as tangent ogive and length of the nose is set to half of the nose diameter. Length and diameter of the center is entered according to the missile dimensions in Figure A.1.

A.1.4 Fin Set Definitions

```
 FINSET1
SECTYP=HEX,
SSPAN(1)=0.000,
SSPAN(2)=0.038,
SSPAN(3)=0.134,
CHORD(1)=0.050,
CHORD(2)=0.050,
CHORD(3)=0.030,
XLE(1)=0.697,
XLE(2)=0.697,
XLE(3)=0.717,
NPANEL=8.0,
PHIF=0.0,45.0,90.0,135.0,180.0,225.0,270.0,315.0,
ZUPPER(1)=0.100,
ZUPPER(2)=0.100,
ZUPPER(3)=0.100,
ZLOWER(1)=0.100,
ZLOWER(2)=0.100,
ZLOWER(3)=0.100,
LMAXU(1)=0.500,
LMAXU(2)=0.500,
LMAXU(3)=0.500,
LMAXL(1)=0.500,
LMAXL(2)=0.500,
LMAXL(3)=0.500,
LFLATU(1)=0.500,
LFLATU(2)=0.500,
LFLATU(3)=0.500,
LFLATL(1)=0.500,
LFLATL(2)=0.500,
LFLATL(3)=0.500,
 END
 FINSET2
SECTYP=HEX,
SSPAN(1)=0.000,
SSPAN(2)=0.100,
CHORD(1)=0.060,
CHORD(2)=0.060,
XLE(1)=1.011,
XLE(2)=1.071,
NPANEL=4.0,
PHIF=45.0,135.0,225.0,315.0,
ZUPPER(1)=0.100,
ZUPPER(2)=0.100,
ZLOWER(1)=0.100,
ZLOWER(2)=0.100,
LMAXU(1)=0.500,
LMAXU(2)=0.500,
LMAXL(1)=0.500,
LMAXL(2)=0.500,
LFLATU(1)=0.500,
LFLATU(2)=0.500,
LFLATL(1)=0.500,
LFLATL(2)=0.500,
 END
```

Zero value is entered for SSPAN(1) value, so that DATCOM places the wing on body. Then, other span locations are placed with respect to the body. Wing locations from

Table A.5: FINSET Namelist Variable Definitions [4]

SECTYP	Type of airfoil section
SSPAN	Semi-span locations
CHORD	Panel chord at each semi-span location
XLE	Distance from missile nose to chord leading edge
NPANEL	Number of panels in fin set
PHIF	Roll angle of each fin measured clockwise top vertical center looking forward
ZUPPER	Thickness to chord ratio of upper surface.
ZLOWER	Thickness to chord ratio of lower surface.
LMAXU	Fraction of chord from section leading edge to maximum thickness of upper surface.
LMAXL	Fraction of chord from section leading edge to maximum thickness of lower surface.
LFLATU	Fraction of chord of constant thickness section of upper surface.
LFLATL	Fraction of chord of constant thickness section of lower surface.

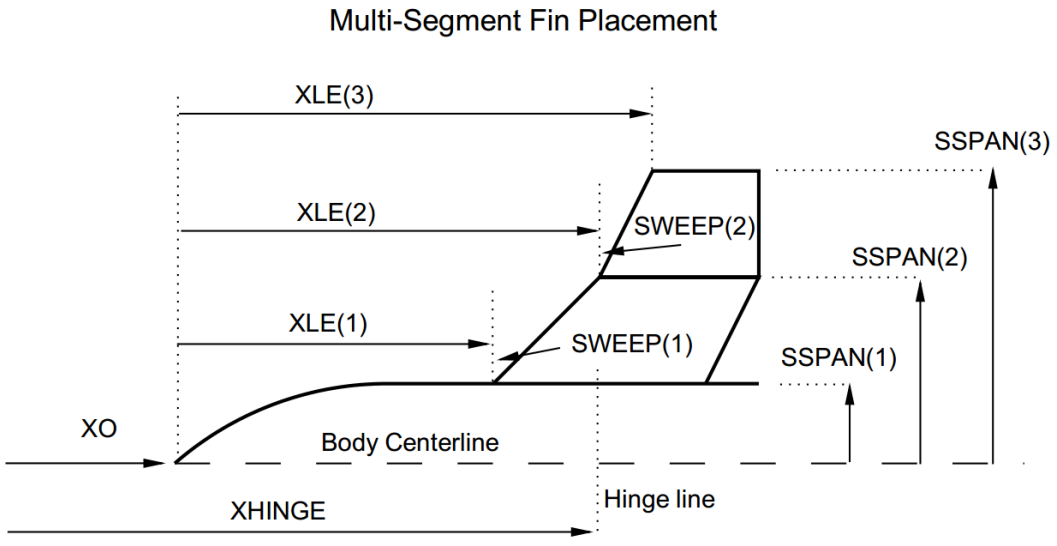

Figure A.3: FINSET Variables - 1 [4]

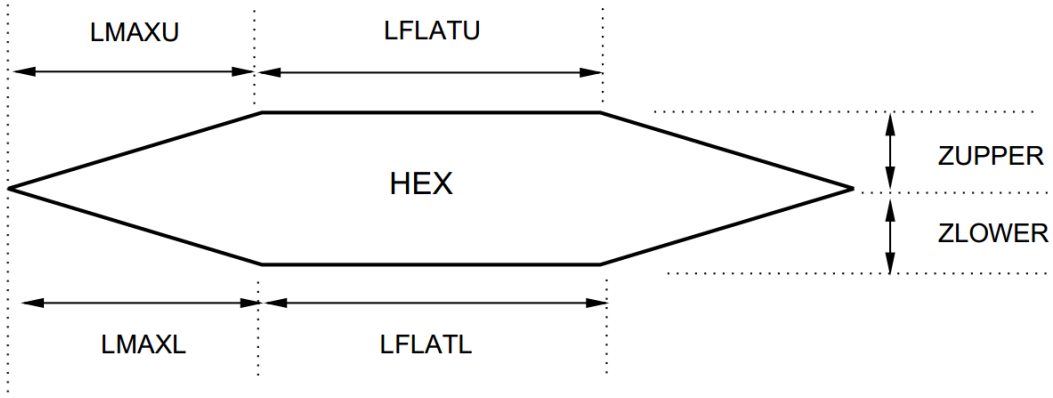

Figure A.4: FINSET Variables - 2 [4]

Table A.6: DEFLCT Namelist Variable Definitions [4]

DELTA1	Deflection angles for each panel
DELTA2	Deflection angles for each panel

nose are entered according to the missile dimensions in Figure A.1. Javelin has two sets of fins. First wing set is located to the middle of the body, it has 8 elements placed symmetrically and they are all fixed. 8 wings are placed around body by entering an angle array to the PHIF variable. The second fin set is at the aft of the missile, has 4 wings and the wings are moveable. There is no information about the missile's wing shape, hence hexagonal shape is assumed and reasonable shape ratios are entered. Note that there are two "FINSET" parts. There has to be as many FINSET entries as there are fin sets on the missile.

A.1.5 Fin Deflections

```
1 DEFLCT
2 DELTA2=0.0,0.0,0.0,0.0,
3 END
```

Aerodynamic surface deflections are entered in this namelist. Since only the aft fin set are movable, deflection angles are written for second fin set. Any unspecified deflection for a fin set is taken as zero. While calculating aerodynamic coefficients that are function of the deflection angle, DATCOM must be run for a number of deflection

angles, changing deflection angle values at each run. Usually surface deflections are defined as elevator, rudder and aileron in three axes. To comply with the convention, these three deflection angles should be converted to 4 fin deflections in cross form. Following equations can be used for conversion:

$$
\begin{aligned}
&\delta_e : elevator \\
&\delta_r : rudder \\
&\delta_a : aileron \\
&\delta_1 = \delta_e + \delta_r + \delta_a \\
&\delta_2 = \delta_e - \delta_r + \delta_a \\
&\delta_3 = -\delta_e - \delta_r + \delta_a \\
&\delta_4 = -\delta_e + \delta_r + \delta_a
\end{aligned}
\tag{A.1}
$$

Fin numbers can be seen in Figure A.5. Here four panel deflections are reduced to the three axes deflections. However, on some specific conditions, even though elevator, rudder and aileron are all zero, individual panel might be different than zero. Hence, for detailed analysis, coefficient dependence may be extended to all four fin deflections.

A.1.6 Control Cards

```
1 DAMP
2 SOSE
3 DIM M
4 FORMAT((20(2X,F10.4)))
5 WRITE DB12 341 360
```

In this section, commands that affect the program execution are input. In order to get dynamic coefficients “DAMP” control card should be added. “SOSE” selects the Second-Order Shock Expansion method for axisymmetric bodies at supersonic speeds. SOSE should be selected if any Mach number is higher than 2.0 [4]. “DIM” indicates the input and output length dimension. “WRITE” control card is used to get specific locations of specific arrays that DATCOM calculates. It can be used to get certain coefficients to be written into “for004.dat” file. For example “WRITE

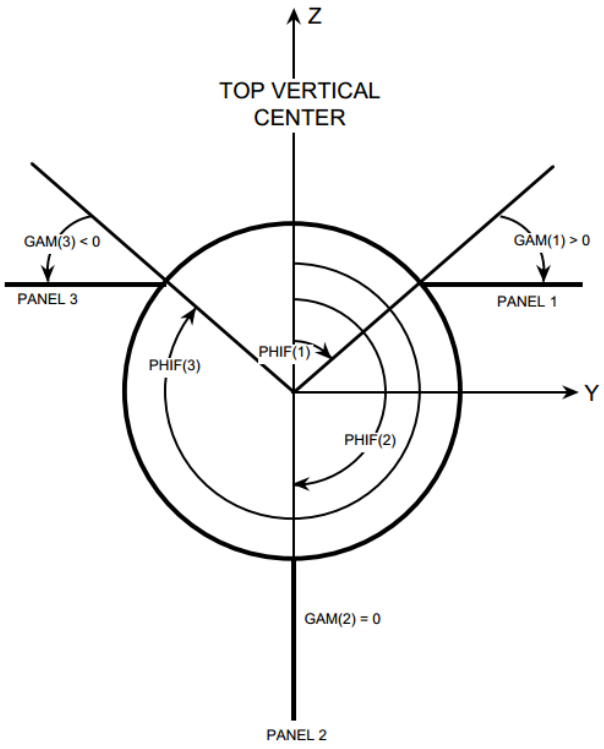

Figure A.5: Fin Numbering [4]

DB12 341 360" command causes array DB12, location 341 to 360 to be written into "for004.dat" file. This control card can be used to obtain specific coefficients (Table A.7 and Table A.8) in MATLAB environment. The fact that "for004.dat" file only consists of numerical data, unlike "for006.dat", makes it convenient to obtain aerodynamic coefficients one by one using "WRITE" command.

"FORMAT" is used to set the format in which the numerical data is written into "for004.dat". It can be modified to further simplify data reading process.

A.1.7 Aerodynamic Coefficient Dependence

Dependence table is given in [17] as shown in Figure A.6. Considering the axisymmetrical missile, if negligible entries are ignored and dynamic coefficients are added, following equations Eq. (A.2) and Eq. (A.3) of dependence is obtained. Dependence table can be expanded in order to model the aerodynamics more accurately.

Table A.7: WRITE Array Names [4]

Configuration	**DUMP array name**	**WRITE array name**
Body alone	SBODY	SBODY
Fin 1 alone	SF1	SFIN1
Fin 2 alone	SF2	SFIN2
Fin 3 alone	SF3	SFIN3
Fin 4 alone	SF4	SFIN4
Body + 1 fin set	SB1	SB1
Body + 2 fin set	SB12	SB12
Body + 3 fin set	SB13	SB123
Body + 4 fin set	SB14	SB1234

Table A.8: WRITE Array Locations [4]

Array Loc.	**Var.**	**Definition**	**Units**
1-20	C_N	Normal force coefficient	-
21-40	C_m	Pitching moment coefficient	-
41-60	C_A	Axial force coefficient	-
61-80	C_Y	Side force coefficient	-
81-100	C_n	Yawing moment coefficient	-
101-120	C_l	Rolling moment coefficient	-
121-140	$C_{N\alpha}$	Normal force derivative with angle of attack	$1/[^\circ]$
141-160	$C_{m\alpha}$	Pitching moment derivative with angle of attack	$1/[^\circ]$
161-180	$C_{Y\beta}$	Side force derivative with sideslip angle	$1/[^\circ]$
181-200	$C_{n\beta}$	Yawing moment derivative with sideslip angle	$1/[^\circ]$
201-220	$C_{l\beta}$	Rolling moment derivative with sideslip angle	$1/[^\circ]$

Variable	all = 0	α	β	δ_a	δ_e	δ_r
$F_{A_{x_{1_s}}}$	drag at zero value for all variables	induced drag	negligible for small: β	negligible for small: δ_a	negligible for small: δ_e	negligible for small: δ_r
$F_{A_{y_{1_s}}}$	zero	negligible for small: α	side force due to: β	zero	zero	side force due to: δ_r
$F_{A_{z_{1_s}}}$	lift at zero value for all variables	lift due to: α	negligible for small: β	negligible	lift due to: δ_e	negligible
$L_{A_{1_s}}$	zero	rolling moment due to sideslip is affected by: α	rolling moment due to: β	rolling moment due to: δ_a	zero	rolling moment due to: δ_r
$M_{A_{1_s}}$	pitching moment at zero value for all variables	pitching moment due to: α	negligible for small: β	negligible	pitching moment due to: δ_e	negligible
$N_{A_{1_s}}$	zero	yawing moment due to sideslip is affected by: α	yawing moment due to: β	yawing moment due to: δ_a	zero	yawing moment due to: δ_r

Figure A.6: Aerodynamic Coefficient Dependence Table [17]

Force coefficients:

$$\begin{aligned} C_X &= C_X(M, \alpha, \beta) \\ C_Y &= C_Y(M, \beta, \delta_r, \dot{\beta}, r) \\ C_Z &= C_Z(M, \alpha, \delta_e, \dot{\alpha}, q) \end{aligned} \tag{A.2}$$

Moment coefficients:

$$\begin{aligned} C_l &= C_l(M, \alpha, \beta, \delta_a, p) \\ C_m &= C_m(M, \alpha, \delta_e, \dot{\alpha}, q) \\ C_n &= C_n(M, \beta, \delta_a, \dot{\beta}, r) \end{aligned} \tag{A.3}$$

Note that in Missile DATCOM, force coefficients are shown in capital letters (A, N, Y) in subscripts and moment coefficients are shown in small letters (l, m, n). In this appendix Missile DATCOM convention is adopted; however, in the rest of

the document force coefficients are labeled as X, Y, Z and moment coefficients are labeled as L, N, M.

A.1.8 Aerodynamic Coefficients of Alternative 2 Missile

Here aerodynamic coefficients of the Alternative 2 missile, used in the thesis, are given. Moment coefficients are referenced to the missile nose.

	$\alpha = 0°$, $\delta_e = 0°$	$\alpha = 5°$, $\delta_e = 0°$			$\alpha = 0°$, $\delta_e = 5°$		
Mach	C_X	C_X	C_M	C_Z	C_X	C_M	C_Z
0.5	0.2305	0.2301	-5.3402	-0.7828	0.2305	-4.3379	-0.3297
1.2	0.8730	0.8720	-6.0111	-0.8446	0.8730	-6.2061	-0.4909
2.5	0.5565	0.5550	-7.2530	-1.0551	0.5565	-1.9793	-0.1552
3.5	0.4604	0.4606	-6.1767	-0.8867	0.4604	-1.3582	-0.1065

APPENDIX B

ATMOSPHERE MODEL

International Standard Atmosphere (ISA) employs the following equations:

γ	Specific heat ratio	1.4
T_0	Absolute temperature at mean sea level	$288.15°K$
ρ_0	Air density at mean sea level	$1.225kg/m^3$
L	Lapse rate	$0.0065°K/m$
g	Gravitational acceleration	$9.80665m/s^2$
R	Characteristic gas constant	$287.0531j/(kg°K)$

$$T = \begin{cases} T_0 - Lh, h < 11000m \\ T_0 - L11000, h \geq 11000m \end{cases}$$

$$a = \sqrt{T\gamma R}$$

$$\rho = \begin{cases} \rho_0 \frac{T}{T_0}^{(\frac{g}{LR}-1)}, h < 11000m \\ \rho_0 \frac{T}{T_0}^{(\frac{g}{LR}-1)} e^{(\frac{g}{LR}(11000-h))}, h \geq 11000m \end{cases}$$

where h is input altitude; T, a and ρ are the temperature, speed of sound and air density at input altitude, respectively.

APPENDIX C

LATERAL THRUSTERS

Lateral thrusters discussed in this work is assumed to be mono or bi propellant type. In mono propellant systems, pressurized propellant goes through a catalyst bed and ignites creating high temperature gases, these exhaust gases are send away from the thruster nozzle to create a reaction force on the body (Figure C.1). In bi propellant system the only difference is the ignition. Instead of a catalyst bed a secondary chemical, called oxidizer, is mixed with the propellant for ignition.

These systems typically have specific impulse around 250-300 seconds. The propellant type is the main factor on the specific impulse value. Thruster force can range from tens of Newtons to hundreds of Newtons [10]. Rocket equation can be used to calculate the mass of the propellant. That is:

$$m_{thr} = \frac{F_{thr}\Delta t}{I_{sp}g_0} \tag{C.1}$$

where F_{thr} is the thruster force, Δt is the time thruster operates, I_{sp} is the specific

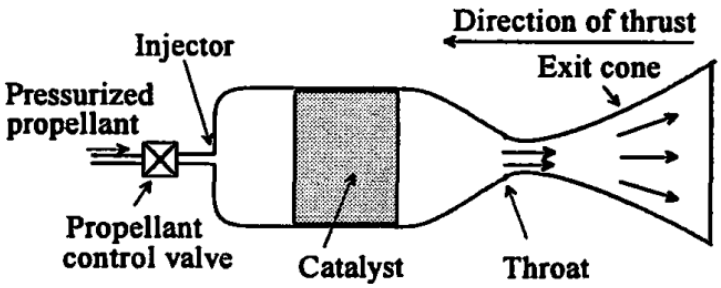

Figure C.1: Schematic Diagram of a Mono-propellant Thruster Engine [10]

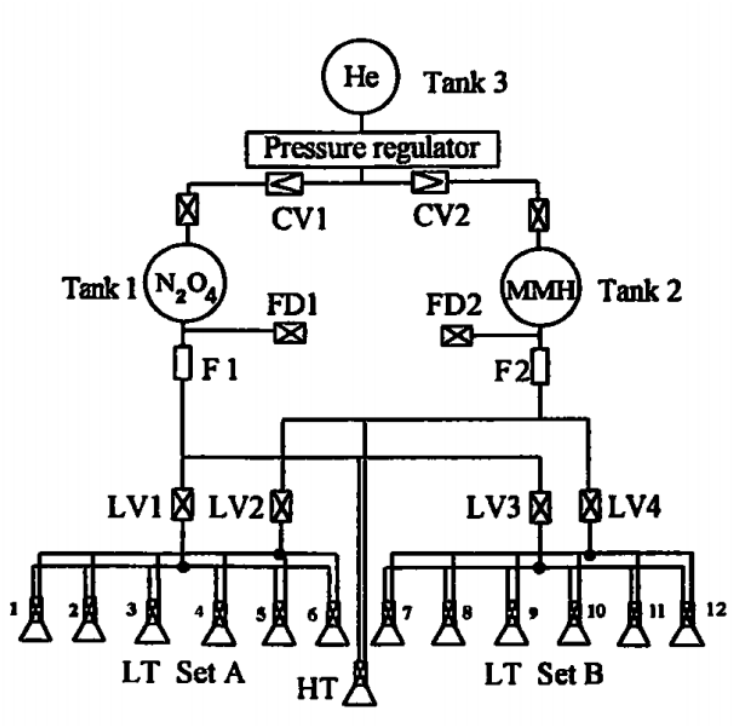

Figure C.2: Schematic Diagram of a Bi-propellant System [10]

impulse of the system and g_0 is the gravitational acceleration at the sea level. In this study specific impulse is assumed to be 275 seconds and thruster force is chosen as 200 N. Single thruster is assumed to be active for at most 10 seconds. Then propellant mass can be calculated as:

$$\begin{aligned} m_{prop} &= 4 \times \frac{200 \times 10}{285 \times 9.81} \\ m_{prop} &\approx 3kg \end{aligned} \tag{C.2}$$

Note that the expression is multiplied by 4 because there are 4 thrusters on the missile. The nozzle and rest of the system's mass is assumed to be 2 kg per thruster [2], [12], [13]. Then total system comes to be about 11 kg. This mass is assumed to be included in the guidance and control section discussed in Appendix D.

APPENDIX D

MISSILE MASS CHARACTERISTICS ESTIMATION

Mass characteristics of the missile discussed in this thesis is calculated with the equations in [14]. [14] is a work done with plenty of missile types and ranges in order to generalize missile total and subsection weight and size with simple equations.

Diameter and the length of the missile is determined as 0.15 m and 2 m which is standard with this type of missiles. Range is chosen as 30 nm (nautical miles) and top speed is chosen as 3.5 Mach. Then suitable equations from [14] are chosen to calculate mass and size values.

$$
\begin{aligned}
V_{total} &= (\pi d^2 l_{total})/4 \\
m_{total} &= 142.2 Vol^{0.74} (EQ-4) \\
m_{propellant} &= -284.9 + 633.6d - 0.105 m_{total} + 0.949\rho (EQ-77) \\
V_{propellant} &= (m_{propellant} - 2.7)/112 (EQ-22) \\
l_{propellant} &= V_{propellant} 4/(\pi d^2) \\
m_{guidance} &= 117.6d + 1.6 range - 0.14\rho (EQ-85) \\
V_{guidance} &= (m_{guidance}/83.9)^(1/0.63)(EQ-53) \\
l_{guidance} &= V_{guidance} 4/(\pi d^2) \\
m_{warhead} &= 0.1\rho - 0.2 range + 0.2 m_{total} - 2.4 l_{total} (EQ-93) \\
V_{warhead} &= (m_{warhead}/103.9)^(1/0.78)(EQ-69) \\
l_{warhead} &= V_{warhead} 4/(\pi d^2)
\end{aligned}
\tag{D.1}
$$

In Eq. (D.1) m, V, l denotes mass, volume and length, respectively. ρ is the missile density and d is the missile diameter. (EQ-XX) expressions indicate the equations

Name	MICA	IRIS-T	AA-11	Umkhonto	9M33	Roland
Mass [kg]	112	87.4	105	130	170	67
Warhead [kg]	12	-	7.4	23	16	6.5
Length [m]	3.1	2.94	2.93	3.32	3.16	2.4
Diameter [mm]	160	127	165	180	209.6	160
Flight Altitude [km]	11	20	-	15	12	5.5
Speed [Mach]	3	3	2.5	2	3	1.6
Wingspan [mm]	320	450	510	500	-	500
Range [km]	50	25	30	60	15	8

Table D.1: Characteristics of Similar Missile Systems

picked from [14]. Note that these equations are valid for *feet* for length units and *pounds* for mass units.

From these equations following values are obtained:

$$\begin{aligned} m_{total} &= 76kg \\ m_{propellant} &= 62kg \\ l_{propellant} &= 0.95m \\ m_{guidance} &= 40kg \\ l_{guidance} &= 1.7m \\ m_{warhead} &= 11kg \\ l_{warhead} &= 0.2m \end{aligned} \tag{D.2}$$

There are some problems with the results, especially in the guidance section. The equations used are not perfect; hence, the results are treated as a reference value together with data from similar systems given in Table D.1 and the values declared in the beginning of Chapter 3 are determined.

Nonetheless [14] is a valuable work as it gathered lots of missile mass data with various mission profiles and ranges.